LBNL-41975

ERNEST ORLANDO LAWRENCE BERKELEY NATIONAL LABORATORY

The Influence of Surface Topography on the Forming Friction of Automotive Aluminum Sheet

Pamela A. Kramer

Materials Sciences Division

May 1998

Ph.D. Thesis

REFERENCE COPY
Does Not
Circulate

Bldg. 50Ø Library - Ref.
Lawrence Berkeley National Laboratory

LBNL-41975
Copy 1

DISCLAIMER

This document was prepared as an account of work sponsored by the United States Government. While this document is believed to contain correct information, neither the United States Government nor any agency thereof, nor the Regents of the University of California, nor any of their employees, makes any warranty, express or implied, or assumes any legal responsibility for the accuracy, completeness, or usefulness of any information, apparatus, product, or process disclosed, or represents that its use would not infringe privately owned rights. Reference herein to any specific commercial product, process, or service by its trade name, trademark, manufacturer, or otherwise, does not necessarily constitute or imply its endorsement, recommendation, or favoring by the United States Government or any agency thereof, or the Regents of the University of California. The views and opinions of authors expressed herein do not necessarily state or reflect those of the United States Government or any agency thereof or the Regents of the University of California.

LBNL 41975

THE INFLUENCE OF SURFACE TOPOGRAPHY ON THE FORMING FRICTION OF AUTOMOTIVE ALUMINUM SHEET

Pamela Ann Kramer

Department of Materials Science and Mineral Engineering
University of California, Berkeley

and

Center for Advanced Materials
Materials Sciences Divison
Lawrence Berkeley National Laboratory
1 Cyclotron Road
Berkeley, CA 94720

May 1998

This work is supported by the Director, Office of Energy Research, Office of Basic Energy Science, Material Sciences Division of the U.S. Department of Energy under Contract No. DE-AC03-76SF00098

The Influence of Surface Topography on the Forming Friction of Automotive Aluminum Sheet

by

Pamela Ann Kramer

B.S. (University of California, Berkeley) 1988
M.S. (University of California, Berkeley) 1992

A dissertation submitted in partial satisfaction of the

requirements for the degree of

Doctor of Philosophy
in

Engineering - Materials Science
and Mineral Engineering

in the

GRADUATE DIVISION

of the

UNIVERSITY OF CALIFORNIA, BERKELEY

Committee in charge:

Professor J.W. Morris, Jr., Chair
Professor Robert O. Ritchie
Professor Lisa A. Pruitt

Spring 1998

THE INFLUENCE OF SURFACE TOPOGRAPHY ON THE FORMING FRICTION OF AUTOMOTIVE ALUMINUM SHEET

by

Pamela Ann Kramer

Ph.D. Dissertation
for the University of California, Berkeley

ABSTRACT

Interest in utilizing aluminum alloys in automobiles has increased in recent years as a result of the desire to lower automobile weight and, consequently, increase fuel economy. While aluminum alloy use in cast parts has increased, outer body panel applications are still being investigated. The industry is interested in improving the formability of these sheet alloys by a combination of alloy design and processing. A different avenue of improving the formability of these alloys may be through patterning of the sheet surface. Surface patterns hold the lubricant during the forming process, with a resulting decrease in the sheet-die surface contact. While it has been speculated that an optimum surface pattern would consist of discrete cavities, detailed investigation into the reduction of forming friction by utilizing discrete patterns is lacking.

A series of discrete patterns were investigated to determine the dependence of the forming friction of automotive aluminum alloys on pattern lubricant carrying capacity and on material strength. Automotive aluminum alloys used in outer body panel applications were rolled on experimental rolls that had been prepared with a variety of discrete patterns. All patterns for each alloy were characterized before and after testing both optically and, to determine pattern lubricant capacity, using three dimensional laser profilometry. A draw bead simulation (DBS) friction tester was designed and fabricated to determine the forming friction of the patterned sheets. Tensile testing and frictionless DBS testing were performed to ascertain the material properties of each sheet. The most striking result of this work was the inversely linear dependence of forming friction on the lubricant carrying capacity of the discrete patterns. Other important observations include the fact that forming friction trends for particular patterns remained the same between alloy sheets of similar thickness, with forming friction increasing both with material strength and with pattern degradation resulting from roll wear. In addition, patterns 2 μm or less in depth were destroyed by post-test surface roughening while patterns greater than 2 μm in depth maintained most of their shape, following the rise and fall of the rougher post-test surface topography. The inversely linear dependence of forming friction on discrete pattern lubricant carrying capacity and the increase of forming friction with material strength were used to develop a constitutive equation for use in describing the forming friction behavior of the discretely patterned surfaces.

DEDICATION

For Sam, who had to put up with me.
For Mom and Dad, who've been there themselves.
I couldn't have done it without you.

TABLE OF CONTENTS

Abstract i
Dedication ii
Table of Contents iii
List of Figures vi
List of Tables x
Acknowledgements xi
1. Introduction 1
1.1 AUTOMOTIVE ALUMINUM UTILIZATION 1
1.2 ALUMINUM FORMABILITY 2
1.3 PART FORMING 2
1.4 AUTOMOTIVE ALLOY PATTERN USE 4
1.5 SURFACE DEFINITION AND PATTERN DESIGN 5
1.6 FORMABILITY VERSUS PAINTABILITY 6
1.7 PATTERNING AND ROLL FINISH 7
1.8 DRAW BEAD SIMULATOR TESTING 9
1.9 PREVIOUS WORK 10
1.10 CURRENT WORK 11
2. Experimental Procedure 13
2.1 DRAW BEAD SIMULATOR TEST MACHINE 13
2.2 TEST MATERIAL 14
2.3 MATERIAL CHARACTERIZATION 15
2.4 PATTERN CHARACTERIZATION 16
2.4.1 Characterization Methods 16
2.4.2 Pattern Lubricant Carrying Capacities 17
2.4.3 Post-Test Pattern Appearance 18
2.5 DRAW BEAD SIMULATOR TESTS 19
2.5.1 Draw Bead Simulator Test Parameters 19
2.5.2 Draw Bead Simulator Machine and Specimen Validation 20
2.5.2 #1 Die Deflection Measurements 20
2.5.2 #2 Gauge Setup versus Load Cell Setup Tests 21
2.5.2 #3 Local versus Denver DBS Tests 21
2.5.2 #4 Specimen-Bead Contact Measurement 21
2.5.2 #5 Single-Sided versus Double-Sided Tests 22
2.5.2 #6 Specimen Width Comparison 22

2.5.2 #7 Estimated Error 22
2.5.3 Draw Bead Simulator Pattern Dependence Tests 23
3. Results 24
3.1 MATERIAL CHARACTERIZATION 24
3.1.1 Alloy Composition 24
3.1.2 Alloy Grain Structure 25
3.1.3 Alloy Tensile Properties 26
3.1.4 Alloy Frictionless Forming Properties 28
3.2 PATTERN CHARACTERIZATION 30
3.2.1 Optical Measurements - Untested Patterns 30
3.2.2 Profilometry Measurements - Untested Patterns 39
3.3 DRAW BEAD SIMULATOR MACHINE AND SPECIMEN VALIDATION 41
3.3.1 Die Deflection Tests 41
3.3.2 Strain Gauge versus Load Cell Setup Tests 41
3.3.3 Local versus Denver DBS Tests 42
3.3.4 Specimen-Bead Contact Measurements 43
3.3.5 Single-Sided versus Double-Sided Tests 43
3.3.6 Specimen Width Comparison 44
3.3.7 Estimated Error 45
3.4 DEPENDENCE OF DBS-μ ON PATTERN 45
3.4.1 Influence of MF, EDT Pattern and Alloy on Forming Friction 45
3.4.2 Influence of EBT Pattern and Alloy on Forming Friction 46
3.5 POST-DBS TEST SURFACE APPEARANCE 53
3.5.1 Overall Tested Surface Appearance 53
3.5.2 Influence of Alloy on Tested Surface Appearance 55
3.5.3 Influence of Single-Sided vs. Double-Sided Test on Tested Surface Appearance 58
3.5.4 Change in Lubricant Carrying Capacity After Testing 58
4. Discussion 61
4.1 VALIDATION OF DBS TEST RESULTS 61
4.1.1 Machine Validity 61
4.1.2 Specimen Validity 62
4.2 MATERIAL EFFECTS 63
4.2.1 Effects of Composition and Processing on Mechanical Properties 63
4.2.2 Effect of Mechanical Strength on Forming Friction 65
4.2.3 Effect of Alloy Properties on Post-Test Surface Roughening 66

4.2.3 #1 Surface Roughening 66
4.2.3 #2 Formability and Paintability Implications 67
4.2.3 #3 Mill Finish Pattern Roughening 67
4.3 PATTERN EFFECTS 68
4.3.1 Effect of Sheet Reduction and Roll Wear 68
4.3.2 Mill Finish and Electro-Discharge Texture Patterns 69
4.3.3 Electron Beam Texture Patterns 70
4.3.4 Lubricant Carrying Capacity 71
4.4 CONSTITUTIVE EQUATION RELATING FORMING FRICTION TO SHEET PARAMETERS 71
5. Summary 74
6. Conclusions 75
6.1 PATTERNING 75
6.2 MATERIAL 75
7. Future Work Recommendations 76
7.1 PATTERNING 76
7.2 MATERIAL 76
7.3 DBS TEST 76
8. References 77
APPENDIX A Fabrication and Modification of a DBS Forming Friction Test Machine .. 84
APPENDIX B DBS Test QuickBasic Program 88
APPENDIX C Representative Micrographs of AA2008, AA6009, and AA6111 103
APPENDIX D EBT Forming Friction Strain Gauge and Load Cell Results 104
APPENDIX E DBS Load Cell Setup Forming Friction Data For All Patterns in Column Form 105
APPENDIX F Calculation of Surface Parameters 107

LIST OF FIGURES

Figure 1 Forming process showing die and punch with close up of draw bead (from I6) 3

Figure 2 Friction regimes defined by Wilson (from I7) 4

Figure 4 DBS Tooling Geometries: a) roller bead test, b) fixed bead test. 10

Figure 5 Front View of DBS test machine. 13

Figure 6 Top view of DBS test setup showing grips and pulling assembly..... 14

Figure 7 Rear view of DBS test setup showing fixed bead setup (before insertion) with specimen; the guide rollers shown keep the specimen level. 14

Figure 8 Schematic showing patterning across sheet surfaces..... 15

Figure 9 Schematic of tensile test specimen..... 16

Figure 10 Ideal volume calculation parameters for $V= 4/3\pi rhl$; r is the distance to the rim center, l is the rim width and h is the ring depth. (from E6) 17

Figure 11 Histogram of surface heights a) for patterns >2 μm in depth and b) for patterns <2 μm in depth..... 18

Figure 12 Schematic of a) fixed, b) mixed, and c) roller bead test setups. 20

Figure 13 Roller bead drawing forces normalized by sheet thicknesses and ultimate tensile strengths plotted against thickness, after Schey (R5), showing the dependence of frictionless drawing forces on the sheet thickness. 29

Figure 14 Plot of AA2008, AA6009, and AA6111 roller bead drawing forces across the EBT sheet width, and of AA2008 MF and EDT and AA6009 MF sheets; AA6111 forces have been corrected for the thickness difference. All tests performed within one pattern number for both A and B sides were averaged. 29

Figure 15 Micrographs of AA2008 Patterning a) MF (6009 similar), and b) EDT 30

Figure 15 Micrographs of AA2008 EBT Patterning c) 1A, d) 2A, e) 3A, f) 4A, g) 5A, h) 6A, i) 7A, j) 8A..... 31

Figure 15 Micrographs of AA2008 EBT Patterning k) 1B, l) 2B, m) 3B, n) 4b, o) 5B, p) 6B, q) 7B, r) 8B..... 32

Figure 16 Micrographs of AA6009 EBT Patterning a) 1A, b) 2A, c) 3A, d) 4A, e) 5A, f) 6A, g) 7A, h) 8A..... 33

Figure 16 Micrographs of AA6009 EBT Patterning i) 1B, j) 2B, k) 3B, l) 4b, m) 5B, n) 6B, o) 7B, p) 8B 34

Figure 17 Micrographs of AA6111 EBT Patterning a) 1A, b) 2A, c) 3A, d) 4A, e) 5A, f) 6A, g) 7A, h) 8A..... 35

Figure 17 Micrographs of AA6111 EBT Patterning i) 1B, j) 2B, k) 3B, l) 4b, m) 5B, n) 6B, o) 7B, p) 8B 36

Figure 18 Examples of a) and b) EBT pattern measurements, c) 60° interlocking hexagonal EBT ring distribution, and d) 45° EBT ring distribution..... 38

Figure 19 Representative untested bearing area curves for deeper EBT patterns a) 2008.1 1A and b) 6009 1A and shallower EBT patterns c) 2008.1 2A and d) 6009 2A. Typical e) MF and f) EDT bearing area curves are comparable to the shallower EBT pattern curves. The distinctive knee in the deeper pattern curves is absent for shallower pattern curves, indicating a pattern depth on the order of the surface waviness. The lower knee for (b) represents a greater pattern volume than for the nominally identical (a). 40

Figure 20 Measured pattern volume, calculated from three dimensional profilometry data, is shown as a function of ideal pattern volume, calculated from roll patterning data for a) 2008 EBT.1 and EBT.2, and 6009 EBT and b) 6111 EBT.1 and EBT.2 sheets. 41

Figure 21 Linear relationship between local DBS forming friction strain gauge setup results and load cell setup results. 42

Figure 22 Local DBS test results for all MF and EDT tests plotted as a function of DBS tests performed at the University of Colorado, Denver, to validate the local test machine. 42

Figure 23 Comparison of "retested" specimens cut from the portion of the 25.4 mm (1 in) wide specimens tested at Denver, and non-prestrained MF and EDT specimens..... 43

Figure 24 Comparison of single-sided and double-sided DBS test results for all MF and EDT testing performed locally and at Denver showing a linear relationship 44

Figure 25 Comparison of all 25.4 mm (1.00 in) and 50.8 mm (2.00 in) wide specimen tests, with "retest" specimens corrected for previous straining, showing a virtual one to one correspondence between the two specimen test widths.. 44

Figure 26 Column plot of DBS-μ for 2008 and 6009 MF and 2008 EDT patterns showing vastly different forming friction for MF-L and MF-T from the directional patterning and nominally equal EDT-L and EDT-T forming friction from the more non-directional patterning..... 45

Figure 27 a) EBT DBS forming friction values for all 1.09 mm (0.043 in) thick specimens, showing a repeatable effect from particular patterns between alloys. The lower forming-μ values arise from lower UTS values. b) EBT DBS forming friction values for all 0.914 mm (0.036 in) thick specimens 46

Figure 28 a) Forming friction results for similar EBT patterns showing the influence of mechanical strength on the single-sided DBS test friction value..... 47

Figure 29 The dependence of single-sided DBS test forming friction on a) ideal and b) measured pattern volumes for specimens cut in the sheet rolling direction for 2008 EBT.1, 2008 EBT.2, and 6009 EBT sheets. The forming friction shows a linear dependence on both ideal and measured pattern volumes... 48

Figure 30 The dependence of single-sided DBS test forming friction on a) ideal and b) measured pattern volumes for specimens cut 90° to the sheet rolling direction for 2008 EBT.1, 2008 EBT.2, and 6009 EBT sheets. The forming friction is virtually independent of the pattern volume in the transverse direction, from the impact of the residual MF pattern on the sheet surfaces..... 49

Figure 31 A single, inversely linear relationship between single-sided DBS test forming friction and discrete lubricant carrying area for 2008 EBT.1, 2008 EBT.2, and 6009 EBT measured patterns cut a) parallel to the sheet rolling direction. As with pattern volumes, specimens cut b) transverse to the sheet rolling direction were independent of pattern area..... 50

Figure 32 Dependence of single-sided DBS test forming friction on a) ideal and b) measured pattern volumes for specimens cut both in and transverse to the rolling direction for the elongated patterns of the 6111 EBT sheets..... 51

Figure 33 Three dimensional plots of profilometry data for a nominally identical a) 2008 and b) 6111 pattern, showing the greater uplift in the 6111 pattern from smearing during rolling as well as c) from roll wear..... 52

Figure 34 Column plot illustrating greater forming friction in the single-sided DBS test from pattern degradation resulting from greater roll wear. Side A represents worn roll, side B represents newer, less worn, roll; test scatter is shown by error bars. 53

Figure 35 Tested versus untested 1BL surfaces for AA2008 and AA6009 showing pattern lengthening from stretching during testing, greater initial contribution from the untested AA6009 pattern from greater smearing during rolling, and greater tested roughnesses from AA2008..... 54

Figure 36 Three dimensional plot of tested surface showing the EBT imprinted pattern following the roughened surface topography. 54

Figure 37 Comparison of tested vs. untested longitudinal and transverse surfaces for a) AA2008.1, b) AA2008.2, c) AA6009, and d) AA6111, showing greater roughening for AA2008-T and greater initial pattern contribution for AA6111..... 55

Figure 38 Three dimensional roughness averages (3D R_a) for untested versus tested a) longitudinal specimens and b) transverse specimens showing surface homogenization and greater post-test roughness of the 2008 sheets. 56
Figure 39 a) 3D Skewness and b) 3D Kurtosis for untested versus tested longitudinal specimens and tested transverse specimens showing homogenization of the different surfaces. 57
Figure 40 Plot of wavelength change for fixed and mixed MF sheet tests showing same degree of roughening..... 58
Figure 41 Plot of tested versus untested pattern lubricant carrying capacity, where the tested volume includes surface roughening effects..... 59
Figure 42 Height histogram of tested surfaces, a) large and b) small rings, with the tested surfaces for the deeper patterns showing a loss of the distinctive representation of the discrete pattern. 59
Figure 43 Bearing area curves for tested a) 6009 EBT 1A, b) 2008.1 EBT 1A, c) 6009 EBT 2A, and d) 2008.1 EBT 2A patterns. a) and b) show a removal of the lubricant pocket effectiveness (no more knee) for the deeper patterns, while all plots and show a change in the overall height for the tested surfaces.... 60
Figure 44 Schematic of a) how an ideal pattern on a roll smears on the sheet surface during rolling, b) resulting in an elongated pattern appearance. 69
Figure 45 Comparison of load cell mixed bead test data to fixed bead test data for similar surfaces tested elsewhere (D17)..... 70
Figure A1 Side view schematic of DBS tooling box, indicating parts..... 85
Figure A2 Calibration curves for strain gauges a) on V-notch and b) below V-notch. 86
Figure D1 DBS-μ strain gauge and load cell setup results for 2008 EBT.1..... 104
Figure D2 DBS-μ strain gauge and load cell setup results for 2008 EBT.2..... 104
Figure D3 DBS-μ strain gauge and load cell setup results for 6009 EBT..... 104
Figure E1 DBS-μ results for 2008 MF, 2008 EDT, and 2008.1 EBT sheets. 105
Figure E2 DBS-μ results for 2008 MF, 2008 EDT, and 2008.2 EBT sheets. 105
Figure E3 DBS-μ results for 6009 MF and 6009 EBT sheets..... 105
Figure E4 DBS-μ results for a) 6111.1 EBT, and b) 6111.2 EBT sheets. 106

LIST OF TABLES

Table 1 Number and Type of Alloy Surface Finishes Available 15
Table 2 Description of DBS test set and direction set terminology 20
Table 3 DBS test matrix 21
Table 4 Estimated Error Values for 25.4 mm (1.00 in) Wide Specimen DBS Tests ... 23
Table 5 Measured Alloy Compositions of As-Received MF, EDT, and EBT Sheet (wt%) 24
Table 6 Grain Aspect Ratios for AA2008, A6009, and AA6111 sheets, where RP is the rolling plane, l is the grain length, w is the grain width, and t is the grain thickness. 26
Table 7 Engineering yield, ultimate, and elongation values for the longitudinal direction of AA2008, AA6009, and AA6111 patterned sheet. 27
Table 8 Engineering yield, ultimate, and elongation values for the transverse direction of AA2008, AA6009, and AA6111 patterned sheet. 27
Table 9 EBT pattern ring information for AA2008 EBT sheets listed by pattern number and side, showing directional and average ring diameters, distributions, and spacings 37
Table 10 EBT pattern ring information for AA6009 EBT sheets listed by pattern number and side, showing directional and average ring diameters, distributions, and spacings 37
Table 11 EBT pattern ring information from AA6111 EBT sheets listed by pattern number and side, showing directional and average ring diameters, distributions, and spacings 38

ACKNOWLEDGEMENTS

My thanks go to Jin Chan for his invaluable assistance and knowledge of everything, and to Carol Tseng for her help and honest opinions. I cannot leave out the tireless generosity of Seung Hyuk Kang, Chris Krenn and Koji Sato, or the tribological knowledge of Peter Skarpelos. The support of my office mates, Heidi Reynolds and Carlos Gonzales, was also invaluable.

I am indebted to the generous contributions of both material and information by Jim Story and Harry Zonker. I am immensely grateful to Robert McCune and Larry Reatherford for allowing me to monopolize their laser profilometer. My gratitude also goes to Peter Joshua for donating the use of the software to translate the profilometry data. My heartfelt thanks go to Professor Sanchez for the use of his DBS machine for comparison testing, and to Dave Robertson for his help in running the machine.

Most of all, I wish to thank Professor Morris for his unwavering support through my graduate career.

1. INTRODUCTION

Automotive aluminum alloys are currently increasing in use to help lower the weight and increase the fuel efficiency of today's automobiles. One of the ways thought to help maximize the formability of these alloys in outer body panel applications is to design a surface pattern that holds lubricant to minimize the contact, and thus the forming friction, between the sheet surface and the die forming the part. In an iterative fashion, this surface design has been taking place for automotive steel alloys. Some constraints on such design, however, are the desire to achieve an acceptable painted finish on the deformed part and concern with the transfer of the chosen design during final rolling with patterned rolls. One method of assessing different designed patterns in the automotive industry is friction testing, which is an indicator of part formability. Relating these formability results and quantifiable surface measurements has, however, been difficult. The work here was designed specifically to find such a relationship for the dependence of forming friction on discretely patterned surfaces.

1.1 Automotive Aluminum Utilization

There is a large incentive in today's automotive industry to create lighter, more fuel efficient automobiles. U.S. Congressional pressure to increase Corporate Average Fuel Economy (CAFE) and the Partnership for a New Generation of Vehicles (PNGV) are the main driving forces behind this incentive. The PNGV is a joint effort by U.S. auto makers and the federal government, announced in September 1993, with the goal of producing an affordable, family sized sedan with a CAFE of 35 km/l (80 mpg) within ten years.[I1] One of the easiest ways to increase the fuel efficiency of an automobile is to reduce its overall weight. Common ways to reduce weight include using thinner sheet for autobody panels, using a unibody construction rather than a frame construction, and using alloys with higher specific strength. All of these methods are presently in use, with the first one having reached its maximum with today's alloys. Manufacturers are restricted from using sheet thinner than that which is currently used in today's automobiles because of the difficulty of ensuring panel stiffness and dent resistance. The use of thinner sheet is demonstrated daily by the ease with which newer car doors dent when impacted, in contrast to the comparatively dent-resistant older cars.

Aluminum alloys, with higher specific strength than steel alloys, are increasingly utilized in automobile construction, both in cast part and in sheet form, to help lower weight and increase fuel efficiency.[I2] Automotive aluminum sheet outer body panel usage is generally limited to less complicated, shallower parts such as hoods, because of formability concerns. Exterior body panel aluminum alloys have lower formability than steel alloys used for the same application because of lower uniform elongations and

generally greater anisotropy in their forming properties resulting from a mixture of different crystallographic textures.[I3] While these problems are being worked on with improvements arising from alloy composition and processing, other approaches to improving formability need to be explored to help increase the use of aluminum alloys in outer body panel applications. One possible approach for a given alloy is through surface patterning.

1.2 Aluminum Formability

Utilizing the properties of the alloys themselves, automotive aluminum alloys are formed into body panels in the naturally aged, or -T4 condition. This room temperature aged state is capable of greater uniform elongation, and therefore better formability, than any elevated temperature aged condition. Unfortunately the greater uniform elongation capability arises from lower alloy strength, an undesired feature in a finished part. This is compensated for by elevated temperature aging, and consequent precipitation hardening, of the panels after the autobody is assembled, during the cycle where the coatings of paint are baked on to the surface of the body. Current alloy compositions attempt to maximize both -T4 sheet formability and precipitation hardening-based strength gains after forming during the paint bake cycle.

In addition to composition, processing is also used to maximize the formability of aluminum sheet, as it can greatly affect the crystallographic texture components present in the sheet.[I4] Processing today differs from that even five years ago in order to maximize the isotropic textures, and minimize the anisotropic textures, in order to improve the directional formability of these alloys.[I5] The ultimate desire is to create a sheet that is equally formable in all directions.

1.3 Part Forming

The formability of automotive outer body panels from a particular alloy is controlled by the alloy's deep drawing capability which, in turn, is controlled by the alloy's composition and processing. Deep drawing is a process where sheet metal is drawn into a die by a punch (Figure 1)[I6] to form a complex part. The sheet is restrained from flowing into the die too quickly by clamping around the die edges with a flat binder. If the clamping force restraining the sheet is appreciably greater than the drawing force pulling the sheet into the die, the sheet will tear. Conversely, if the drawing force is greater than the restraining force by too great a margin, the material will be drawn into the die too quickly and wrinkling will result. In many operations the restraint provided by the flat binder is inadequate, and drawbeads are added to the binder. Draw beads are D-shaped rods set into the flat binder at critical restraining points which utilize both bending deformation and sliding friction to restrain the sheet (Figure 1).

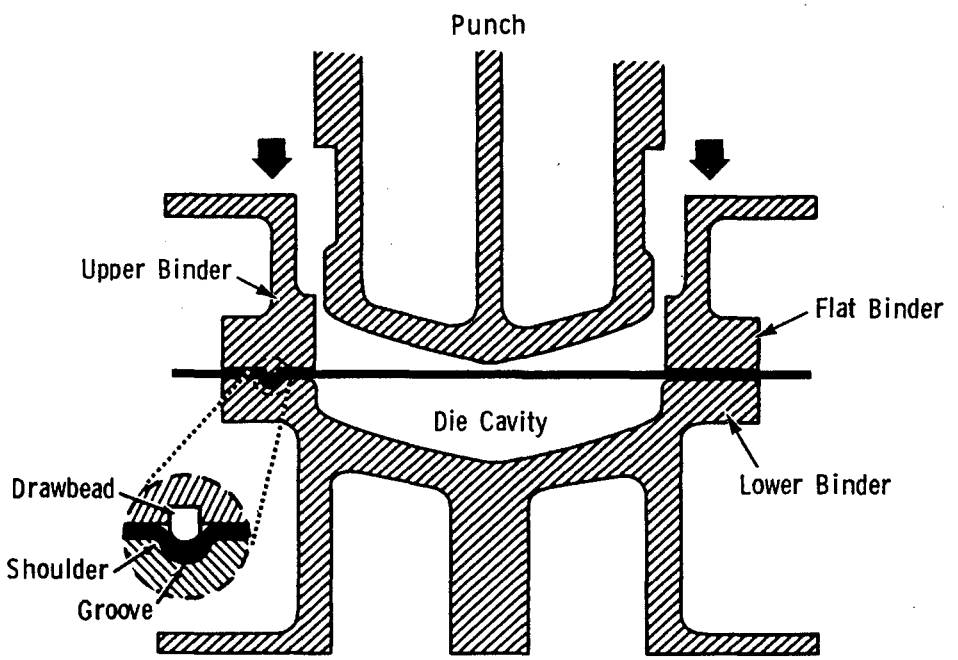

Figure 1 Forming process showing die and punch with close up of draw bead (from I6)

For a given sheet alloy, with a given composition and processing, one way to improve the deep-drawability of a part is to reduce the forming friction, or surface contact, between the sheet surface and the forming die. One of the most effective ways to reduce the surface contact is to utilize a lubricant during the forming process, a common practice in automotive stamping. The lubricant effectiveness is maximized when the sheet surface holds the lubricant in place, a process that a sheet pattern can greatly affect. Contact minimization results in reduced frictional resistance of the sheet to part formation, where greater friction may indicate that the sheet is sticking to the die, with the possibility of the sheet tearing rather than yielding and flowing along the die surface. Sheet-die contact minimization also results in a minimization of possible surface damage from adhesion and galling that might cause the part to be rejected.

While four main lubrication regimes have been defined (Figure 2), the majority of deep drawing forming operations take place in the mixed field lubrication regime where some asperity contact takes place and some hydrostatic lubrication takes place.[I7-I9] It should be noted that as understanding of this regime has progressed, some authors have taken into account the dynamic method of the process as well as deformation of the asperities and renamed hydrostatic as microhydrodynamic or micro-plastohydrodynamic (micro-PHD).[I8,I9] This latter terminology will be used below if material deformation is involved. The other lubrication regimes include boundary lubrication, where an extremely thin lubricant layer coats the surfaces and asperity deformation dominates, and

thin and thick film lubrication, where no asperity contact takes place and the lubricant completely separates the two surfaces.[I7]

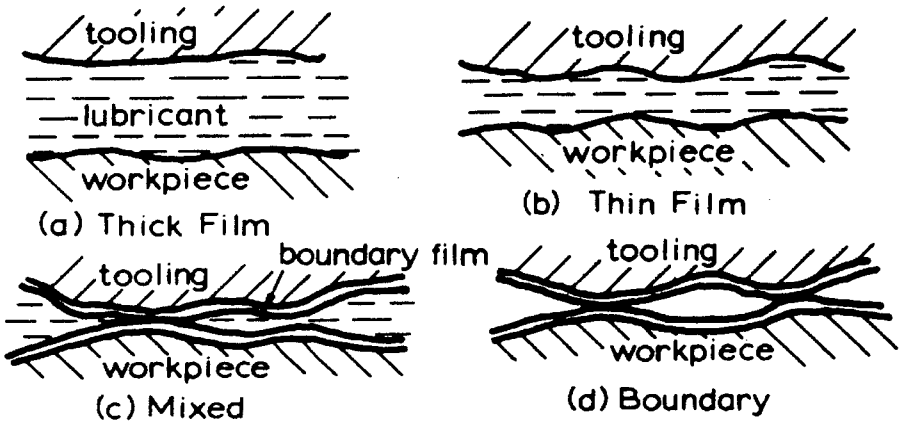

Figure 2 Friction regimes defined by Wilson (from I7)

While all these regimes are considered to be active during different parts of the deep drawing process, the interaction of the sheet surface with the die during the mixed field lubrication regime is critical to pattern design because it is during this forming regime that the pattern influence on lubricant retention is the greatest. In other words, to facilitate the protective action of the lubricant, the sheet surface needs to be able to physically hold the lubricant both to provide micro-PHD resistance and to continue to feed lubricant out to the higher, possible contact areas as the surface profile flattens. The work here, discussed in greater detail below, was designed to help clarify the dependence of forming friction on the lubricant retention capability of automotive aluminum alloys used in outer body panel applications in order to improve the formability of these alloys.

1.4 Automotive Alloy Pattern Use

Historically, the majority of sheet metal used by the automotive industry in outer body panels has consisted of various types of steel alloys.[I2,I10] Even today, with the push toward lighter automobiles, the majority of automotive sheet metal used is still steel.[I2,I10-I17] This has resulted in the majority of forming research in the area of automotive sheet alloys taking place on low carbon steels. The real push to increase understanding of the relationship between surface patterning and forming friction of steel sheet heightened when the automotive industry switched from bare steel to galvanized-zinc coated or zinc-alloy coated steel; the soft Zn-coated steel was found to be much more difficult to form than the bare steel used previously. Even the shot-blasted surface pattern in use at the time, better at retaining lubricant than the previously used mill finish, did not do enough to minimize the interaction between the soft zinc coating and the hard steel dies, resulting in sticking and galling and increased part rejection. Iterative pattern

advances have greatly improved the formability of these coated alloy sheets, and investigation into surface pattern effects on these sheets is still ongoing.

With the increasing use of automotive aluminum sheet in outer autobody panel applications, many of the problems encountered with the changeover from bare steel to Zn-coated steel sheet appear to be repeating themselves with aluminum. The vast majority of automotive aluminum sheet currently in use is patterned with the highly directional mill finish. This has the result that the surface of the sheet may not adequately retain enough lubricant in certain forming directions to prevent adhesion between the aluminum and the die. This is as critical for aluminum as it is for Zn-coated steel, as aluminum is highly adhesive and tends to gall readily.[I18-I22] Unfortunately automotive aluminum alloy sheet is generally not patterned for economic reasons. Any patterning of the sheet results in greater cost, and therefore a lower capability of being cost-competitive with patterned Zn-coated steel sheet. While elongation and anisotropy forming issues currently necessitate a less complex outer body panel design for the vast majority of Al alloys, the incentive to increase Al alloy outer body panel use is growing. Increasing use of Al alloys will necessitate adapting the alloys to the more complex parts currently made out of steel alloys. Consequently both alloy design and patterning of the Al alloy sheet surfaces to improve formability are becoming of greater concern.

1.5 Surface Definition and Pattern Design

A surface may be defined in a number of ways, including pattern shape and directionality, roughness averages, peak to valley height, and the wavelengths that actually make up the surface. Optical characterization is most commonly used to determine shape and directionality while surface profilometry tends to be used to quantify roughness parameters. Both two and three dimensional surface profilometry techniques have been used more frequently in recent years to determine the wavelengths that make up the surface by performing Fourier analysis. A Fourier transformation takes the profilometry data and breaks it down into the contribution, or power, of each wavelength that exists on the profiled surface. Different perceptions of what wavelengths constitute roughness exist for different surfaces. For example, glass surfaces would consider roughness to be in the nanometer range and waviness in the tens of microns range. For the macroscopically patterned surfaces considered here waviness is considered to consist of wavelengths greater than 800 μm (0.031 in), roughness covers the wavelength range from 800 μm (0.031 in) down to 20 μm (787 μin), and microroughness includes wavelengths below 20 μm (787 μin). Results based on wavelength analyses will be discussed below.

In an approach different from wavelength analysis, it has been put forth that the best surface topography for containing the lubricant consists of small surface cavities.[I8,I9,I23,I24] Research on isolated microcavities 100 μm (3937 μin) in diameter and between 10 μm (394 μin) and 20 μm (787 μin) deep that were introduced into a sheet surface demonstrated roughly a magnitude drop in strip drawing friction versus a normal mill finish sheet pattern.[I23] Prior to this isolated microcavity work, one investigation into Lasertex patterning made a recommendation of 250 μm (9842 μin) spacing and Ra > 1.5 μm (59 μin) for 200 μm (7874 μin) diameter cavities, in order to maintain indentation isolation.[I24] In order to increase knowledge in this area the discrete patterning tested here, discussed in greater detail below, was designed to help solidify recommendations for future pattern designs.

1.6 Formability versus Paintability

In addition to formability, patterning affects the paintability, or final painted appearance, of automobiles. To form a surface, the common belief is the rougher the surface the better. To obtain a smooth painted surface the opposite is thought to be true, with mirror-finish being the desired starting state. This has the result that the press shop that forms the parts and the paint shop which paints the formed parts desire sheet patterns that are in direct conflict with one another. Thus in designing a pattern for formability, the design must be constrained by the desire to achieve good paintability. Research focusing on the paintability of sheet surfaces has indicated that, for certain paint systems, shorter surface feature wavelengths may be painted over and not visible to the naked eye while longer wavelengths are visible through the painted surface.[I24-I27] Recent work has indicated that wavelengths under 500 μm (0.020 in) have a greater influence on reducing forming friction than wavelengths over 500 μm (0.020 in).[I28] These shorter wavelength features are believed to be small cavities on top of asperities that provide micro-PHD resistance during forming. It appears, therefore, that controlling the imprinted wavelengths on sheet surfaces can allow a sheet to have both acceptable forming and painting properties, removing the conflict between formability and paintability and clarifying the constraint on the surface design.

In addition to particular wavelength components of untested surfaces, surface roughening from the forming operation affects both the subsequent formability and paintability of these surfaces. Roughening results from both individual grain rotation during forming to accommodate strain in the material, and from rotation of groups of grains of similar crystallographic texture. The amount of roughening is known to increase with increasing grain size,[I9,I29] but some question has arisen as to which grain size parameter is the most important.[I30] As alloy composition and processing control the

microstructure of a material, they are major factors in determining the post-forming surface roughness. The research performed here investigated post-test surface roughening of outer body panel aluminum alloys, and investigated the correlation with different grain size parameters.

1.7 Patterning and Roll Finish

Patterns are imprinted on automotive sheet metal by performing the final sheet rolling operations with patterned rolls, where the pattern on the roll is coined onto the surface of the sheet metal. The roll pattern is imparted to automotive steel alloys during the final two cold rolling operations. The first cold rolling operation imprints an initial pattern and reduces the as-received hot-rolled sheet thickness around 70%, the coil of steel is heat treated, then the final "skin pass" roll imprints the final pattern on top of the initial pattern and reduces the sheet thickness between 0.5% and 2%. The double imprinting operation is not used with aluminum alloys because of heat treating requirements. In order to maintain formability, no further work hardening takes place after the heat treatment, which occurs immediately after the final reduction. Thus the final cold rolling reduction as well as the pattern transfer takes place during the final rolling operation of aluminum alloys, which can reduce a sheet thickness up to 15%. In order to maintain acceptable pattern transfer, however, work has shown that reductions must be limited to less than 4%.[I31] In the present work an ideal pattern is considered to be one where perfect coining of the roll pattern onto the sheet takes place with no distortion, while a "real" pattern is that measured using profilometry of the sheet surface and includes the influences of smearing, sliding, and roll wear.

Some patterning techniques discussed briefly here are illustrated in Figure 3. As is evidenced by the advances in roll patterning technology discussed below, and by research into the transfer of the roll pattern to the sheet surface, the pattern itself has undergone evolution as the search persists for the sheet finish that will result in not only optimum forming properties, but also optimum painting properties.[I23-I37] Mill finish (MF), the oldest finish used, originated from the grinding of the rolls in the mill between rolling operations. The circumferential grinding marks on the roll, resulting from a grinding pad moving along the length of the roll as it rotates, imprint on the sheet as a series of longitudinal peaks and valleys. One of the first post-grinding patterns utilized was shot-peening, where the surface of the roll was bombarded with shot. The finer the shot used, the finer the crater pattern created on the roll surface. Many steel mills today have old, now unused, shot peening machines on site. Currently, after grinding in the mill most rolls are sent out to sub-contractors for electro-discharge texturing (EDT), a process in which a spark is used to blast away very small pieces of the roll surface. As this

technique is used with increasing frequency, the control over the process is improving, with finer patterns available today compared to those applied previously.[138]

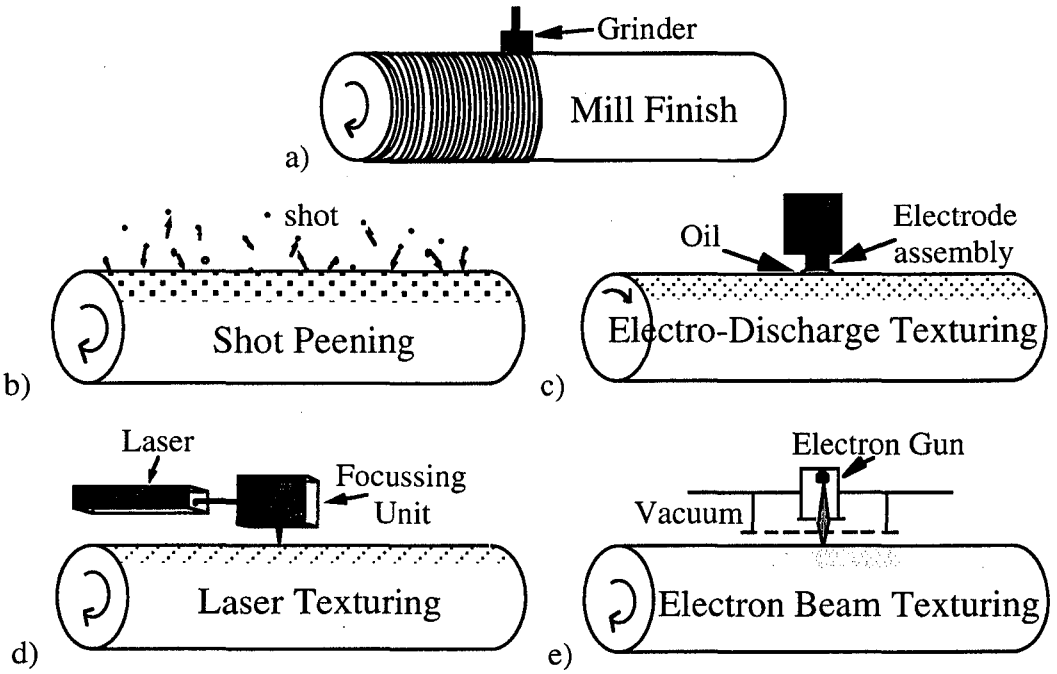

Figure 3 Illustration of different roll texturing processes: a) Mill Finish, b) Shot Peening, c) Electro-Discharge Texturing, d) Laser Texturing, and e) Electron Beam Texturing

Another, more discrete, after-grinding pattern imprinted on the roll is laser texturing (LT), where a laser is used to melt part of the roll, and either CO or O_2 gas is used to blow the molten metal out of the hole. Depending on the angle at which the gas is blown onto the surface, either a ring or semi-circular hill around the valley result. Electron Beam Texturing (EBT), the most recent technique of after-grinding roll-pattern application, has the finest resolution of any of the techniques in use today. In this expensive technique, originally developed for the printing industry, the entire roll is lowered into a vacuum chamber and patterned with an electron beam; the force of the beam blows the molten metal up onto the roll surface to create a ring around a valley. Both laser texturing and EBT impress regular, isolated valleys into the surface of the sheet metal, resulting in a well-defined lubricant carrying volume. It is important to realize that while the search for the optimum formable and paintable surface has resulted in large advances in roll patterning, much of the advancement has been through trial and error rather than through a systematic study of the patterning effects. The research discussed below was designed to contribute to the understanding of patterning effects in a systematic manner, allowing further, more informed, advances in pattern design.

1.8 Draw Bead Simulator Testing

One method of evaluating the effectiveness of different surface patterns is the draw bead simulator. The draw bead simulator (DBS) is a friction testing machine developed by Harmon Nine in the 1970s to assist in the evaluation of sheet metals and lubricants used for stamping operations.[I6] The DBS machine simulates the controlling action of the drawbead in the forming process. While a number of different machines exist that simulate various aspects of the forming process,[I39] the draw bead simulator has been found to be useful in indicating the deep drawing performance of both sheet metal alloys and different lubricants, and so has come into common usage in the forming industry as a quality control device.

The draw bead restraining force consists of both bending deformation and sliding friction. The two components are separated out by performing two tests of identical tooling geometry: a roller bead test for bending deformation only and a fixed bead test for combined bending deformation and sliding friction (Figure 4). The roller bead test is assumed to have negligible friction from the support rollers, and no sliding friction component, and the sliding friction generated during fixed bead testing is assumed to be Coulombic in nature. Thus, the bending deformation component of the roller bead test is directly subtracted from the bending deformation plus sliding friction components of the fixed bead test to determine an experimental number for sliding friction. The simple equation used for determining the coefficient of friction[I6], μ, is:

$$\mu = \frac{D_{fixed} - D_{roller}}{\pi C_{fixed}} \qquad \text{(Eqn. 1)}$$

where D is the drawing force for fixed and roller beads, π is the geometric contact angle of both sides of the sheet with the fixed beads, and C is the clamping force for the fixed bead test. This equation is accepted to be a rough and simple equation used for the purposes of ranking the friction response of materials and lubricants.

In certain situations, it is necessary to perform sliding friction tests on only one side of a sheet, rather than both, as is indicated above. The experiments designed here utilized this single-sided test because the patterns on the two sides of the discretely patterned sheet did not match. The forming friction equation above, used when performing double-sided tests, was modified[I40] to represent single-sided tests, where only one side of the sheet is tested with a fixed bead, by dividing the geometric contact angle by two:

$$\mu = \frac{2(D_{fixed} - D_{roller})}{\pi C_{fixed}} \qquad \text{(Eqn. 2)}$$

where D is the drawing force for fixed and roller beads, $\pi/2$ is the geometric contact angle of both sides of the sheet with the fixed bead, and C is the clamping force for the fixed bead test.

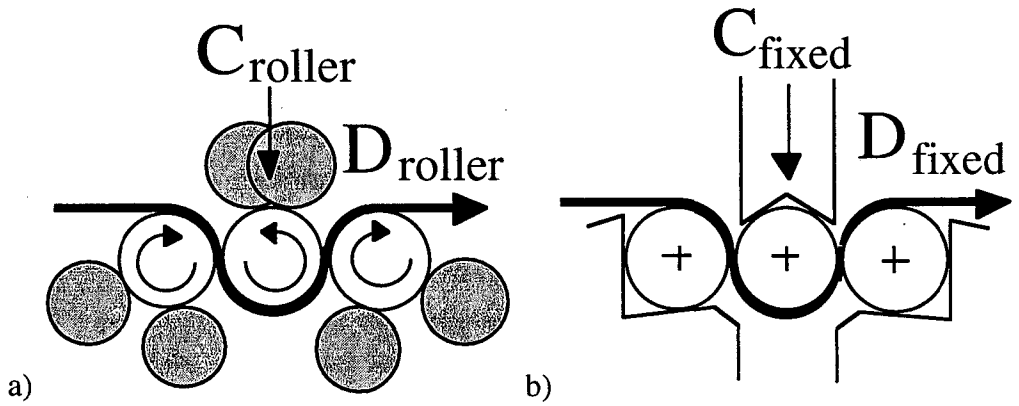

Figure 4 DBS Tooling Geometries: a) roller bead test, b) fixed bead test.

A number of authors have explored the validity of certain assumptions modelling the DBS test[I41-I51] while others have greatly facilitated understanding of the DBS test by exploring various physical machine and specimen parameters and their effect on the DBS test results.[I8,I52-I58] The test parameters investigated here, such as the validity of the single-sided test equation, are investigated and discussed in greater detail later.

1.9 Previous Work

Previous forming research, most of which was performed using both coated and uncoated steel alloys, tended to concentrate on searching for a relationship between tool and/or sheet metal surface parameters and sliding friction.[I59-I71] Some of this research was performed on discretely patterned Lasertex or EBT patterns, but the vast majority was performed on either the highly directional mill finish pattern or the more random EDT pattern. Of this research, no direct relationship has been found between at least sixteen simple two dimensional arithmetic parameters based on the surface profile, such as various ways of calculating surface roughness, and the values of sliding friction measured. One of the trends that has been noted is that greater surface roughnesses lower the friction. While exceptions to this trend have been noted,[I11] this general relationship is considered insufficient to characterize sheet surfaces, as it characterizes only the amplitude and not the wavelength or wave shape of the roughness profile.[I19]

One researcher used a hybrid parameter of asperity spacing and height combined with a surface roughness parameter to calculate the mean free volume for Zn-coated steel sheet.[I71] He found a linearly inverse relationship between this volume parameter and forming friction, where the slope was dependent on the crystallographic texture

differences of the Zn coatings. Another researcher discovered a more reliable correlation between forming friction and a particular regime of the Fourier power spectrum for Zn-coated sheet steel alloys patterned with EDT rolls.[I28,I68] The indication of this research was that wavelength contributions under 500 μm (0.020 in) had a greater effect on reducing forming friction than wavelengths over 500 μm (0.020 in). It is not as likely that the same relationship would exist for discretely patterned surfaces, however, because of their deterministic nature. An example of this would be infinitely deep discrete patterns less than 500 μm (0.020 in) in diameter and spaced under 500 μm (0.020 in) apart, adding tremendously to the wavelength contribution, but not reducing the forming friction any more than some critical, shallower depth.

It was this lack of information on the dependence of forming friction on discrete patterns that motivated the current research discussed below. The work here was performed with the goal of determining such a relationship and forming a constitutive equation based on this relationship that may be used in the future to guide pattern design.

1.10 Current Work

Increasing interest in the use of automotive aluminum alloys for outer body panel applications stems from congressional mandates to increase automotive fuel efficiency. These alloys are, however, less formable than steel alloys used in the same applications because of a combination of lower uniform elongation and anisotropic properties based on crystallographic texture. One of the ways to help maximize the formability of these alloys and make them more usable in complex parts, as opposed to the relatively simple parts they are used in now, is to design a surface that holds lubricant in such a way that it minimizes the contact, and thus the forming friction, between the sheet surface and the die forming the part. In the automotive industry one method used to assess the formability of different alloys, lubricants and patterns is DBS friction testing. Relating these and other formability results to quantifiable surface parameters has, however, been difficult. Furthermore, while excellent overviews of all aspects of the automotive forming of aluminum alloys exist,[I72-I76] a thorough understanding of the relationship between pattern parameters and forming friction in these alloys is still incomplete. The work here was conducted to fill this knowledge gap by using experimentation specifically designed to find the dependence of forming friction on discretely patterned surfaces.

In order to determine a constitutive relationship between discrete patterns and forming friction, three automotive aluminum alloys used in outer body panel applications were rolled on EBT patterned rolls that contained eight different patterns across each roll. Two of the alloys were rolled with two different eight-patterned rolls, and the third was rolled with two matching eight-patterned rolls. For comparison, MF patterned sheet split-

ingot processed from the same material was obtained for the first two alloys, and EDT patterned sheet split-ingot processed from one of the first two alloys was also obtained; EDT patterned sheet split-ingot processed from the second alloy was unavailable, as were MF and EDT patterned sheet split-ingot processed from the third alloy. A DBS test machine was fabricated to perform forming friction tests on all surface patterns. Validity of the data from this new test machine were of possible concern, so comparative MF and EDT tests were performed on a machine elsewhere that has been involved in a series of round robin DBS tests.[155] Tensile tests and roller bead tests were used to determine material properties, and to help assess the effect of material strength on the forming friction of these alloys. Single-sided DBS tests were performed on all EBT patterns while both single- and double-sided DBS tests were performed on MF and EDT patterns to check the assumption that the contact area of the sheet surface with the fixed bead during the single-sided sliding friction test was exactly half that of the double-sided test. All patterns were three dimensionally profiled both before and after DBS testing. The EBT pattern profilometry data was used to calculate the pre-DBS test pattern lubricant carrying capacity, both volume and area, of each pattern for each alloy. Post-test profilometry data was used to determine a minimum critical discrete pattern depth and the degree of surface roughening. The MF and EDT pre-test pattern profilometry data was used to assess the directional wavelength contributions of the respective patterns, and to determine if the 500 μm wavelength association with forming friction seen with Zn-coated sheet steel applied to these aluminum alloys. Finally, a constitutive equation for use in discrete pattern design was derived from the forming friction dependence on pattern volume.

2. EXPERIMENTAL PROCEDURE

2.1 Draw Bead Simulator Test Machine

A draw bead simulator was designed and constructed utilizing a tension/ compression servo-hydraulically driven load frame already in existence.[E1] Specific details of the design and construction of this machine are given in Appendix A. The draw bead simulator tooling consisted of two sets of dies, with a male and female fixed bead die set and a male and female roller bead die set. Figure 5 shows a photograph of the overall test setup, while Figure 6 shows a top view of the grips and drawing assembly and Figure 7 shows a rear view of the fixed bead dies with a specimen inserted before the top die is lowered into place. The die beads consisted of 9.525 mm (0.375 in) diameter D2 tool steel rods hardened to HRC 62. The drawing force for the test, measured using a load cell behind the specimen grips, was provided by a screwdrive driven by a computer controlled servomotor. The clamping force, provided by the computer controlled servo-hydraulic test machine, was measured using four button load cells inserted directly under the top die. Specimen location and test velocity were measured using a linear motion transducer, while bead depth was measured using a linear voltage differential transducer (LVDT) attached to the load frame pull rod and calibrated for bead position. Load cell and LVDT calibrations were performed before the strain gauge setup tests, described in Appendix A, and again before the load cell setup tests.

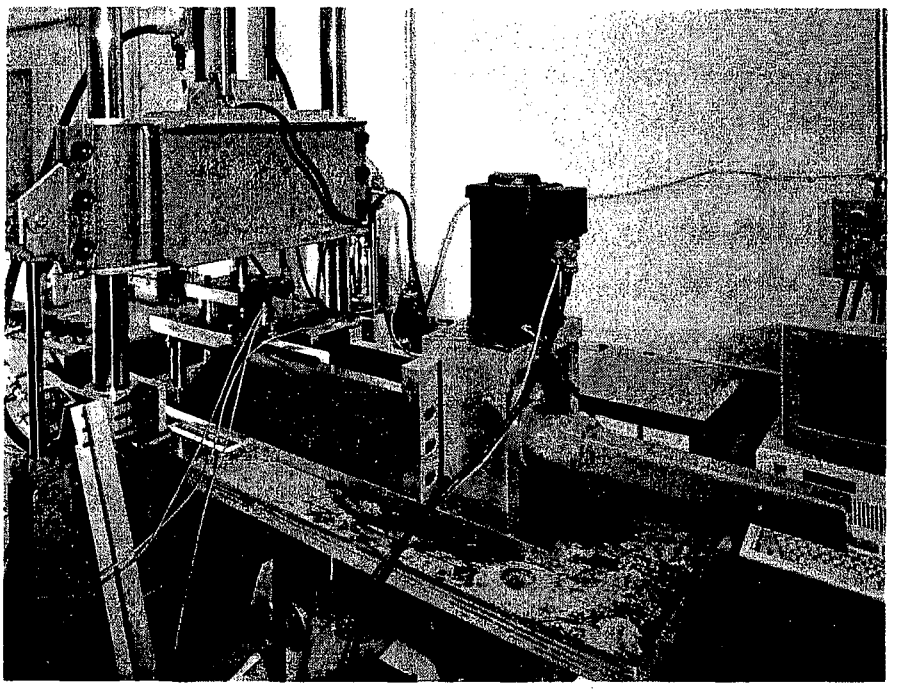

Figure 5 Front View of DBS test machine.

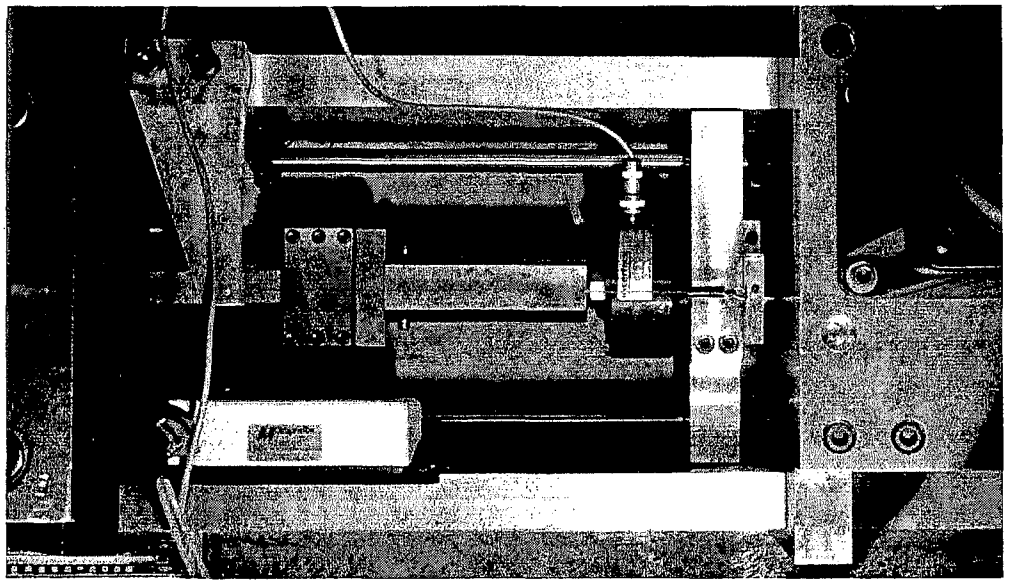

Figure 6 Top view of DBS test setup showing grips and pulling assembly.

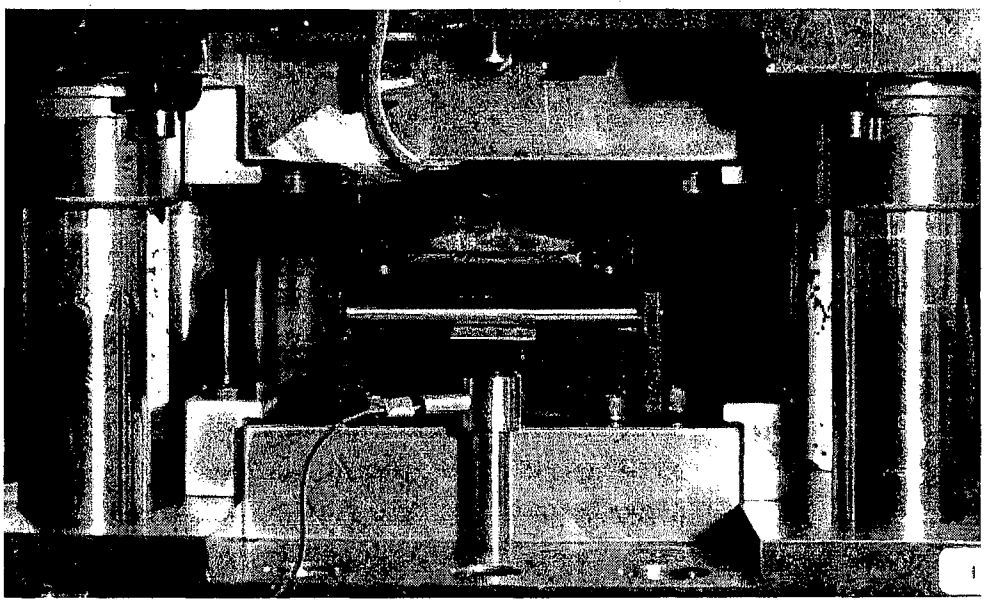

Figure 7 Rear view of DBS test setup showing fixed bead setup (before insertion) with specimen; the guide rollers shown keep the specimen level.

2.2 Test Material

Three different automotive aluminum alloys used in outer body panel applications were obtained.[E2] These alloys, imprinted with a variety of surface finishes (Table 1), were obtained in the naturally aged condition used for part forming. EBT sheets consisted of eight different patterns across each sheet side (Figure 8). AA2008 and AA6009 sheets, rolled with two different eight-patterned rolls, contained sixteen different single-sided patterns. AA6111 sheets, rolled with matching eight-patterned rolls,

contained eight different double-sided patterns. EBT patterns between the different alloys were nominally the same size and distribution, with different patterns having different depths as well as different ring sizes and distributions. The sixteen different EBT patterns were used in this study to determine the dependence of forming friction on discrete pattern volume. Pattern information from the sheet surfaces is quantified and discussed. MF patterned AA2008 and AA6009 sheets were used along with an EDT patterned AA2008 sheet to compare the more commonly used patterning techniques to EBT. Split-ingot processed MF and EDT sheets from the remaining alloys were not available. The AA2008 and AA6009 sheets were 1.09 mm (0.043 in) thick, while the AA6111 sheets were 0.914 mm (0.036 in) thick. The appearance of the EBT patterns on the 6111 sheets, resulting from a greater final thickness reduction, is compared to those on the 2008 and 6009 sheets. The effect of roll wear on the pattern is also discussed.

Alloy	Surface Finishes
2008-T4	MF, EDT, 2 sheets (.1 and .2) of 16 different EBT topographies, 8 per sheet side
6009-T4	MF, 1 sheet of 16 different EBT topographies, 8 per sheet side
6111-T4	2 sheets (.1 and .2) of 8 EBT topographies, matching on both sheet sides

Table 1 Number and Type of Alloy Surface Finishes Available

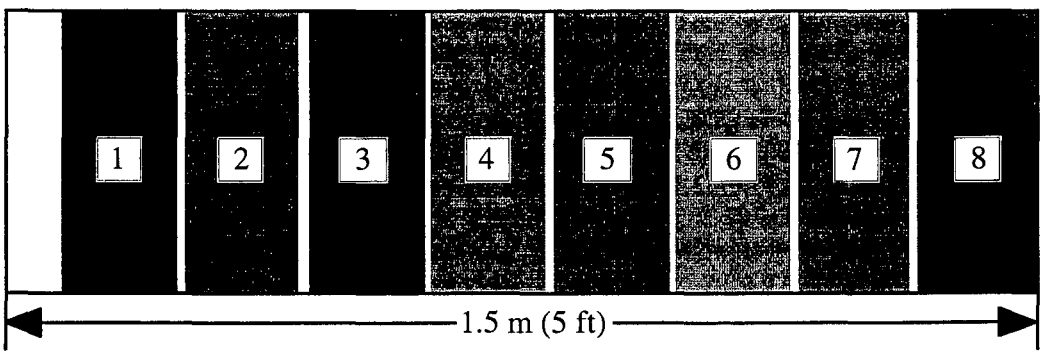

Figure 8 Schematic showing patterning across sheet surfaces.

2.3 Material Characterization

The microstructure of each alloy sheet was determined by mounting specimens from each alloy type in three perpendicular directions, i.e., in the plane of the rolling direction, perpendicular to the rolling plane along the rolling direction, and perpendicular to the rolling plane transverse to the rolling direction. Specimens were polished to 0.05 μm (2 μin) and etched with Keller's Etch (1 ml HF, 1.5 ml HCl, 2.5 ml HNO_3, 95 ml distilled H_2O) to reveal grain boundaries. Grain size and aspect ratio differences between the different alloys are quantified and related to post-DBS test surface roughening.

Each alloy used in this study was split-ingot cast, i.e., the initial cast ingot was split before reducing the ingot thickness down to sheet under nominally identical conditions

until the combination final reduction and patterning roll. As a consequence, no significant compositional or mechanical property differences were expected to exist between the different sheets within an alloy type. These assumptions were both checked. The chemical composition of samples from each sheet type was determined using Wavelength Dispersive X-Ray (WDXRF) analysis for Cu and a Vacuum Emission Spectrograph for the rest of the elements; two readings were taken from each sample and averaged.[E3] Mechanical property differences were checked by performing tensile tests and roller bead, or "frictionless," DBS tests. Tensile specimens were polished to 600 grit before testing to remove surface patterning and notch effects. A schematic of the tensile specimen used here is shown in Figure 9. All tests were performed on a computer controlled servo-hydraulic tensile test machine at room temperature at a strain rate of 10^{-3}. Elongation was measured using a 25.4 mm (1 inch) gage length 50% extensometer calibrated before each test session. Frictionless DBS tests were performed during the course of normal DBS friction testing of each alloy pattern set.

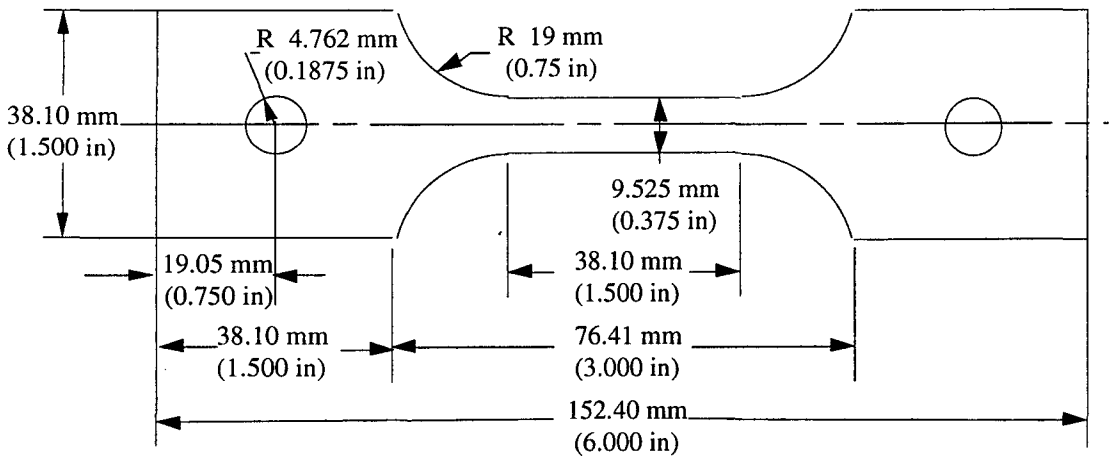

Figure 9 Schematic of tensile test specimen.

2.4 Pattern Characterization

2.4.1 Characterization Methods

All patterns were characterized using optical microscopy to determine feature size and orientation. Three dimensional profiling was performed on representative specimens of all surfaces both pre- and post-DBS testing using a laser profilometer with a 1 μm (39 μin) spot size both before and after DBS testing to enable the calculation of pattern volume, or lubricant carrying capacity.[E4] A representative 1.0 mm x 1.0 mm (0.039 in sq.) square area of each surface was scanned at an x and y resolution of 2.5 μm (39.4 μin), and a z resolution of < 0.1 μm (3.9 μin). For all patterns this area was assumed to be representative of the entire sheet surface.

All flat specimens were best fit planar leveled because the sheet specimens did not lie perfectly flat on the laser profilometer's travel table. Leveling occurred by subtracting a plane defined by regression lines calculated in the x and y directions of the surface. All tested specimens, curved in the test direction from the testing process, were planar leveled then polynomially leveled to the second degree in the test direction. Polynomial leveling subtracted a curved plane fitted to the mean of the surface curvature. Some tested specimens were also polynomially leveled to the second degree transverse to the test direction for comparison. Bearing area curves were calculated for all surfaces, and pre-test pattern differences as well as pre- and post-test comparisons are performed. Two dimensional wavelength characterization using FFT power spectra was performed from the profilometry data for all specimen types to compare pre- and post-DBS test surfaces.

2.4.2 Pattern Lubricant Carrying Capacities

The ideal EBT pattern lubricant carrying capacity, where perfect coining of the perfect roll pattern onto the sheet surface was assumed, was calculated from information about ring size and spacing on the rolls.[E5] The volumetric calculation (Eqn. 3) used the theorem of Pappus and the area of a parabolic section to calculate the volume of a circular ring with a parabolic cross-section assuming perfect rings and perfect coining.[E6] The theorem of Pappus was chosen because it was the simplest way found to calculate the area of a torus, or circular imprint with a particular cross section. It defines the volume for a given plane section of area A rotated about an axis in the plane. For a semicircular revolution the volume is $V = As$ where s is the length of the circular arc traced by the area's center of gravity. For a complete revolution the volume is $V = 2\pi rA$. Based on the actual surface profiles, the area of a parabolic section was chosen as the cross section of the imprint rather than a perfect half-circle. Here V represents the ring volume, r represents the radius to the center of the ring rim, A represents the cross-sectional area, h represents the ring depth, and l represents the parabola width (Figure 10).

$$V = 2\pi rA = 2\pi r(\frac{2}{3}hl) = \frac{4}{3}\pi rhl \qquad \text{(Eqn. 3)}$$

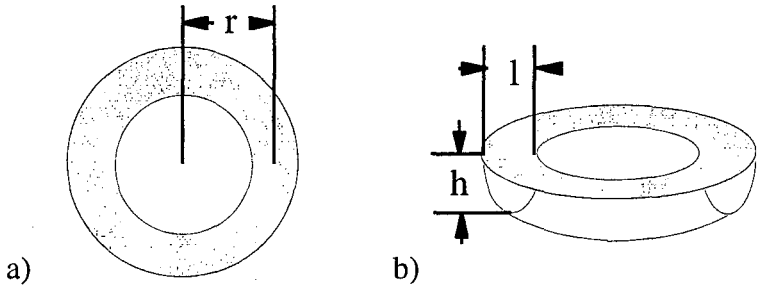

Figure 10 Ideal volume calculation parameters for V= $4/3\pi rhl$; r is the distance to the rim center, l is the rim width and h is the ring depth. (from E6)

The real EBT pattern lubricant carrying capacity was calculated from the laser profilometry data. Each profilometry data point was considered to reside in a square 2.5 μm (98 μin) on a side. Pattern volume was obtained by subtracting imprinted surface values from the "unimprinted" sheet surface height. These individual height values were summed, and the total was multiplied by 6.25 μm^2 (9688 μin^2) to give the pattern volume. Pattern area was obtained by calculating the number of points below the MF shelf value and multiplying by 6.25 μm^2 (9688 μin^2). The shelf value used in these calculations was the average value of the surface with only a MF pattern, i.e., the height of the surface below which all EBT pattern volume was assumed to exist. This shelf value was derived using a histogram representing all height values from a given surface (Figure 11). For larger, deeper EBT patterns, the value was taken as the average of the peak representing the MF surface, which resided above the peak representing the EBT pattern imprint. For smaller, shallower EBT patterns where there was only one peak the value was taken as the average value of that peak. This may have resulted in an underestimation of the pattern volume and area of those surfaces. Sheet pattern volumes are compared to the ideal roll pattern volumes, and both real and ideal volumes and real areas are considered in a constitutive relationship to the DBS forming friction of those patterns.

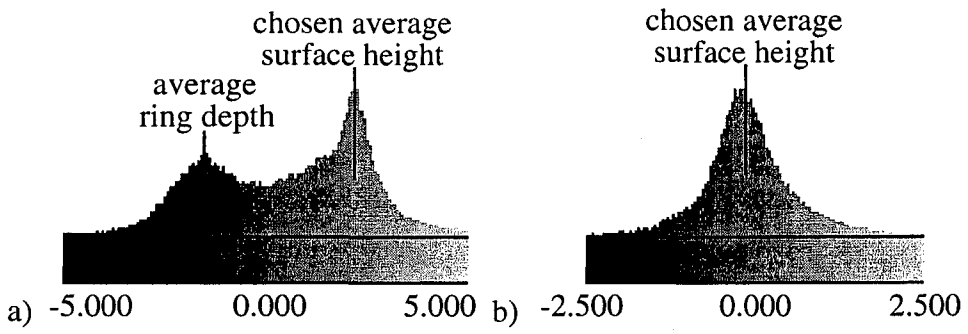

Figure 11 Histogram of surface heights a) for patterns >2 μm in depth and b) for patterns <2 μm in depth.

2.4.3 Post-Test Pattern Appearance

Post-DBS test surface roughening of the different patterns is compared to pre-DBS test surface appearances, and the influence of pattern depth on retention of a pattern after testing is discussed. Post-DBS test surface roughening between similar patterns of the different alloys is compared, and differences are discussed in terms of possible influence on further forming friction.

2.5 Draw Bead Simulator Tests

2.5.1 Draw Bead Simulator Test Parameters

All DBS test specimens within a topography were cut from a single alloy sheet using a shear with stops set for high accuracy of specimen width. This accuracy is important, as specimen width variations have been shown to affect test results.[E7] A set of seven or eight specimens in a row were sheared, with the outer pieces being used for the roller bead tests and the inner for the fixed or mixed bead tests. This specimen configuration was used to subtract out any local variations in sheet properties, as thickness and strength variations both across and along a sheet have been shown to influence test results.[E7] Specimens were deburred on all edges using a fine file and Buehler 600 grit SiC paper to eliminate the possibility of specimen burrs damaging test beads and influencing test results.

DBS test specimens were drawn a distance of 152 mm (6 in) at a velocity of 85 mm/sec (200 in/min) using a 23 cm (9 in) long specimen. Mixed bead, single-sided, tests utilized a male fixed bead and female roller beads while fixed bead, double-sided, tests used both male and female fixed beads, and roller bead tests used both male and female roller beads (Figure 12). All strain gauge setup tests were performed with the top, male, die tightened to approximately 34 N-m (300 in-lb). All load cell setup tests were performed with the top die preloaded upon die insertion to between 667 N (150 lb) and 725 N (163 lb), with the load distributed evenly between the front and the back of the die, and the bottom die tightened to approximately 34 N-m (300 in-lb). To minimize lubricant variation, all tests were performed using lubricant from a single batch of Parker+Amchem MP-404 prelube.[E8] This lubricant has a viscosity of 72.8 mPa-s (72.8 Centipoise) at 38°C (100°F).[E9] All specimens were cleaned with acetone and a clean shop wipe before applying lubricant. Excess lubricant was applied to all specimens, and to the fixed beads before the first fixed or mixed bead test in a test set, so that lubricant film thickness was established by the process.[E10] All roller bead tests were run without lubricant for cleanliness, based on the assumption of negligible friction. The fixed beads were ground in the longitudinal direction using 600 grit SiC paper between test sets.[E11] Each test set consisted of four or five mixed or fixed bead tests and two or three roller bead tests (Table 2); the number of tests depended on the number of specimens cut and on the width of the pattern on the sheet. A direction set consisted of all surfaces for one sheet side and one direction of an alloy lot. Calibration specimens were run before and after each direction set to check and correct for any drift in output from machine or environmental effects. Both individual test values and average test set values were used in Eqns. 1 and 2 to calculate forming friction.

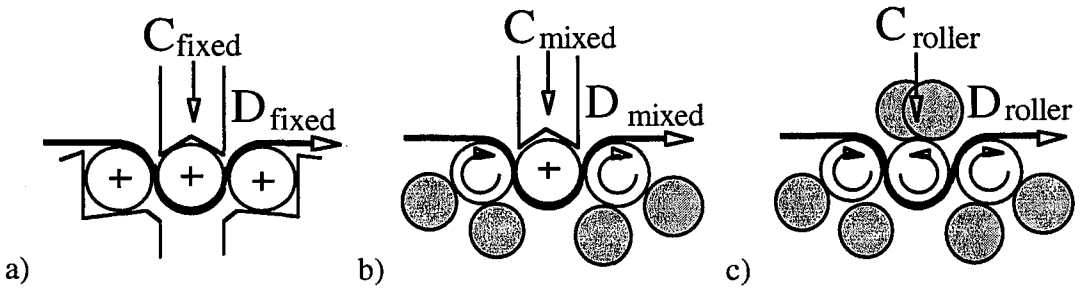

Figure 12 Schematic of a) fixed, b) mixed, and c) roller bead test setups.

	# Sheet Sides Tested	# Patterns Tested	# Directions Tested
Test Set	one	one	one
Direction Set	one	eight	one

Table 2 Description of DBS test set and direction set terminology.

2.5.2 Draw Bead Simulator Machine and Specimen Validation

As with any new machine, there was some concern over the validity of the results from the fabricated Draw Bead Simulator. In order to ensure confidence in the test results, a number of measures were taken to explore both the machine parameters and the specimen parameters. First, die deflection was measured to ensure the test strip was not being pinched during drawing. Second, results between the gauge and load cell test setups were compared to determine if the overall trends differed between the two setups, which would indicate something fundamentally wrong with the machine. Third, specimens were tested on another DBS machine and compared to the local tests. Fourth, bluing tests were performed to determine actual contact angles of the sheet with the top and bottom dies. This was done to determine the validity of the assumption stated above that the geometric angle of contact in the normal, or double-sided, DBS friction equation may simply be halved for the single-sided test. Fifth, single-sided and double-sided tests were performed on both machines (from #3) to further check this assumption. Sixth, these comparison tests were performed on specimens of two different widths to confirm the validity of using a narrower specimen for the EBT patterned material. Last, the estimated error for all tests was calculated and compared to actual test scatter.

2.5.2 #1 Die Deflection Measurements

To ensure that the specimens were not being pinched during testing between the male bead and either the front or the rear female bead, deflection of the fixed bead dies was measured using both 25.4 mm (1.00 in) and 50.8 mm (2.00 in) bare steel 0.81 mm (0.032 in) thick specimens. Die deflections were measured with a shim gauge. The specimens were tested without lubricant in order to measure maximum possible die deflections.

2.5.2 #2 Gauge Setup versus Load Cell Setup Tests

MF and EDT patterned material was tested single-sided using both test setups on the fabricated DBS machine. EBT single-sided tests and roller bead tests using the strain gauge setup with a mistakenly barely tightened female roller bead die were repeated using the load cell setup described above. All EBT tests were performed on specimens 25.4 mm (1.00 in) wide in order to obtain enough specimens from each pattern on a sheet. These results are compared within and between alloy types to determine if there was a change in pattern-based trends between the two test setups.

2.5.2 #3 Local versus Denver DBS Tests

DBS tests were performed locally on the fabricated machine and on a DBS test machine at the University of Colorado, Denver, that has been used in round robin testing.[E12] The results of the tests (Table 3) are compared and considered in validation of the data from the fabricated machine.

Location	Pattern	Test Type	Specimen Width	Machine Setup
Denver	MF, EDT	Mixed	25.4 mm (1 in)	Load Cell
Denver	MF, EDT	Fixed	25.4 mm (1 in)	Load Cell
Denver	MF, EDT	Mixed	50.8 mm (2 in)	Load Cell
Denver	MF, EDT	Fixed	50.8 mm (2 in)	Load Cell
Local	MF, EDT (Denver tested)	Mixed	25.4 mm (1 in)	Strain Gauge
Local	MF, EDT (Denver tested)	Fixed	25.4 mm (1 in)	Strain Gauge
Local	MF, EDT (Denver tested)	Mixed	50.8 mm (2 in)	Strain Gauge
Local	MF, EDT (Denver tested)	Fixed	50.8 mm (2 in)	Strain Gauge
Local	MF, EDT	Mixed	25.4 mm (1 in)	Strain Gauge
Local	MF, EDT	Fixed	25.4 mm (1 in)	Strain Gauge
Local	MF, EDT	Mixed	25.4 mm (1 in)	Load Cells
Local	EBT	Mixed	25.4 mm (1 in)	Strain Gauge
Local	EBT	Mixed	25.4 mm (1 in)	Load Cells

Table 3 DBS test matrix

2.5.2 #4 Specimen-Bead Contact Measurement

Double-sided DBS tests were performed with bluing grease applied to both the test sheet and the bead surfaces before testing. Tests were performed using both 25.4 mm (1.00 in) and 50.8 mm (2.00 in) wide 0.81 mm (0.032 in) thick bare steel specimens to investigate the possibility of the sheet skipping while travelling over the beads and to measure the contact angle of the sheet with the beads. The angle of contact was measured to check the validity of the assumption stated earlier (Section 2.8) that the geometric contact angle in the DBS forming friction equation for double sided tests (Eqn. 1) could simply be halved for the single sided tests (Eqn. 2).

2.5.2 #5 Single-Sided versus Double-Sided Tests

Different specimen configurations were tested both on the fabricated machine and in Denver to explore the other specimen choices made here. Single-sided and double-sided DBS tests were performed using MF and EDT specimens to further investigate the validity of the assumption of halving the geometric contact angle of the sheet with the beads when calculating single-sided versus double-sided forming friction. This was a possible concern, for the majority of EBT testing was expected to be performed single-sided because of the different patterns on the two sheet sides.

The Denver test machine setup required 46 cm (18 in) long specimens, the last 152 mm (6 in) of which were drawn through the test beads. The tested specimens were cut down to 23 cm (9 in), and the half not deformed by the Denver DBS test beads was tested on the fabricated DBS machine using the strain gauge setup with the top and bottom dies tightened to approximately 34 N-m (300 in-lb). Single-sided, double-sided and roller bead tests were repeated using the same strain gauge setup on 25.4 mm (1.00 in) wide specimens cut from the alloy sheets to check if there was an effect from previous straining on the non-DBS deformed specimens cut from the tested Denver samples. Single-sided 25.4 mm (1.00 in) specimen width tests were repeated on previously untested material using the load cell setup to check behavior between the two setups.

2.5.2 #6 Specimen Width Comparison

Two different specimen widths, 25.4 mm (1.00 in) and 50.8 mm (2.00 in), were tested on both the fabricated machine and the Denver machine and the results compared. Specimen width was of concern because 25.4 mm (1.00 in) wide specimens had to be used for EBT tests, rather than the generally used 50.8 mm (2.00 in) wide specimens, because of material limitations.

2.5.2 #7 Estimated Error

Estimated error was calculated for all tests to check against the actual test scatter. DBS forming friction for the double sided tests was calculated using Eqn. 1 while Eqn. 2 was used for the single sided tests. Estimated error was calculated for all machines using Eqns. 4, 5, and 6, below. Eqn. 4 represents the general error propagation equation, modified for DBS forming friction. Eqns. 5 and 6 represent the derivations for fixed and mixed bead DBS friction Eqns. 1 and 2, respectively, where D_f represents the drawing load for the fixed or mixed bead test, D_r represents the drawing load for the roller bead test, and C_f represents the clamping load for the fixed or mixed bead test.

$$\delta\mu = \sqrt{\left(\frac{\partial\mu}{\partial D_f}\right)^2 (\Delta D_f)^2 + \left(\frac{\partial\mu}{\partial D_r}\right)^2 (\Delta D_r)^2 + \left(\frac{\partial\mu}{\partial C_f}\right)^2 (\Delta C_f)^2} \qquad \text{Eqn. 4}$$

$$\delta\mu = \sqrt{\left(\frac{1}{\pi C_f}\right)^2 (\Delta D_f)^2 + \left(\frac{-1}{\pi C_f}\right)^2 (\Delta D_r)^2 + \left(\frac{-D_f + D_r}{\pi C_f{}^2}\right)^2 (\Delta C_f)^2} \qquad \text{Eqn. 5}$$

$$\delta\mu = \sqrt{\left(\frac{2}{\pi C_f}\right)^2 (\Delta D_f)^2 + \left(\frac{-2}{\pi C_f}\right)^2 (\Delta D_r)^2 + \left(\frac{-2D_f + 2D_r}{\pi C_f{}^2}\right)^2 (\Delta C_f)^2} \qquad \text{Eqn. 6}$$

Table 4 gives the values used in the estimated error equations for the tests performed at Denver and for both test setups used locally. All three variables for the Denver test setup for 25.4 mm (1.00 in) wide specimens were considered to be the estimated repeatability of the load cells used in the test setup, 9 N (2 lb). This same value of 9 N (2 lb) was used for the drawing load cell error for both the strain gauge and the load cell local test setups. For locally tested 25.4 mm (1.00 in) wide specimens tested on the strain gauge setup, the clamping delta value was considered to be the spread between the up and down slope of the calibration curve, or 110 N (25 lb). For load cell test setups, the clamping delta value was considered to be the same repeatable load cell error as the drawing error, 9 N (2 lb). Only single-sided 25.4 mm (1.00 in) specimen test estimated error was calculated for comparison across all pattern types, because both double-sided and 50.8 mm (2.00 in) test specimens were not DBS tested for all patterns. The differences in calculated error for the strain gauge setup and the load cell setup are discussed.

Location	Test Type	Specimen Width (mm)	ΔD_f (N)	ΔD_r (N)	ΔC_f (N)
Denver	Fixed Load Cell	25.4	9	9	9
Denver	Mixed Load Cell	25.4	9	9	9
Local	Fixed Strain Gauge	25.4	9	9	110
Local	Mixed Strain Gauge	25.4	9	9	110
Local	Mixed Load Cell	25.4	9	9	9

Table 4 Estimated Error Values for 25.4 mm (1.00 in) Wide Specimen DBS Tests Performed at Denver and Locally

2.5.3 Draw Bead Simulator Pattern Dependence Tests

The main point of this work is to determine pattern influence on forming friction. For MF and EDT patterns the results from the tests above (Sections 2.5.2 #2 through #4) were used as a baseline comparison for the EBT results (Section 2.5.2 #2). The EBT results were used to ascertain the influence of both the pattern lubricant carrying capacity and alloy strength on the forming friction of the material. Lubricant carrying capacity includes both the volume of lubricant held by the pattern and the area of lubricant contact with the dies.

3. RESULTS

The results from the tests and analyses performed are given below under the three main categories of material characterization, pattern characterization, and draw bead simulation tests. Material characterization covers alloy composition, tensile properties and frictionless forming properties while pattern characterization gives optical and profilometry results for the untested patterns. The draw bead simulation section includes information on the tests performed to validate both the fabricated DBS tester and the use of the single-sided test specimen, and covers the influence of the surface patterns on forming friction and the change in appearance of the friction tested specimens.

3.1 Material Characterization

3.1.1 Alloy Composition

Analyzed alloy compositions are shown in Table 5, validating the expectation that the split-ingot processing of the alloys did not result in appreciable compositional differences. The two sheets of EBT nominally identical within alloy type for AA2008 and AA6111 are labeled below as EBT.1 and EBT.2. All variations except the Cr content of specimen 2008 EBT.2 and the Mn content between the 6009 specimens are within the 5 to 10% variation expected from the analyses, and these differences may be normal for variation within a large ingot.

Alloy (surface)	Composition								
	Si	Fe	Cu	Mn	Mg	Cr	Zn	Ti	Al
2008 (MF)	0.61	0.18	0.93	0.07	0.38	0.01	0.01	0.01	rem
2008 (EDT)	0.62	0.18	0.94	0.07	0.39	0.01	0.01	0.01	rem
2008 (EBT.1)	0.62	0.18	0.99	0.08	0.41	0.01	0.03	0.01	rem
2008 (EBT.2)	0.64	0.19	0.98	0.06	0.42	0.003	0.01	0.01	rem
6009 (MF)	0.71	0.45	0.35	0.39	0.52	0.04	0.05	0.01	rem
6009 (EBT)	0.72	0.44	0.34	0.47	0.54	0.04	0.04	0.01	rem
6111 (EBT.1)	0.74	0.27	0.86	0.25	0.68	0.03	0.06	0.01	rem
6111 (EBT.2)	0.74	0.27	0.85	0.25	0.69	0.03	0.06	0.01	rem

Table 5 Measured Alloy Compositions of As-Received MF, EDT, and EBT Sheet (wt%)

Keeping in mind the fact that composition and processing control a material's microstructure and that same composition and resulting microstructure control a material's properties, some predictions may be made from these compositions as to the appearance and behavior of the respective alloy sheets. For AA2008, presuming identical processing conditions, the different sheet properties do not look like they will be appreciably different, as all the analyzed values are very close together. For AA6009, the much larger Fe and Mn content, compared to both AA2008 and AA6111, should

contribute to a significant increase in the number of inclusions which, in turn, should provide a greater number of grain nucleation sites and result in a finer grain size. These inclusions should be larger in both the 6009 and the 6111 alloys, as a higher Mn content combines with the Fe to create second phase intermetallic precipitates larger than those resulting if only Fe were present.[R1] The much lower Cu in the AA6009 sheets indicate lower strengths, compared to AA2008 and AA6111 sheets here, arising from a lower concentration of hardening GP zones and solute clusters.[R2] This lower concentration also indicates a lower precipitation-based bake hardening capability in this alloy. It will be interesting to see whether the higher strength predicted from the Hall-Petch relation for the smaller grain size expected of the AA6009 alloys compensates for the strength loss expected from the smaller amount of Cu in these sheets. For nominally identical processing conditions, it is not expected that the small difference between the Mn contents of the two different AA6009 sheets will generate a large difference in properties, as both amounts are very large and their effects should be similar. For the reasons listed above regarding Fe and Mn content in the AA6009 sheets, one would expect to see a larger number of inclusions in AA6111 than in AA2008 sheets, but not as many nor as large as those in AA6009. AA6111 also contains appreciable amounts of Cu, Mg and Si, resulting in two different hardening systems being active at the same time ($CuAl_2$, Mg_2Si, and $CuMgAl_2$). Even in the solid solution and solute cluster stage expected of the -T4 condition, this is likely to result in the highest strengths of all the sheets tested here, in addition to the best bake hardenability. The nominally identical compositions of the two AA6111 sheets lead to the expectation that the two sheet properties will also be nominally identical, presuming identical processing conditions. The Cr, Zn and Ti present in trace amounts in all sheets may contribute to grain refinement from pinning of the grain boundaries during initial ingot casting.[R3] The Zn may also contribute to suppressing stretcher strain marks, large areas of necking on the sheet surface that form during deep drawing and make a sheet surface unacceptable for outer body panel applications.[R3] The trace amounts are not otherwise expected to appreciably contribute to differences in either the grain structure or the mechanical properties of the alloys.

3.1.2 Alloy Grain Structure

All sheets consisted of pancake-shaped grains, larger in the rolling plane than through the thickness of the sheet, resulting from the rolling process. Representative micrographs are shown in Appendix C (Figures C1 through C3). The AA2008 sheets contained an equiaxed bimodal grain size distribution around 40 μm (1575 μin) and 80 μm (3150 μin), with an average grain size of 56 μm (2205 μin) for MF and EDT and 52 μm (2047 μin) for EBT.1 and EBT.2. Average grain thicknesses for the AA2008 sheets

were 23 μm (906 μin) for the MF sheet, 21 μm (827 μin) for EDT, 18 μm (709 μin) for EBT.1, and 25 μm (984 μin) for EBT.2. The AA6009 sheets contained a range of grain sizes, slightly elongated in the rolling direction, from 20 μm (787 μin) to 110 μm (4331 μin), with an average grain size of 43 μm (1693 μin) for the MF sheet and 40 μm (1575 μin) for the EBT sheet. Average grain thicknesses were 14 μm (551 μin) for the MF sheet and 15 μm (591 μin) for the EBT sheet. The AA6111 sheets also displayed a bimodal grain size distribution, slightly elongated in the rolling direction, around 40 μm (1575 μin) and 100 μm (3937 μin), with an average grain size of 60 μm (2362 μin), and thicknesses of 15 μm (591 μin) for both EBT.1 and EBT.2. Grain aspect ratios, given below in Table 6, reflect the grain size measurements given above. Inclusion content of the AA6009 sheets was twice that of the 2008 sheets and 50% greater than that of the AA6111 sheets. Inclusion size in the AA6009 sheets was five times that of the AA2008 sheets (an average diameter of 10 μm (394 μin) vs. 2 μm (79 μin)), while the AA6111 sheets displayed a mix of the small and large precipitates. The larger precipitates heavily decorated the grain boundaries in the alloys while the smaller precipitates mostly resided in the grain interiors.

Alloy	RP (l/w)	RP:Thickness (l/t)	RP:Thickness (w/t)
2008 MF	1.0	2.4	2.4
2008 EDT	1.0	2.6	2.6
2008 EBT.1	1.0	2.8	2.8
2008 EBT.2	1.0	2.1	2.1
6009 MF	1.1	3.2	3.0
6009 EBT	1.1	2.9	2.7
6111 EBT.1	1.1	4.1	3.7
6111 EBT.2	1.1	4.1	3.7

Table 6 Grain Aspect Ratios for AA2008, A6009, and AA6111 sheets, where RP is the rolling plane, l is the grain length, w is the grain width, and t is the grain thickness.

The smaller grain size for the AA6009 sheets and the greater inclusion content and size for the AA6111 and AA6009 sheets over the AA2008 sheets conformed to the predictions based on the alloys' compositions. The larger grain size of the 6111 sheets was not indicated, however, and results from the different final processing of these sheets with a greater rolling reduction, compared to AA2008 and AA6009 sheets, resulting in wider, thinner squashed grains.

3.1.3 Alloy Tensile Properties

Tensile tests were performed on all alloys for each pattern type to characterize the mechanical properties of each sheet. All specimens were polished both on the faces and on the sides to remove notch effects, with the exception of most of the AA6111

longitudinal specimens. A minimum of two tests were performed both parallel to and transverse to the rolling direction of each alloy and each sheet. Average engineering yield strengths, ultimate tensile strengths, and uniform elongations, including minimum and maximum test scatter values, are shown in Table 7 for the longitudinal (L) direction and in Table 8 for the transverse (T) direction.

Alloy	Yield (MPa)	min max (MPa)	UTS (MPa)	min max (MPa)	Uniform ε (%)	min max (%)	Total ε (%)	min max (%)
2008 MF-L	157	156 158	281	279 282	22.2	22.0 22.3	26.4	26.3 26.5
2008 EDT-L	156	153 157	278	273 282	21.2	19.2 24.2	25.8	25.2 27.9
2008 EBT.1-L	163	162 165	288	285 290	20.7	19.2 21.9	24.4	23.4 25.4
2008 EBT.2-L	167	166 168	289	288 290	19.2	18.3 20.2	23.9	23.3 24.5
6009 MF-L	161	159 163	276	276 277	19.5	18.9 20.0	26.6	26.3 26.8
6009 EBT-L	163	163 163	274	271 277	19.1	18.1 20.7	23.7	22.6 24.7
6111 EBT.1-L	204	198 213	334	326 342	23.5	21.7 26.7	27.9	26.4 30.4
6111 EBT.2-L	205	204 205	335	335 336	23.8	23.6 24.0	28.1	28.0 28.3

Table 7 Engineering yield, ultimate, and elongation values for the longitudinal direction of AA2008, AA6009, and AA6111 patterned sheet.

Alloy	Yield (MPa)	min max (MPa)	UTS (MPa)	min max (MPa)	Uniform ε (%)	min max (%)	Total ε (%)	min max (%)
2008 MF-T	142	142 145	267	267 268	24.6	24.0 25.1	34.1	33.7 34.5
2008 EDT-T	143	142 144	269	267 271	24.5	22.4 27.4	32.2	29.2 36.2
2008 EBT.1-T	148	147 148	273	272 274	25.4	25.2 25.5	30.4	29.8 30.9
2008 EBT.2-T	153	152 154	280	280 280	24.9	23.7 26.8	32.7	32.1 33.1
6009 MF-T	151	150 152	272	272 272	23.0	22.8 23.1	27.5	27.4 27.6
6009 EBT-T	149	148 150	264	263 266	20.7	20.2 21.5	25.1	24.5 26.1
6111 EBT.1-T	189	188 191	331	329 333	24.1	23.6 24.4	27.9	27.0 29.3
6111 EBT.2-T	186	185 186	330	330 330	23.1	22.6 23.7	28.1	27.5 28.6

Table 8 Engineering yield, ultimate, and elongation values for the transverse direction of AA2008, AA6009, and AA6111 patterned sheet.

As expected from the compositions of the sheets, AA2008 MF and EDT results were similar, but EBT YS and UTS values were slightly higher. This may be attributable to the fact that the grain sizes were slightly smaller in the EBT sheets than in the MF and EDT sheets. In addition, while the strengths and elongations of the different 2008 alloy sheets are within ten percent of each other, this difference is significant because it directly indicates frictionless roller bead test result differences, discussed later.

Also as expected from composition information, values for AA6009-L overlapped, but AA6009-T EBT UTS and elongation values were consistently lower than those for AA6009-T MF. The smaller grain size of the 6009 sheets appears to have compensated for the lower Cu content in this alloy, with the yield and ultimate strengths falling either within or very close to the range of the 2008 sheet values.

The 6111 sheets followed the compositional prediction of the highest strengths in both the longitudinal and the transverse directions. In addition to the minimum of two tests performed for AA6111 EBT.1-T and EBT.2 -L and -T directions, eighteen tests were performed on AA6111 EBT.1-L specimens unpolished on their patterned faces cut from nine locations across the width of the EBT.1 sheet to determine if patterning influenced the tensile properties. The nine locations included a test strip along one edge of the sheet, and specimens cut from each of the eight patterns across the sheet width. YS and UTS results showed a 3.5% increase near the sheet edges, compared to a 1% scatter in values for all interior tests. Rather than pattern influence, it is likely that the increase toward the sheet edges resulted from processing dynamics rather than from pattern influence, as no influence of pattern on the tensile properties was visible for all other tests. Other than the rise in both yield and ultimate tensile strengths toward the sheet edges (included in the averages and shown as the maximum test values, above), AA6111 tensile values overlapped.

3.1.4 Alloy Frictionless Forming Properties

Roller bead tests were performed to ascertain the frictionless forming characteristics of all alloys. It was necessary to correct for the thickness differences of the AA6111 sheet to allow direct comparison against the AA2008 and AA6009 roller bead drawing forces. This correction is based on the work of Yellup and Schey.[R4,R5] Yellup found that drawing stress varies linearly with sheet thickness and concluded, based on this, that drawing force varies with the square of the sheet thickness. Schey later demonstrated this power law dependence for a variety of steel alloys and for AA5052. Figure 13 plots all roller bead test results obtained here along with Schey's results for AA5052. The drawing load normalized by both the specimen width and the specimen UTS in N/mm^2 is plotted against the specimen thickness. The power law fit shown in Figure 13 acceptably

confirms the dependence of the roller bead drawing force on the square of the thickness for the materials tested here.

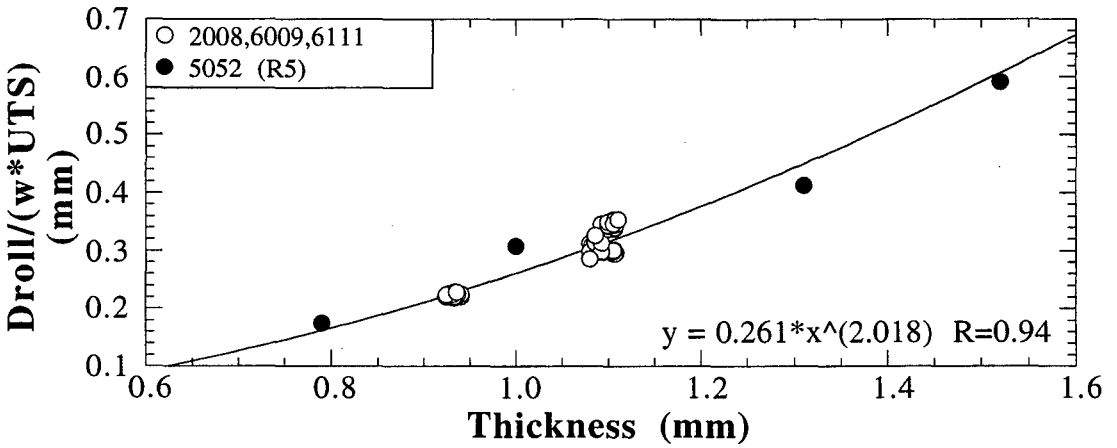

Figure 13 Roller bead drawing forces normalized by sheet thicknesses and ultimate tensile strengths plotted against thickness, after Schey (R5), showing the dependence of frictionless drawing forces on the sheet thickness.

Using this relationship, AA6111 roller bead test results were divided by the square of the AA6111 sheet thickness, 0.835 mm^2 (0.0013 in^2), and multiplied by the square of the AA2008 and AA6009 sheet thicknesses, 1.19 mm^2 (0.0018 in^2). The scaled drawing loads from this calculation were checked using the power law equation shown in Figure 13 using the UTS values shown in Tables 6 and 7. Values calculated from the power law equation showed excellent agreement with values calculated using the thickness-squared ratio. The thickness-corrected AA6111 roller bead drawing forces for the load cell setup are plotted in Figure 14 along with the AA2008 and AA6009 drawing forces, showing minimal variation across the sheets.

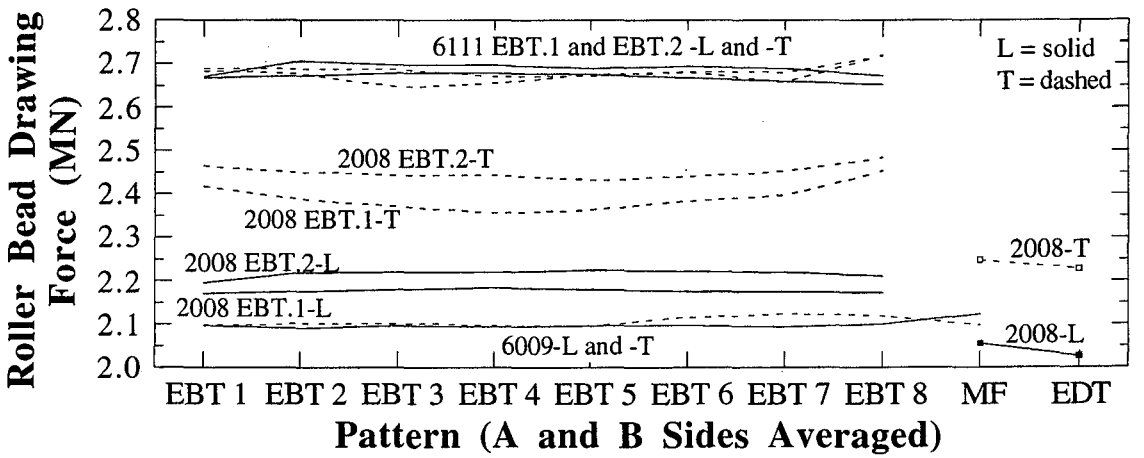

Figure 14 Plot of AA2008, AA6009, and AA6111 roller bead drawing forces across the EBT sheet width, and of AA2008 MF and EDT and AA6009 MF sheets; AA6111 forces have been corrected for the thickness difference. All tests performed within one pattern number for both A and B sides were averaged.

Both AA6111 and AA6009 show similar roller bead drawing loads in the longitudinal and transverse directions. All AA2008 specimens, however, show an increase of between 10% and 12% in roller bead drawing forces in the transverse direction compared to the longitudinal direction. The variation in directional drawing loads for the AA2008 sheets appears to have been indicated by the differences in tensile strengths shown in Tables 3 and 4, above. The drawing load variations for the different pattern finishes were also indicated, as the EBT UTS values were greater than the MF and EDT UTS values.

3.2 Pattern Characterization

3.2.1 Optical Measurements - Untested Patterns

Optical micrographs of the available surface patterns for the 2008 alloys are shown in Figure 15, for the 6009 alloys are shown in Figure 16, and for the 6111 alloys are shown in Figure 17. Tables 9, 10 and 11 give the EBT pattern information measured from the EBT micrographs. Only one set of measurements is given for the 2008 and the 6111 EBT patterns, as EBT.1 and EBT.2 patterns within an alloy type were nominally identical. Side A was chosen to be the sheet side that had a test strip running along one side of the sheet; side B had no test strip imprint. Pattern numbering was based on the location of the pattern on the sheet (Figure 8), with the pattern closest to the test strip designated as Pattern #1 and the pattern farthest away from the test strip designated as Pattern #8. Both average ring diameters and ring rim widths are given, with average diameters measured from ring rim center to rim center, rim widths measured from outer to inner ring edges and ring spacing measured from ring center to ring center (Figure 18).

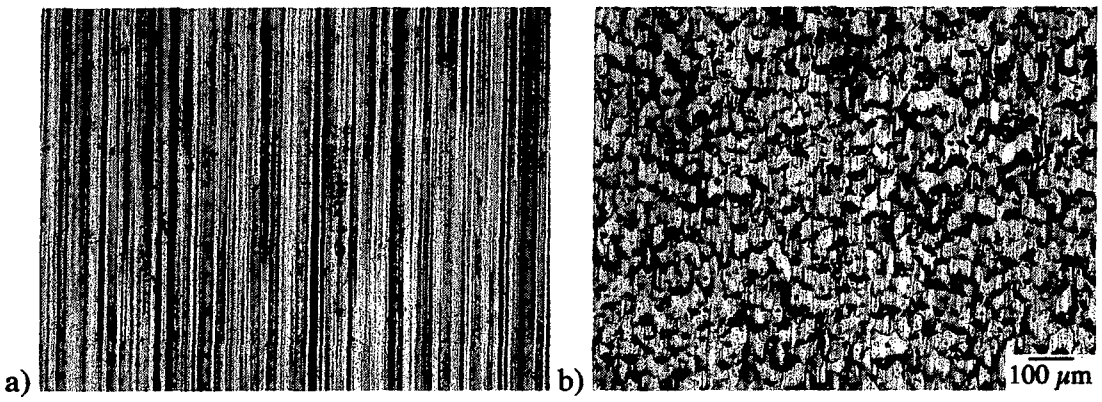

Figure 15 Micrographs of AA2008 Patterning a) MF (6009 similar), and b) EDT

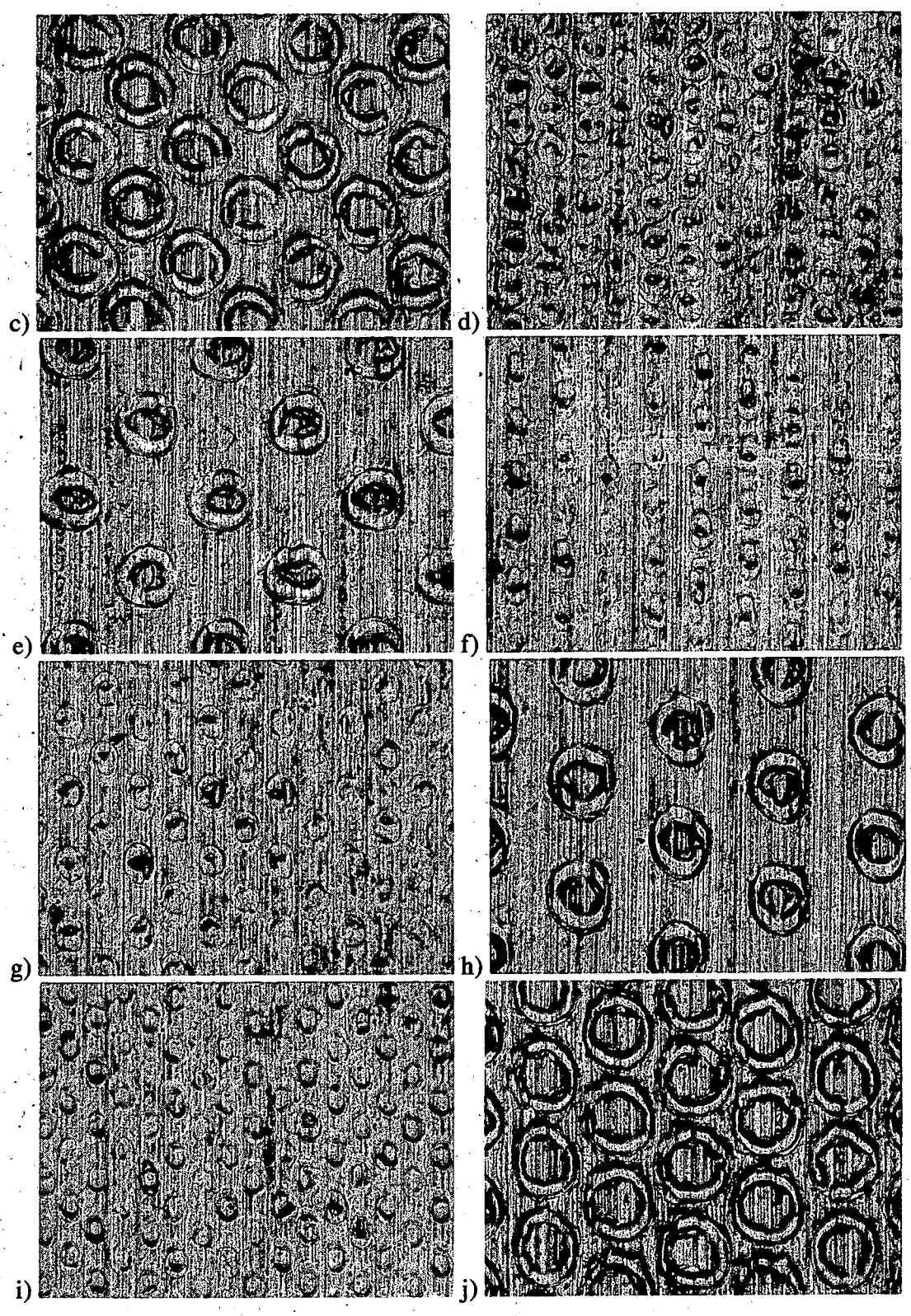

Figure 15 Micrographs of AA2008 EBT Patterning c) 1A, d) 2A, e) 3A, f) 4A, g) 5A, h) 6A, i) 7A, j) 8A

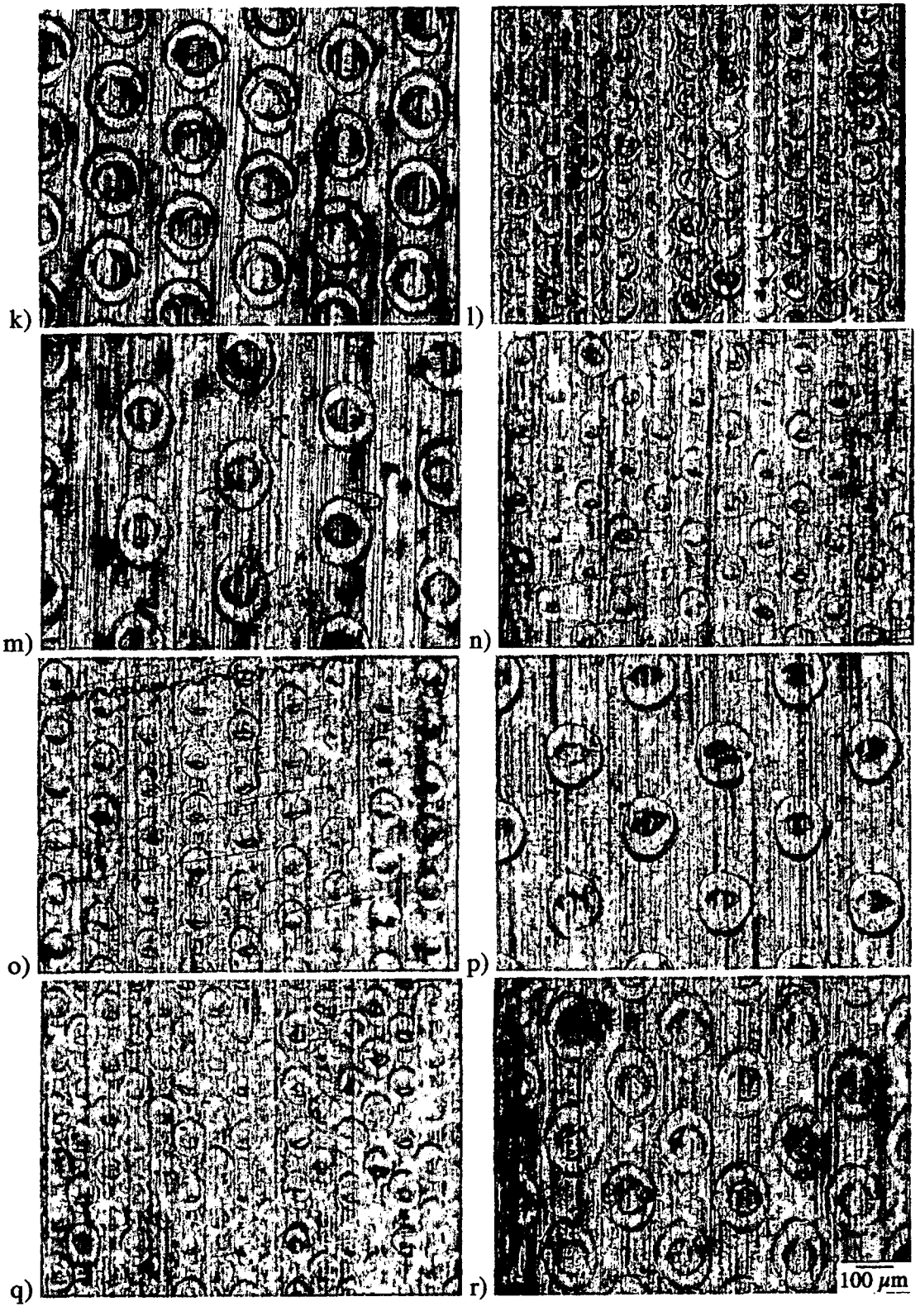

Figure 15 Micrographs of AA2008 EBT Patterning k) 1B, l) 2B, m) 3B, n) 4b, o) 5B, p) 6B, q) 7B, r) 8B

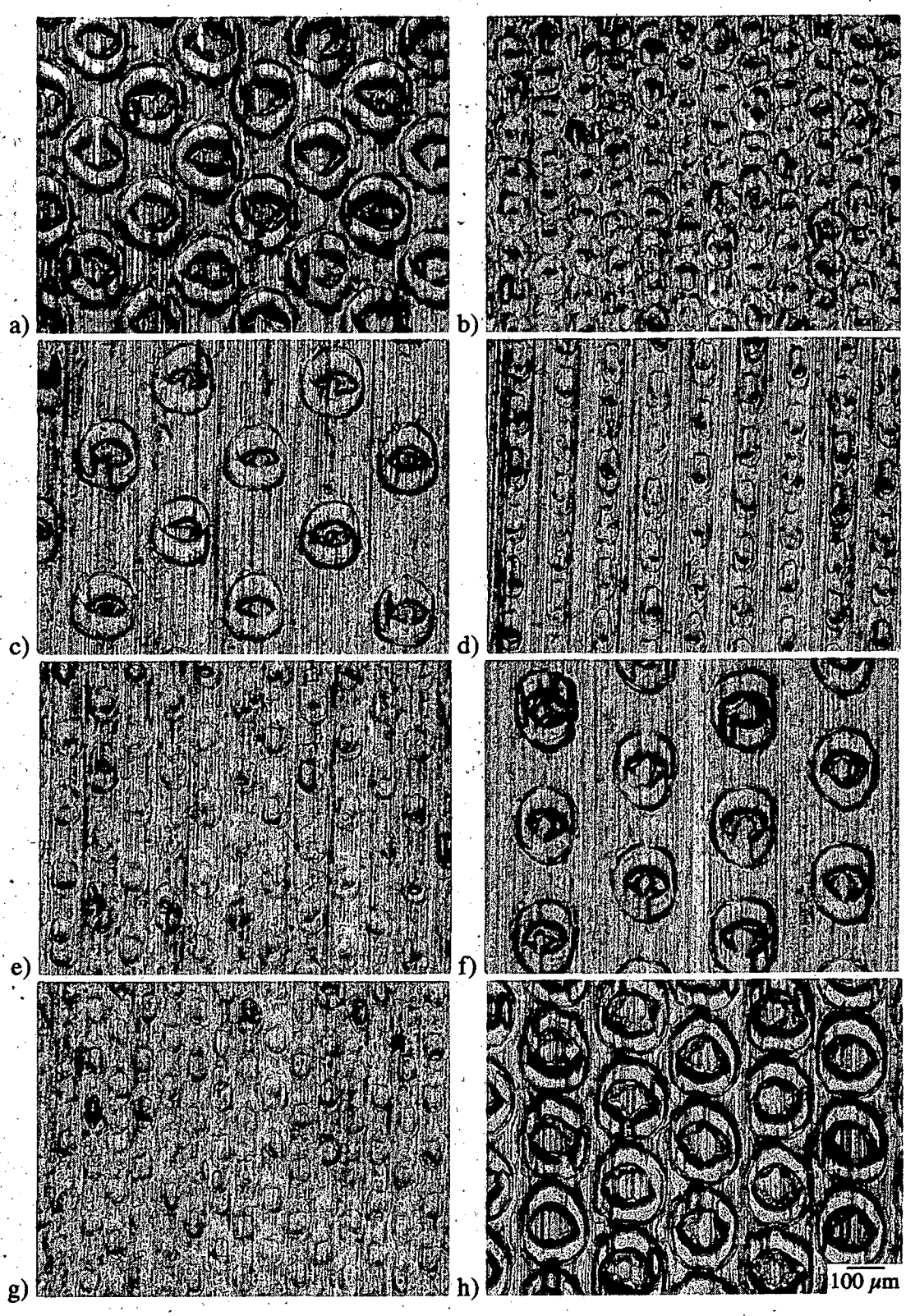

Figure 16 Micrographs of AA6009 EBT Patterning a) 1A, b) 2A, c) 3A, d) 4A, e) 5A, f) 6A, g) 7A, h) 8A

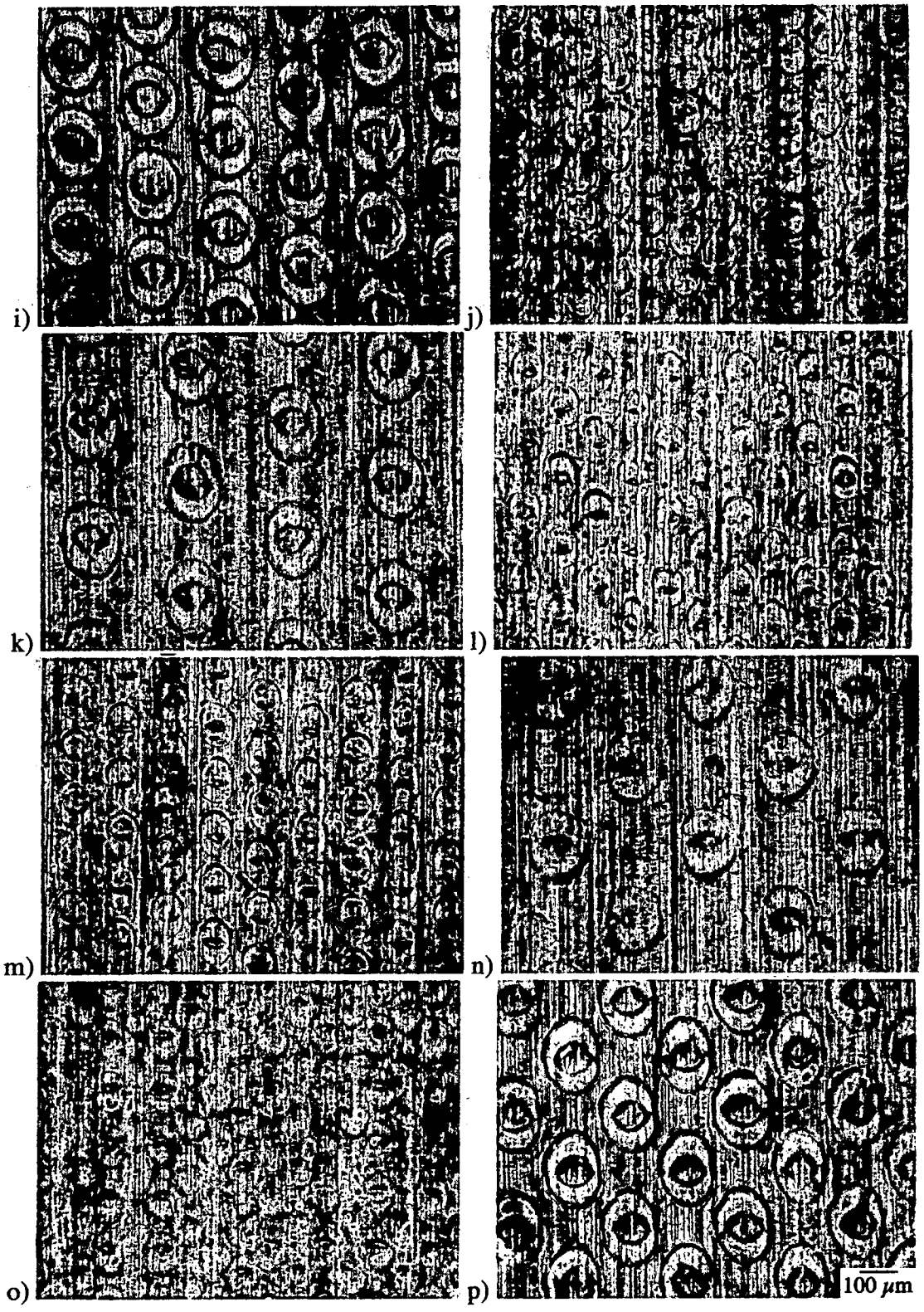

Figure 16 Micrographs of AA6009 EBT Patterning i) 1B, j) 2B, k) 3B, l) 4b, m) 5B, n) 6B, o) 7B, p) 8B

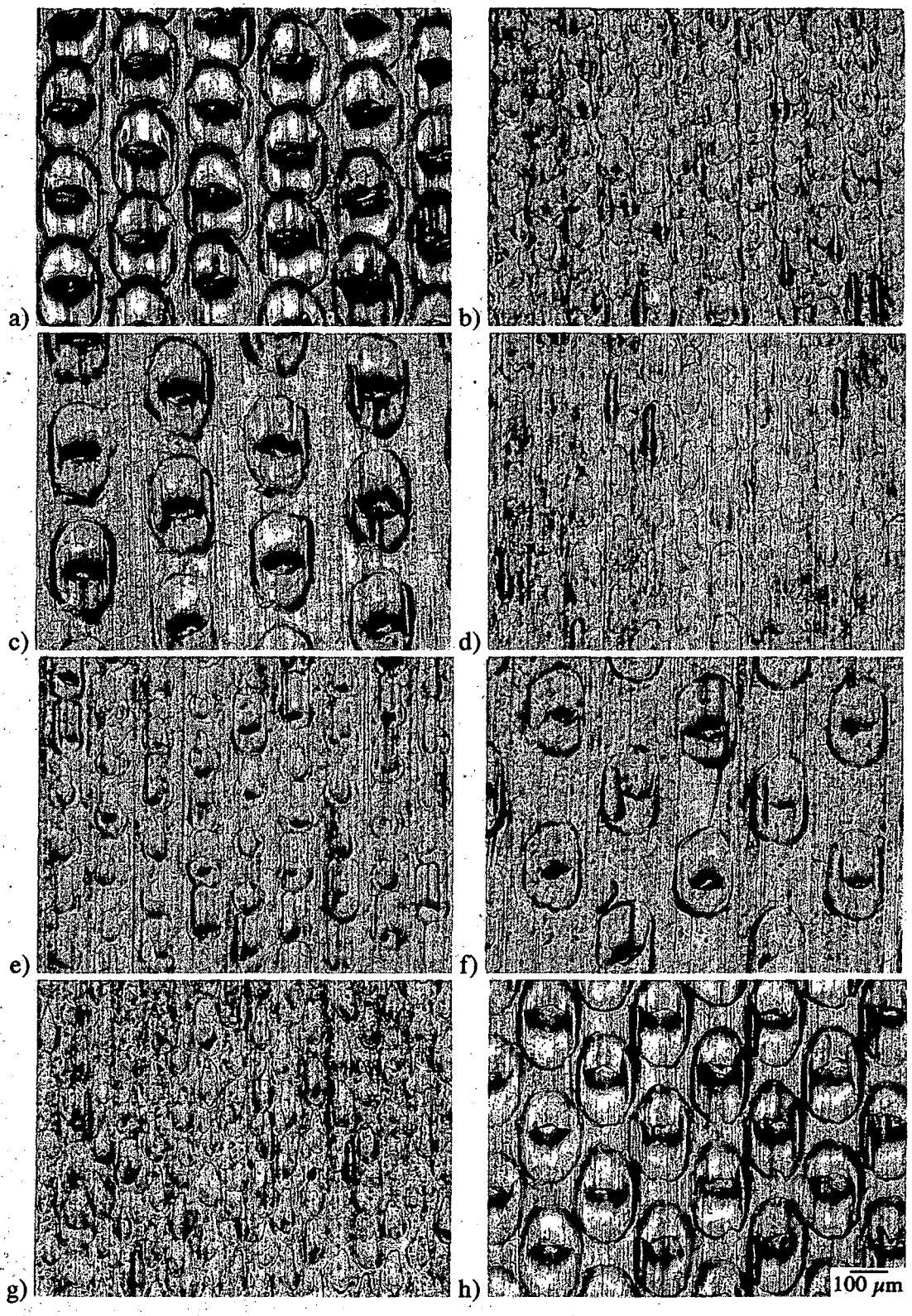

Figure 17 Micrographs of AA6111 EBT Patterning a) 1A, b) 2A, c) 3A, d) 4A, e) 5A, f) 6A, g) 7A, h) 8A

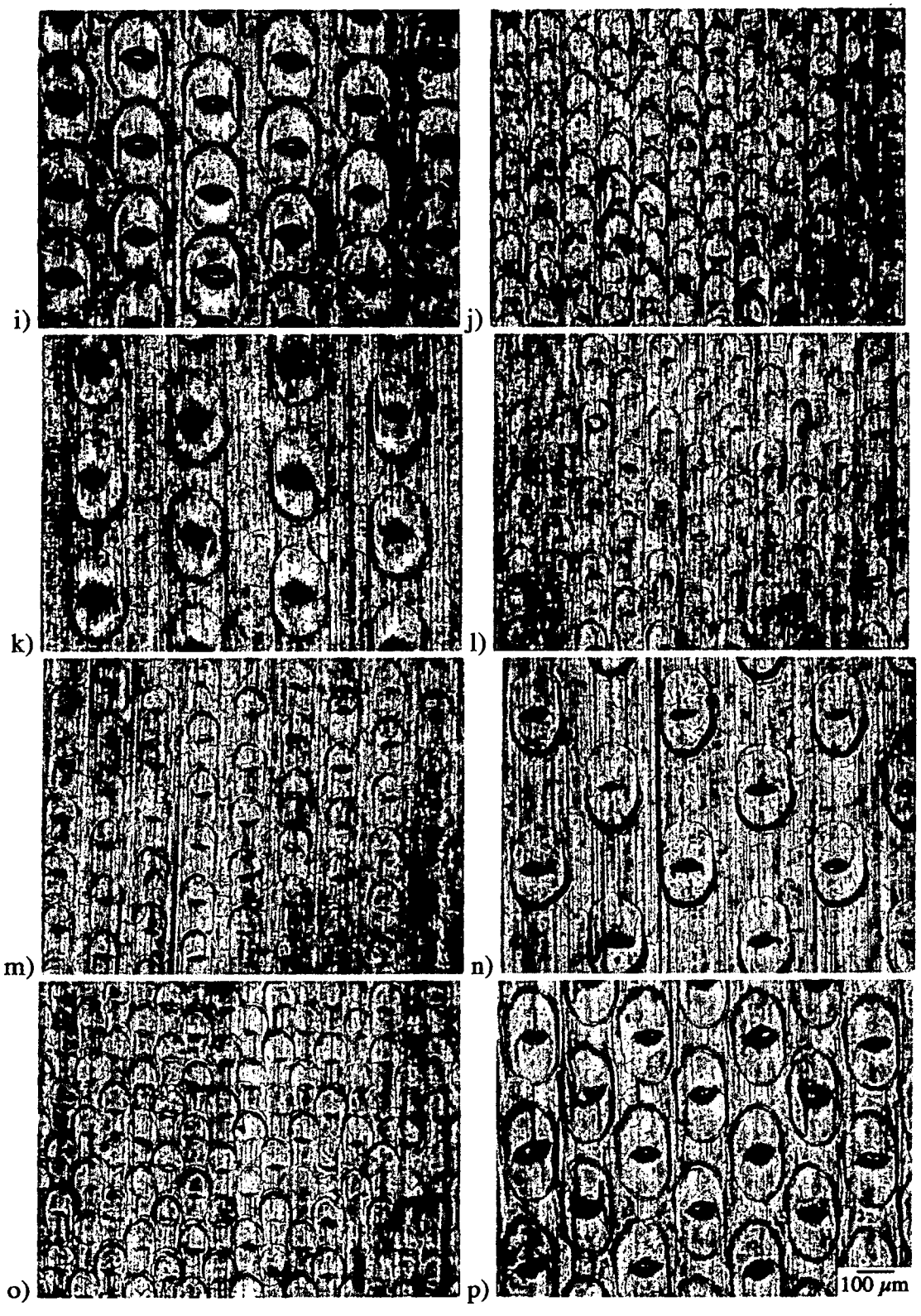

Figure 17 Micrographs of AA6111 EBT Patterning i) 1B, j) 2B, k) 3B, l) 4b, m) 5B, n) 6B, o) 7B, p) 8B

Pattern #	Avg. Ring Diam.-L (μm)	Avg. Ring Diam.-T (μm)	Ring Rim Width-L (μm)	Ring Rim Width-T (μm)	Distribution (degree)	Spacing (μm)
2008.1A	150	150	40	25	45	225
2008.2A	60	60	40	25	60	110
2008.3A	120	140	50	25	45	300
2008.4A	70	50	40	20	60	150
2008.5A	60	55	40	20	45	138
2008.6A	150	140	50	30	60	320
2008.7A	90	55	20	5	45	95
2008.8A	175	160	35	30	60	240
2008.1B	150	130	40	20	60	240
2008.2B	80	70	20	20	60	112
2008.3B	140	125	50	25	60	320
2008.4B	70	60	30	20	45	120
2008.5B	75	70	35	10	60	147
2008.6B	110	120	60	30	45	300
2008.7B	75	70	35	20	45	105
2008.8B	140	120	50	20	45	225

Table 9 EBT pattern ring information for AA2008 EBT sheets listed by pattern number and side, showing directional and average ring diameters, distributions, and spacings.

Pattern #	Avg. Ring Diam.-L (μm)	Avg. Ring Diam.-T (μm)	Ring Rim Width-L (μm)	Ring Rim Width-T (μm)	Distribution (degree)	Spacing (μm)
6009.1A	150	150	60	25	45	225
6009.2A	70	65	45	20	60	112
6009.3A	130	140	65	30	45	300
6009.4A	70	50	45	10	60	150
6009.5A	70	55	50	15	45	140
6009.6A	150	150	60	20	60	320
6009.7A	90	55	30	10	45	105
6009.8A	175	165	50	25	60	240
6009.1B	150	130	60	25	60	240
6009.2B	70	70	45	20	60	112
6009.3B	150	125	70	25	60	320
6009.4B	75	65	45	15	45	140
6009.5B	75	65	50	15	60	147.5
6009.6B	120	110	70	30	45	300
6009.7B	70	70	50	20	45	105
6009.8B	140	120	70	30	45	225

Table 10 EBT pattern ring information for AA6009 EBT sheets listed by pattern number and side, showing directional and average ring diameters, distributions, and spacings.

Pattern #	Avg. Ring Diam.-L (μm)	Avg. Ring Diam.-T (μm)	Ring Rim Width-L (μm)	Ring Rim Width-T (μm)	Distribution (degree)	Spacing (μm)
6111.1A	150	140	100	40	60	237.5
6111.2A	pattern too destroyed to make accurate measurements				60	
6111.3A	160	140	110	25	60	320
6111.4A	90	80	80	10	45	140
6111.5A	pattern too destroyed to make accurate measurements				60	
6111.6A	140	120	110	30	45	300
6111.7A	pattern too destroyed to make accurate measurements				45	
6111.8A	160	130	110	40	45	225
6111.1B	150	130	100	30	60	237.5
6111.2B	70	70	40	20	60	110
6111.3B	160	120	110	25	60	320
6111.4B	80	60	75	20	45	140
6111.5B	80	60	70	15	60	147.5
6111.6B	140	110	110	40	45	300
6111.7B	80	60	70	25	45	115
6111.8B	150	110	120	30	45	120

Table 11 EBT pattern ring information from AA6111 EBT sheets listed by pattern number and side, showing directional and average ring diameters, distributions, and spacings.

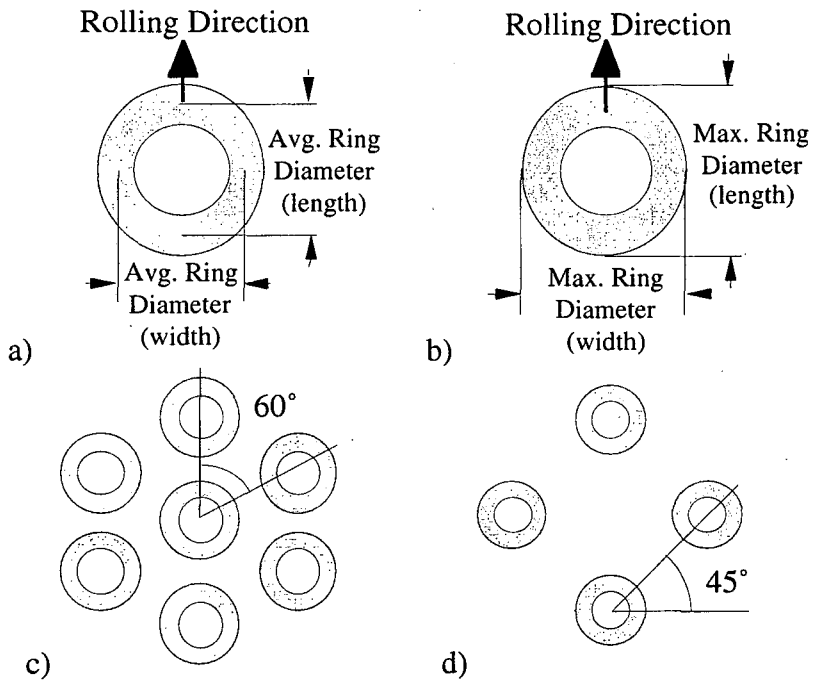

Figure 18 Examples of a) and b) EBT pattern measurements, c) 60° interlocking hexagonal EBT ring distribution, and d) 45° EBT ring distribution

The patterns were split evenly between large (A and B side patterns #1, 3, 6, and 8) and small (A and B side patterns #2, 4, 5, and 7) ring diameters. Large patterns averaged 140 μm (5512 μin) in diameter and greater than 2 μm (79 μin) in depth while small patterns averaged 65 μm (2559 μin) in diameter and less than 2 μm (79 μin) in depth. Pattern ring distribution fell into one of two types, either a 60°, interlocking hexagonal distribution, or a distributed square rotated 45° from both the transverse and the longitudinal directions (Figure 18). Pattern ring spacing ranged from the ring rims almost touching to spacings multiple ring diameters apart.

Pattern rings on the 6111 alloys appeared highly elongated compared to similar patterns on the 2008 and 6009 alloys. In addition to greater elongation, the nominally matching patterns on the two sides of the 6111 EBT alloy sheets show different degrees of degradation exemplified by a breakdown in the pattern ring outline, leading to the destruction of some of the smaller, shallower patterns, and by obvious deep pits in the ring rims.

3.2.2 Profilometry Measurements - Untested Patterns

Profilometry data from all patterns was used to validate optical measurements. Directional FFT power spectra for EBT surfaces confirmed measured wavelengths of optically-resolvable features, such as impression size and spacing, in addition to displaying wavelengths from the residual MF pattern on the sheets. One fact that became apparent using the power spectra was that the residual MF patterning resulted in greater starting roughnesses transverse to the sheet rolling directions.

Bearing area curves calculated from profilometry data show a distinctive knee for the larger, deeper patterns but not for the smaller, shallower patterns (Figure 19). The depth of this knee for the larger patterns correlates to pattern volume, with a greater knee depth indicating greater volume. The lack of a knee for the shallower patterns confirms the height histogram and the optical observations that the shallower pattern depths were on the order of the waviness of the sheet surfaces. The bearing area curves for the MF and EDT surfaces were similar to the shallower EBT pattern curves, as can be seen below (Figure 19).

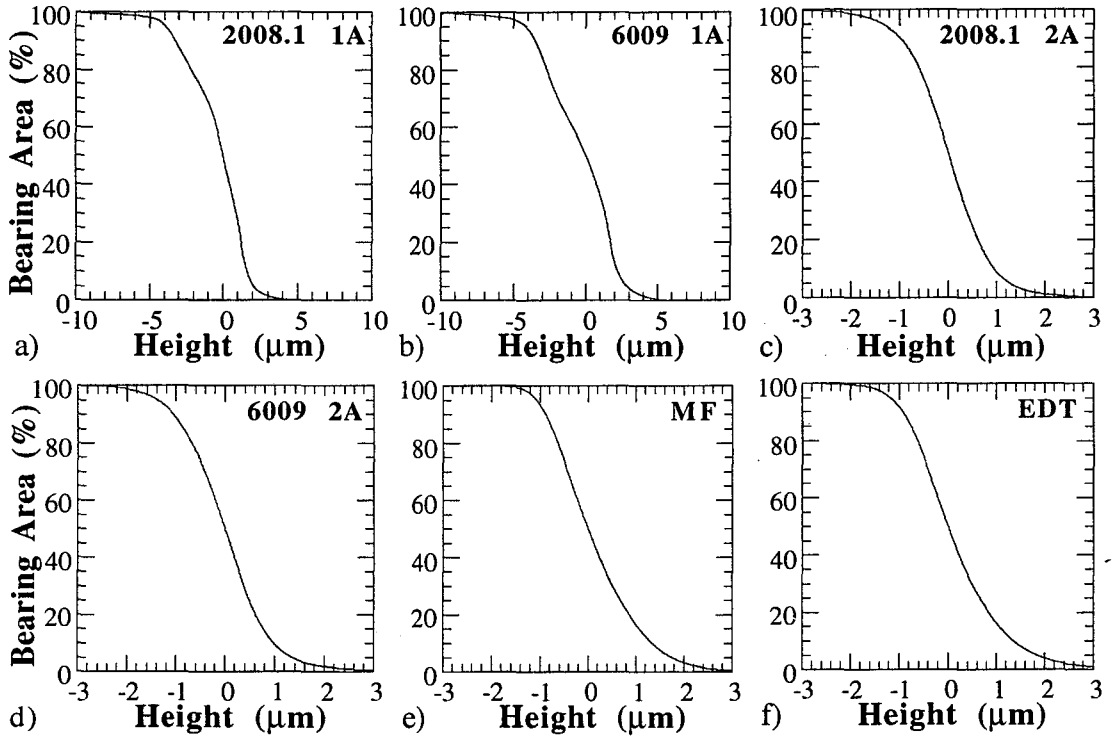

Figure 19 Representative untested bearing area curves for deeper EBT patterns a) 2008.1 1A and b) 6009 1A and shallower EBT patterns c) 2008.1 2A and d) 6009 2A. Typical e) MF and f) EDT bearing area curves are comparable to the shallower EBT pattern curves. The distinctive knee in the deeper pattern curves is absent for shallower pattern curves, indicating a pattern depth on the order of the surface waviness. The lower knee for (b) represents a greater pattern volume than for the nominally identical (a).

Ideal and real lubricant carrying capacities, defined in Section 2.4.2, were calculated for all EBT surfaces. Ideal pattern volume, or the volume of lubricant the ideal pattern will hold, was calculated from the roll patterning information. Measured EBT pattern volumes were calculated from profilometry data of untested patterns by choosing a shelf value below which to calculate the lubricant volume the pattern was capable of holding. Both ideal and real volumes, calculated for an area 1 mm x 1 mm (0.039 in sq.) in size, are compared in Figure 20. The larger measured pattern volumes for the 6009 and 6111 sheets, compared to the 2008 sheet volumes (Figure 20), correspond to a larger degree of pattern elongation, visible in the optical micrographs shown in Figures 15 through 17. The lack of a correlation between the ideal, roll based, pattern volume and the actual pattern volume may arise from roll wear and degradation of the pattern from the ideal, as well as from the method used to quantify the measured volumes.

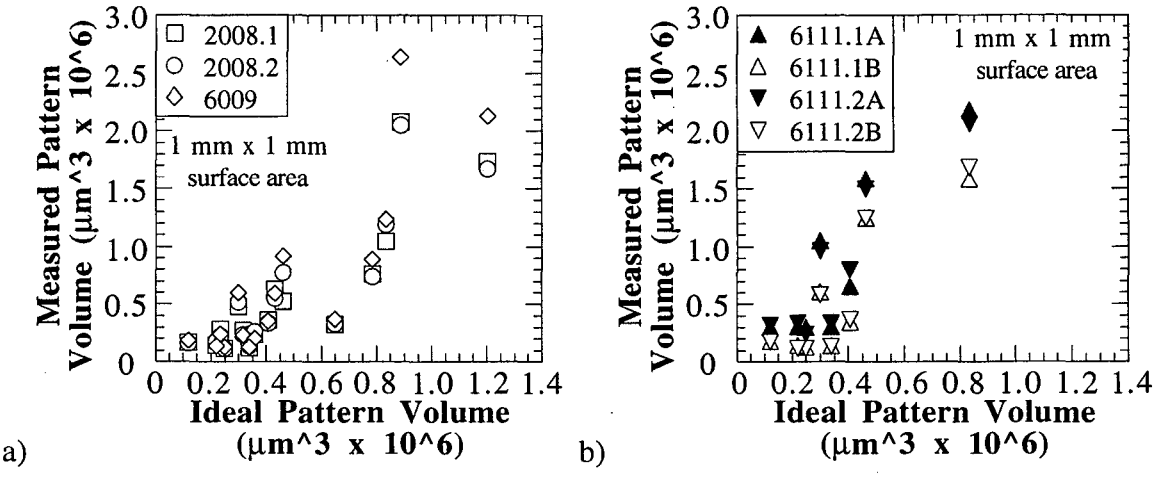

Figure 20 Measured pattern volume, calculated from three dimensional profilometry data, is shown as a function of ideal pattern volume, calculated from roll patterning data for a) 2008 EBT.1 and EBT.2, and 6009 EBT and b) 6111 EBT.1 and EBT.2 sheets.

3.3 Draw Bead Simulator Machine and Specimen Validation

As stated above, validation of the newly fabricated DBS test machine results were of concern both for current and future research on this machine. The precautions taken to ensure machine validity included measuring bead deflection, comparing test results within the two test setups on the fabricated machine, comparing test results between the fabricated machine and another DBS tester, and comparing estimated error to test scatter for all tests. For specimen validity, bluing tests were performed to measure specimen contact with the test beads and single-sided test results were compared to double-sided test results for two specimen widths.

3.3.1 Die Deflection Tests

Deflection measurements showed that the test strip was not being pinched. The rear, entrance female bead moved rearward between 0.025 mm and 0.038 mm (0.001 in and 0.0015 in) during testing, while the male bead moved forward 0.025 mm (0.001 in) and the forward, exit female bead moved forward between 0.025 mm and 0.038 mm (0.001 in and 0.0015 in).

3.3.2 Strain Gauge versus Load Cell Setup Tests

The forming friction results for the local strain gauge test setup, compared to the local load cell test setup results in Figure 21 and Appendix D, display a linear relationship valid for all pattern types and all alloys. This relationship indicates a repeatability for both test setups and lends confidence to the data collected from the fabricated machine.

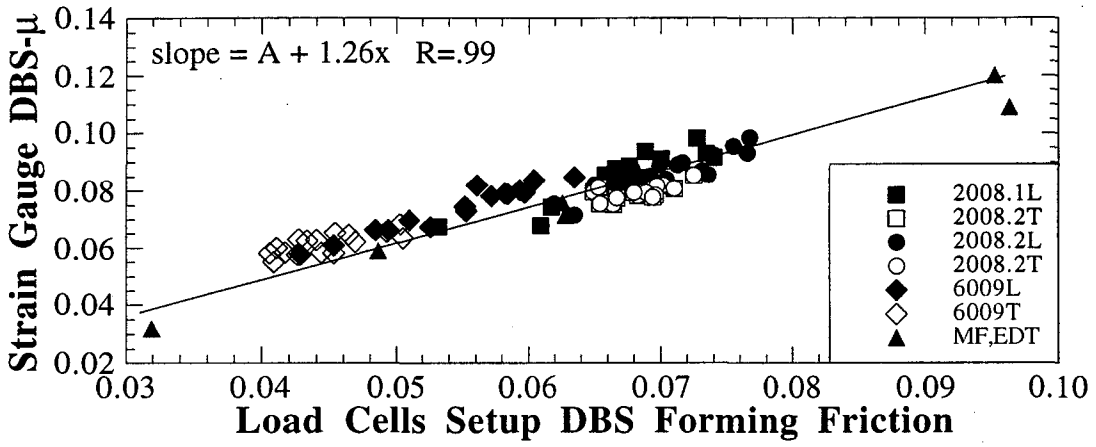

Figure 21 Linear relationship between local DBS forming friction strain gauge setup results and load cell setup results.

3.3.3 Local versus Denver DBS Tests

DBS testing was also performed using MF and EDT patterned material on a DBS machine at the University of Colorado, Denver. The Denver machine has compared favorably to other DBS testers in round robin testing performed by the North American Deep Drawing Research Group (NADDRG), and so was considered a good machine against which to compare the newly fabricated machine. All MF and EDT tests performed locally are plotted in Figure 22 as a function of the MF and EDT tests performed on the Denver machine. The linear fits for mixed bead testing and fixed bead testing are roughly the same slope but slightly shifted, indicating a repeatable linear difference between the two machines, and lending support to the validity of the data collected on the local machine test setups.

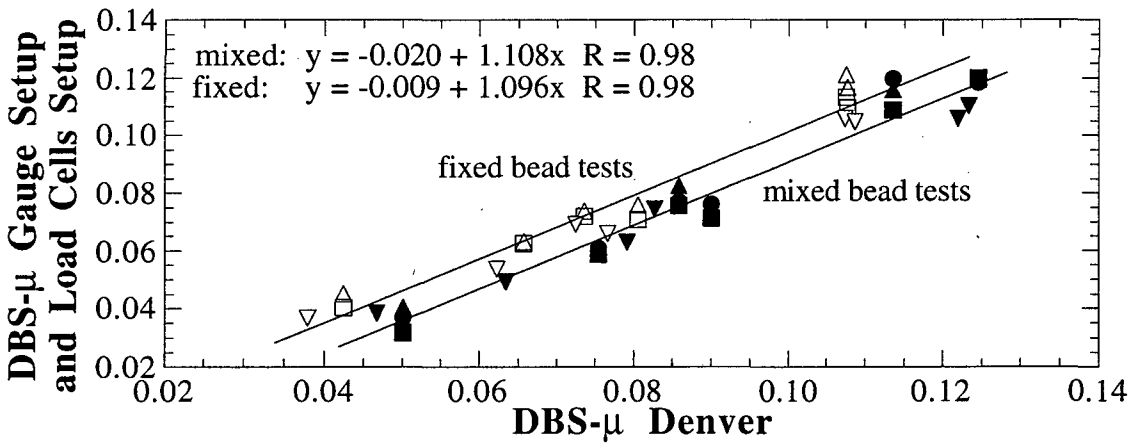

Figure 22 Local DBS test results for all MF and EDT tests plotted as a function of DBS tests performed at the University of Colorado, Denver, to validate the local test machine.

The data in Figure 22 include both retested MF and EDT specimens corrected for their previous straining by the slope in Figure 23, and load cell MF and EDT test data multiplied by the slope for strain gauge setup versus load cell setup test results given in Figure 21. The retest specimens, cut from sections of the longer Denver specimens that did not undergo drawbead deformation, showed a slight decrease in forming friction compared to specimens that underwent no prior straining (Figure 23).

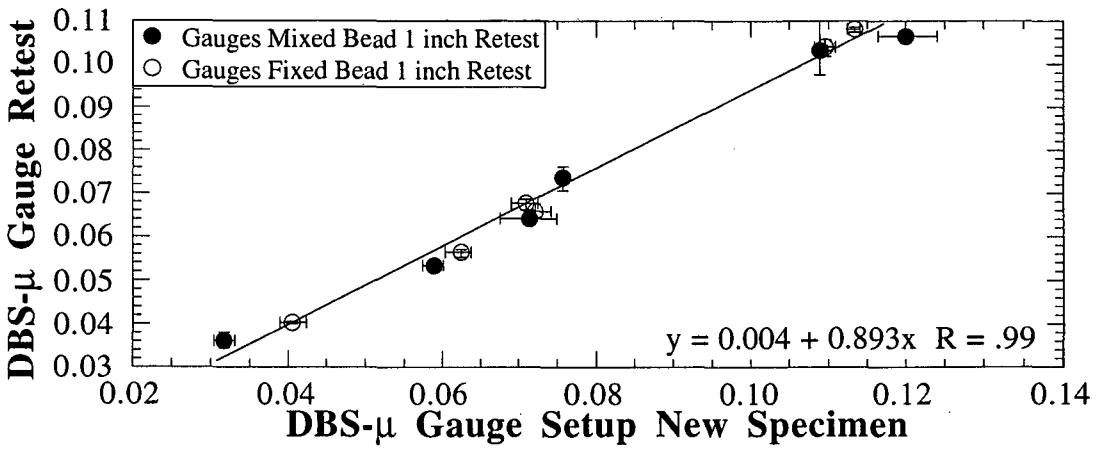

Figure 23 Comparison of "retested" specimens cut from the portion of the 25.4 mm (1 in) wide specimens tested at Denver, and non-prestrained MF and EDT specimens.

3.3.4 Specimen-Bead Contact Measurements

As all EBT specimens had to be tested single-sided, the validity of using single-sided versus double-sided testing was of concern. Tests for both the 25.4 mm (1.00 in) and the 50.8 mm (2.00 in) specimen widths showed that the tested strip did not skip while travelling over the male bead. This agreed with lubricant gathering behavior observed during testing. They also showed that the contact angle with the male bead is between 4 and 10% greater than the angle of contact with the two female beads, with neither contact angle reaching 180° (160 to 170° for the male bead, 75 to 80° on entrance female bead and around 80° for the exit female bead).

3.3.5 Single-Sided versus Double-Sided Tests

To further explore contact angle differences and differences in test dynamics, single- and double-sided tests were performed both locally and on the Denver machine. Figure 24, displaying single-sided tests as a function of double-sided tests, shows that there is a linear relationship between the two test types, validating the use of this test to evaluate the behavior of the EBT specimens.

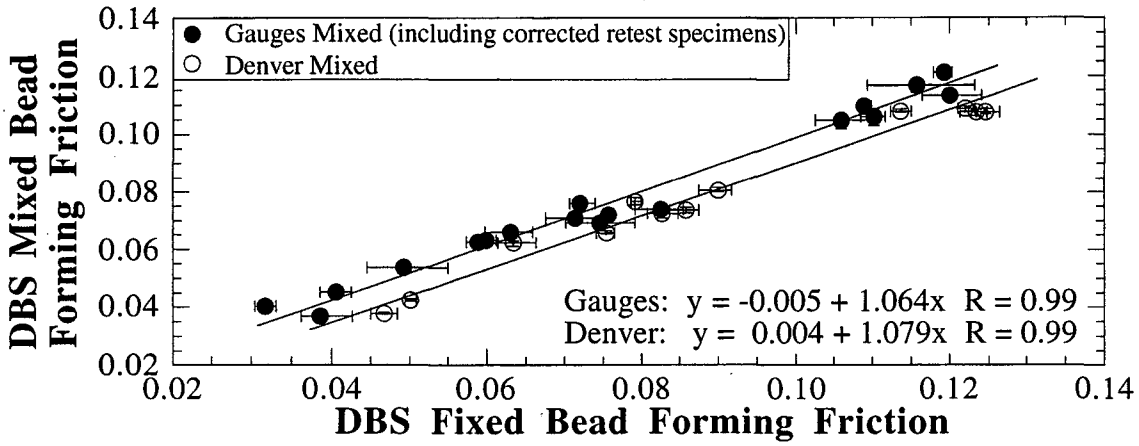

Figure 24 Comparison of single-sided and double-sided DBS test results for all MF and EDT testing performed locally and at Denver showing a linear relationship.

The greater forming friction values shown in Figure 24 for the single sided tests over the double sided tests agree with the greater contact angle observed for the male bead in the bluing tests. While the relationship shown in Figure 24 is linear, it combines with the contact angle measurements to show that a simple halving of the geometric contact angle in the forming friction equation is not perfect if one wants to compare absolute forming friction values between single-sided and double-sided tests.

3.3.6 Specimen Width Comparison

In addition to using single-sided tests, limited pattern widths across the full-wide sheet (Figure 8) dictated the use of 25.4 mm (1.00 in) wide specimens rather than 50.8 mm (2.00 in) wide specimens. Comparison of the DBS forming friction of these two widths cut from the same sheet, shown in Figure 25, validates use of this specimen width, and corroborates previous work by Schey showing a virtual one-to-one correspondence in the forming friction values of the two test specimen widths.[R5]

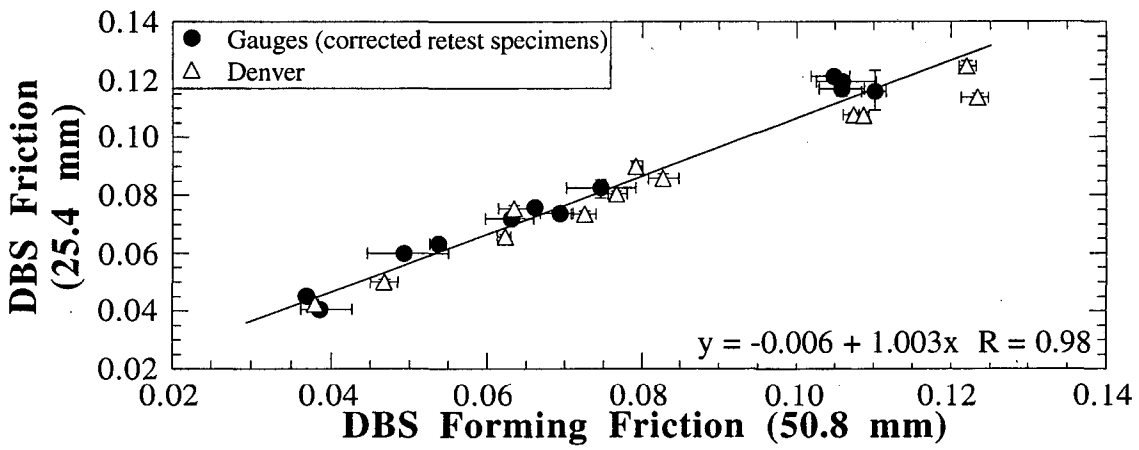

Figure 25 Comparison of all 25.4 mm (1.00 in) and 50.8 mm (2.00 in) wide specimen tests, with "retest" specimens corrected for previous straining, showing a virtual one to one correspondence between the two specimen test widths.

3.3.7 Estimated Error

Overall MF and EDT test scatter for the Denver DBS tester was ~3%, while the fixed bead error, calculated using Eqn. 5, was 3% ±1 % and the mixed bead error, calculated using Eqn. 6, was 4% ± 2%. Switching from the gauges on the die to the load cells under the top die in the fabricated machine reduced compression load scatter within a mixed bead test set from an average of 4% (ranging from 1% to 14%) to less than 1%, reduced test friction scatter from ~8% to ~5%, and reduced overall mixed bead test error, calculated from Eqn. 6, from 8% ± 3% to 5% ± 1%. Fixed bead test error for the gauge setup was 4% ± 1%.

3.4 Dependence of DBS-μ on Pattern

3.4.1 Influence of MF, EDT Pattern and Alloy on Forming Friction

Figure 26 illustrates the fact that both AA2008 and AA6009 MF-L specimens exhibited two to three times the forming friction of MF-T specimens, while AA2008 EDT-L and -T specimens displayed equal forming friction. This result was expected from the patterns themselves, i.e., the highly directional mill finish only being able to retain lubricant in one direction, and the less directional EDT holding lubricant equally well in the two directions tested here. The MF and EDT behavior seen here also confirms other researchers' observations on both steel and aluminum alloys.[R6-R8] The relationship between EDT pattern wavelength and forming friction observed with electrogalvanized (EG) steel EDT patterned surfaces[R9] could neither be confirmed nor denied with these tests, as there was not a great enough variety of EDT patterns available to perform a statistically significant number of tests.

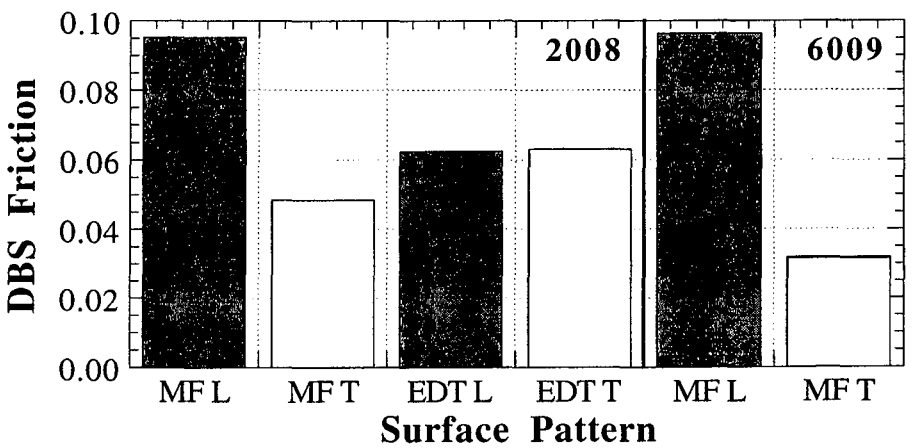

Figure 26 Column plot of DBS-μ for 2008 and 6009 MF and 2008 EDT patterns showing vastly different forming friction for MF-L and MF-T from the directional patterning and nominally equal EDT-L and EDT-T forming friction from the more non-directional patterning.

3.4.2 Influence of EBT Pattern and Alloy on Forming Friction

Finding the dependence of DBS forming friction on discrete EBT pattern lubricant carrying capacity is the main concern of the work performed here. For this dependence to be most useful, the patterns must influence the DBS friction in a repeatable manner between alloys of different strengths. A repeatable influence of the EBT pattern on DBS forming friction was observed between different alloys of the same thickness (Figure 27), with the lower mechanical strengths resulting in lower forming friction values. The trend for the thinner, more elongated patterns of the 6111 sheets is shown separately (Figure 27). DBS forming friction results for all patterns and directions are plotted for reference in column form in Appendix E. Some of the same-thickness DBS-μ data are combined in Figure 28 to further illustrate the monotonic influence of mechanical strength on the forming friction of similar patterns.

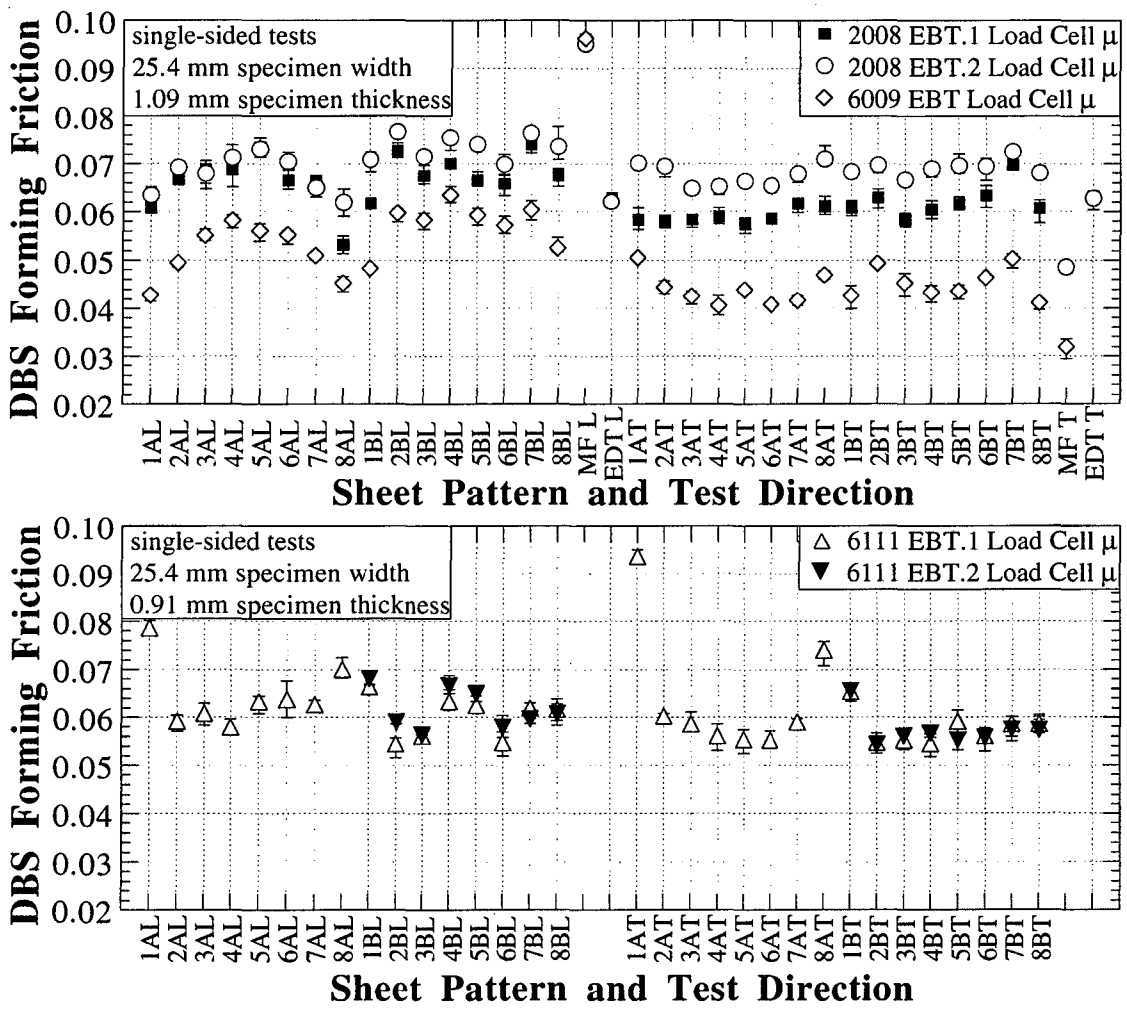

Figure 27 a) EBT DBS forming friction values for all 1.09 mm (0.043 in) thick specimens, showing a repeatable effect from particular patterns between alloys. The lower forming-μ values arise from lower UTS values. b) EBT DBS forming friction values for all 0.914 mm (0.036 in) thick specimens.

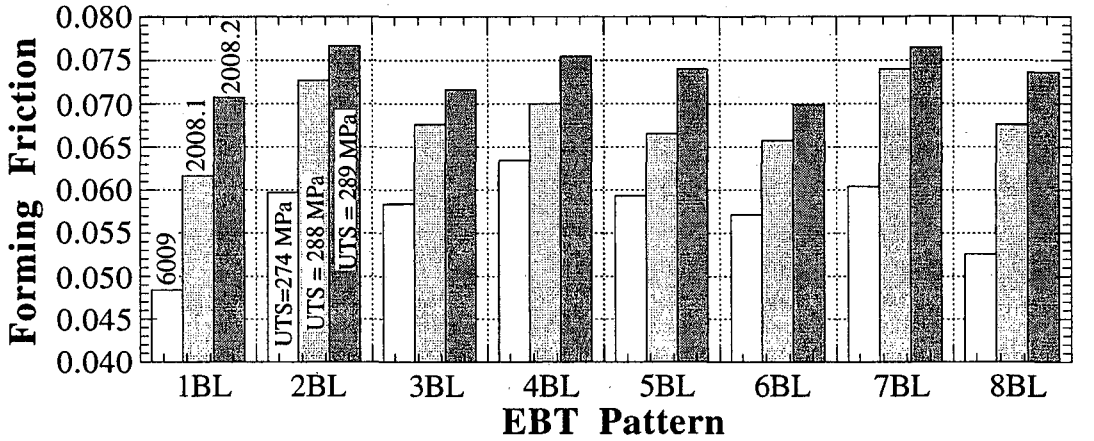

Figure 28 a) Forming friction results for similar EBT patterns showing the influence of mechanical strength on the single-sided DBS test friction value.

The dependence of forming friction on pattern indicated in Figure 27 is replotted in Figures 29 and 30 to illustrate the dependence of forming friction on pattern volumes. Figure 29 shows the dependence of DBS friction in the sheet rolling direction on both the ideal and the measured untested discrete pattern volumes for the AA2008 and AA6009 sheets. The slope lines shown on the plots represent the linearly inverse correlation between the DBS forming friction and the pattern volumes, showing the same trend as the work by Hylton on coated sheet steel.[R10] The dependence of forming friction on pattern volume correlated better for the measured lubricant carrying capacities than for the calculated ideal volumes. While the ideal volumes displayed a single slope for all pattern sizes, the measured volumes indicate a separate influence for the smaller, shallower ring sizes than for the deeper, larger rings. It is likely that the different slopes for the two pattern depth dependencies of the measured volumes arose from the method used to calculate those volumes. While the deeper patterns displayed distinctive bimodal distributions in the height histogram (Figure 11), the shallower patterns displayed a single distribution which resulted from the waviness of the surface interfering with the pattern heights. It is also possible that the extreme shallowness of the rings displayed a deeper dependency from a faster loss of the micro-PHD effect and of lubricant as the sheet thinned and the surface roughened.

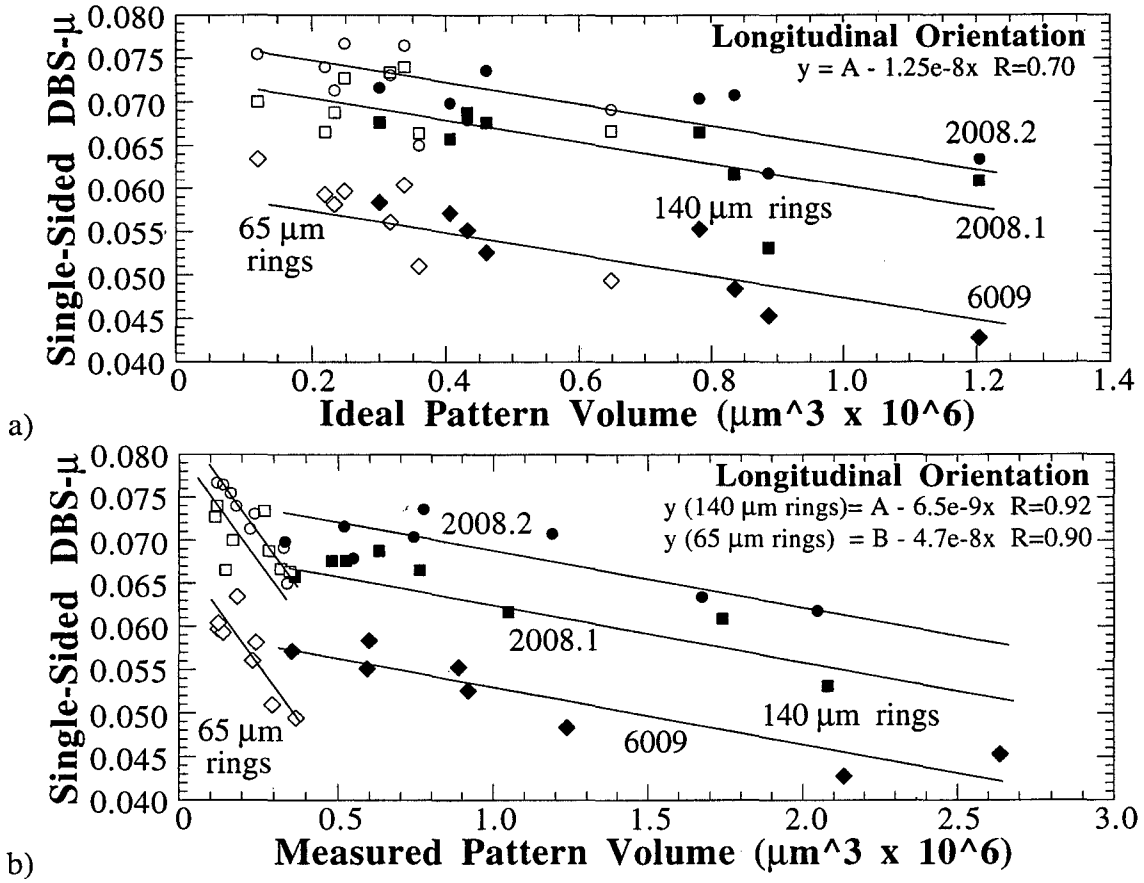

Figure 29 The dependence of single-sided DBS test forming friction on a) ideal and b) measured pattern volumes for specimens cut in the sheet rolling direction for 2008 EBT.1, 2008 EBT.2, and 6009 EBT sheets. The forming friction shows a linear dependence on both ideal and measured pattern volumes.

The forming friction dependence in the transversely oriented specimen direction on ideal and measured pattern volumes is shown in Figure 30. The influence of the residual mill finish pattern completely overwhelmed the discrete patterns tested here, to the point that the resulting forming friction values were nominally identical, regardless of pattern volume. The same relationship was observed for measured pattern area (Figure 31). This overwhelming background influence is supported by the profilometry based power spectra showing the residual presence of the MF pattern.

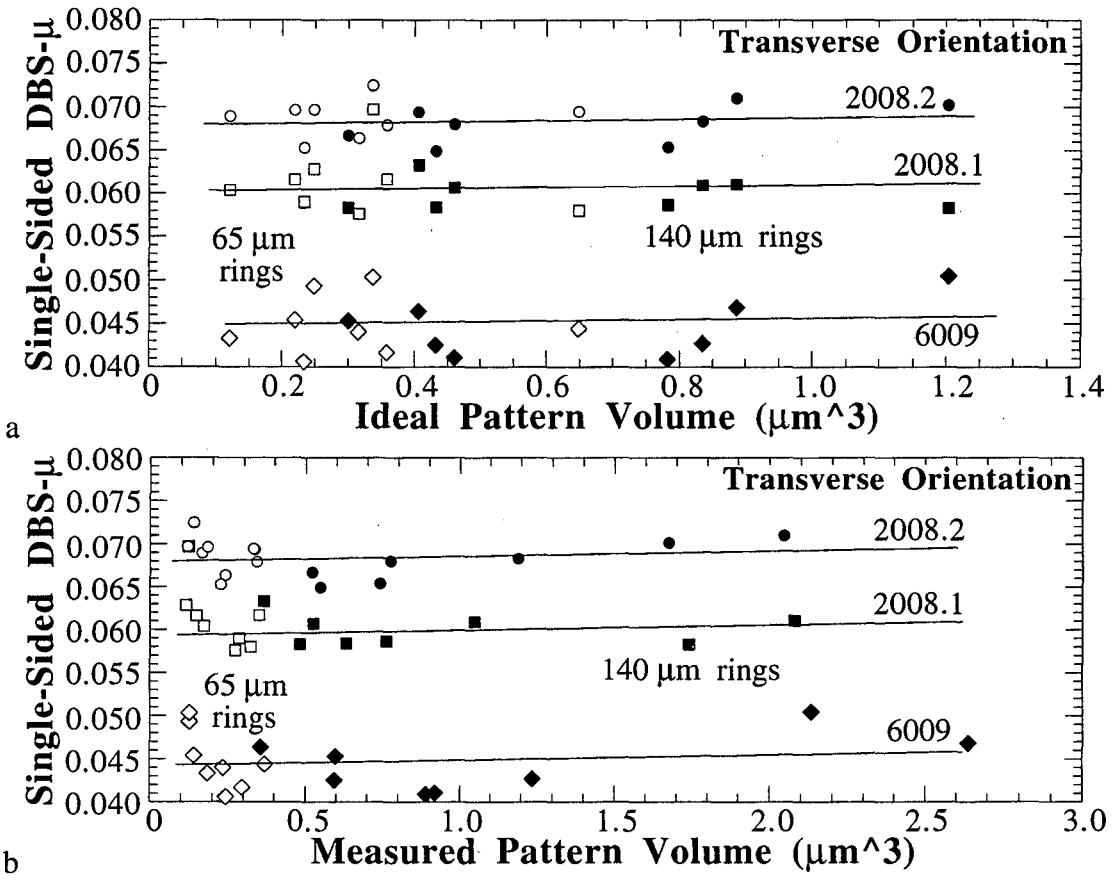

Figure 30 The dependence of single-sided DBS test forming friction on a) ideal and b) measured pattern volumes for specimens cut 90° to the sheet rolling direction for 2008 EBT.1, 2008 EBT.2, and 6009 EBT sheets. The forming friction is virtually independent of the pattern volume in the transverse direction, from the impact of the residual MF pattern on the sheet surfaces.

To further understand the dependence of forming friction on pattern lubricant carrying capacity, the lubricant carrying area associated with the volumes shown above was calculated for the measured patterns. The resulting plot (Figure 31) shows a single inversely linear relationship between longitudinal forming friction and lubricant carrying area. This result correlates with Bowden and Tabor's theory that friction is linearly proportional to real contact area.[R11] As with the volume plot shown above, the scatter in the plot is a direct result of the method used to choose the value at which to calculate this area, the same value below which the volumes displayed above were calculated, and the natural scatter obtained from the friction testing machine. Because of roll wear and other rolling dynamics that were apparently accounted for with the ideal volume calculation, forming friction was not linearly dependent on the ideal lubricant carrying area.

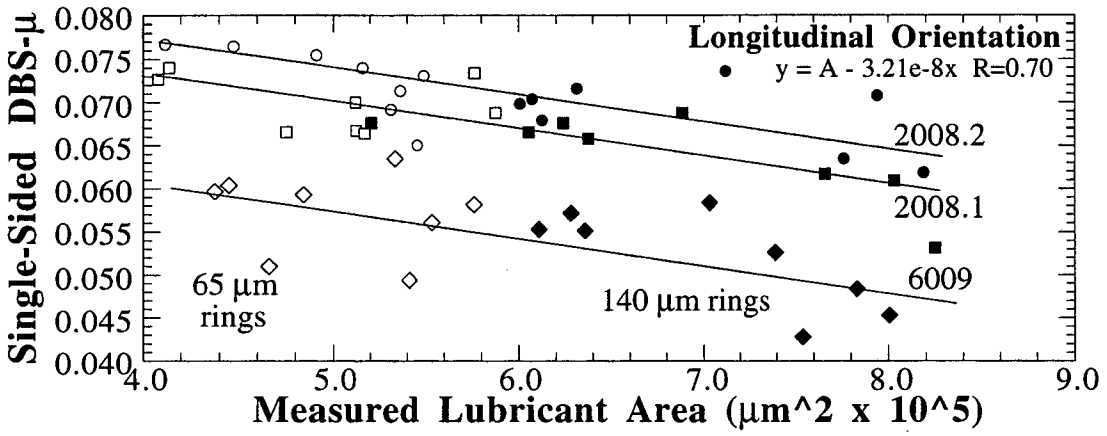

a)

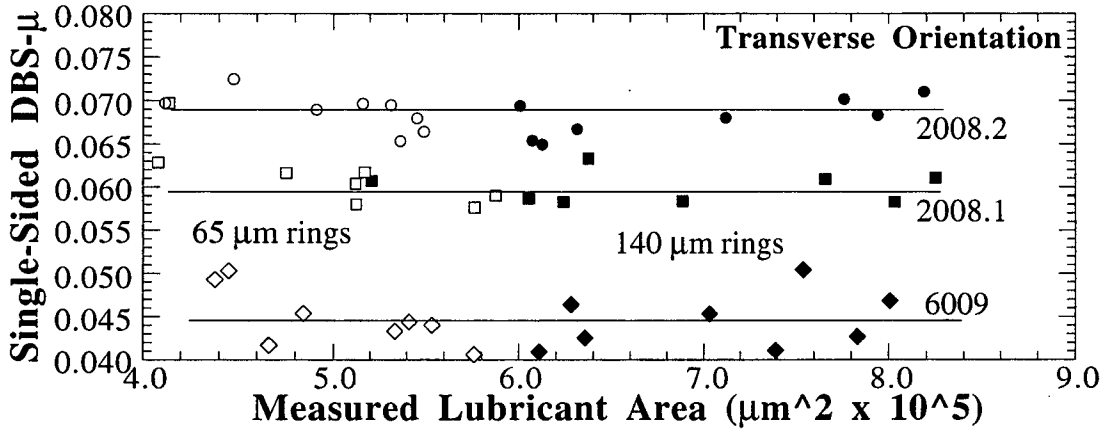

b)

Figure 31 A single, inversely linear relationship between single-sided DBS test forming friction and discrete lubricant carrying area for 2008 EBT.1, 2008 EBT.2, and 6009 EBT measured patterns cut a) parallel to the sheet rolling direction. As with pattern volumes, specimens cut b) transverse to the sheet rolling direction were independent of pattern area.

For the thinner, highly-elongated patterns of the AA6111 sheets, forming friction increased with pattern volume in both the longitudinal and the transverse directions (Figure 32). This increase resulted from the smearing of the pattern, which caused a greater amount of material to be forced upward, above the level of the MF patterned sheet surface (Figure 33). This uplift of material in the center of the rings created a series of discrete contact points, with the contact area increasing with pattern volume. In addition to increasing contact area, riding on these points rather than on the original MF surface resulted in a loss of the beneficial micro-PHD pressure pockets the rings were meant to provide, as no seal between the ring rims and the bead could take place.

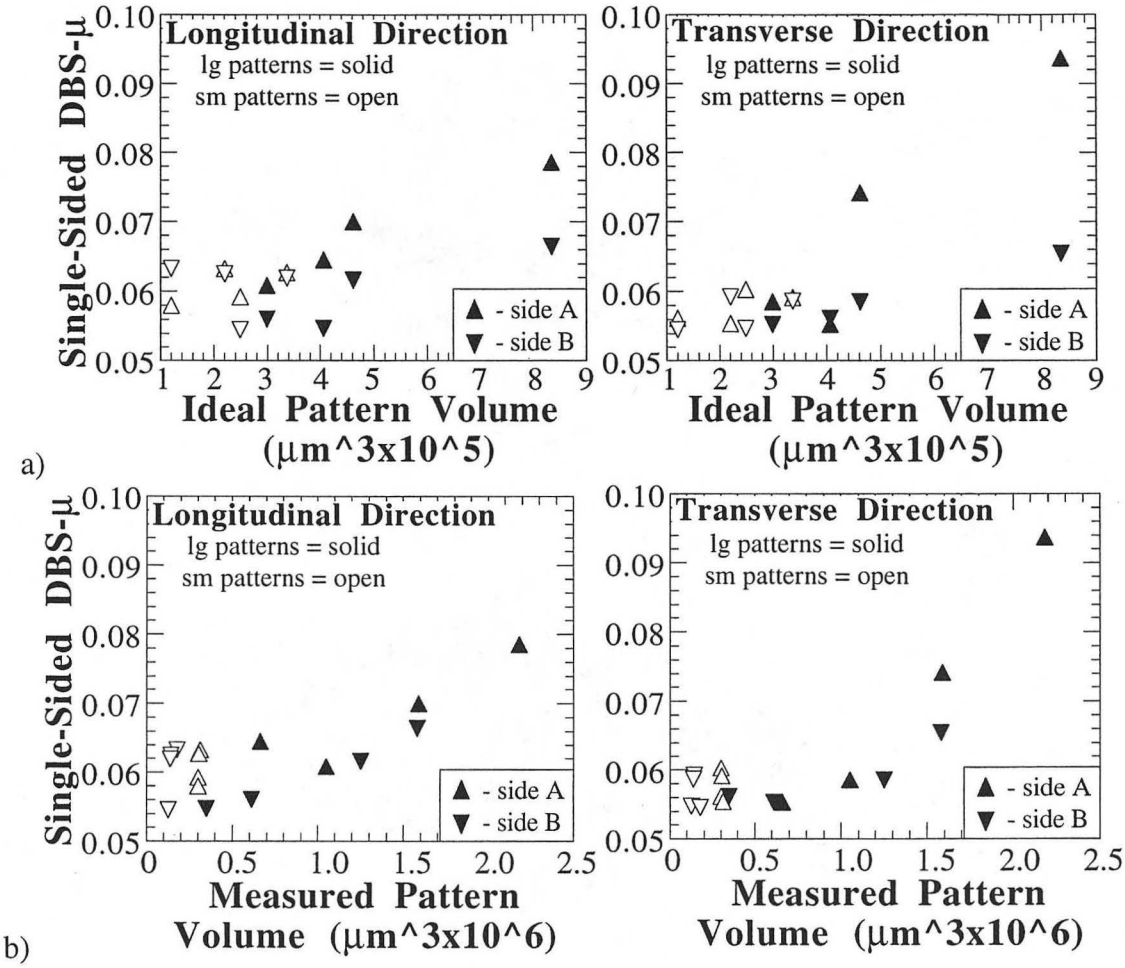

Figure 32 Dependence of single-sided DBS test forming friction on a) ideal and b) measured pattern volumes for specimens cut both in and transverse to the rolling direction for the elongated patterns of the 6111 EBT sheets.

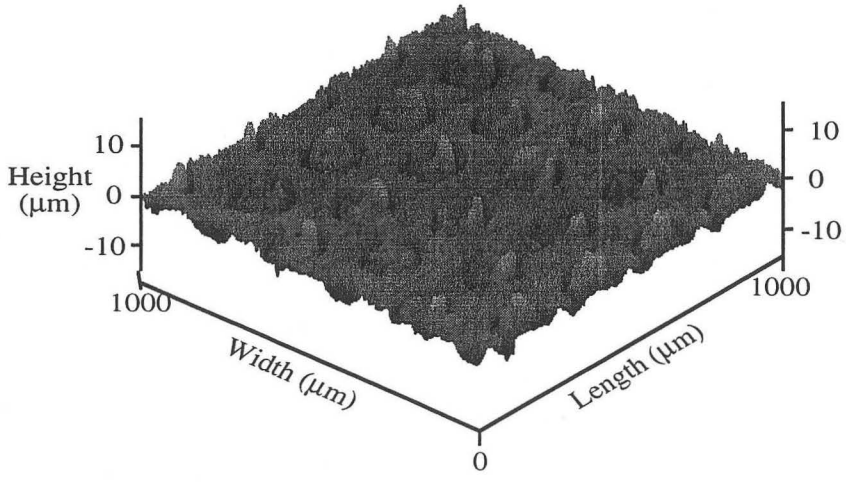

a)

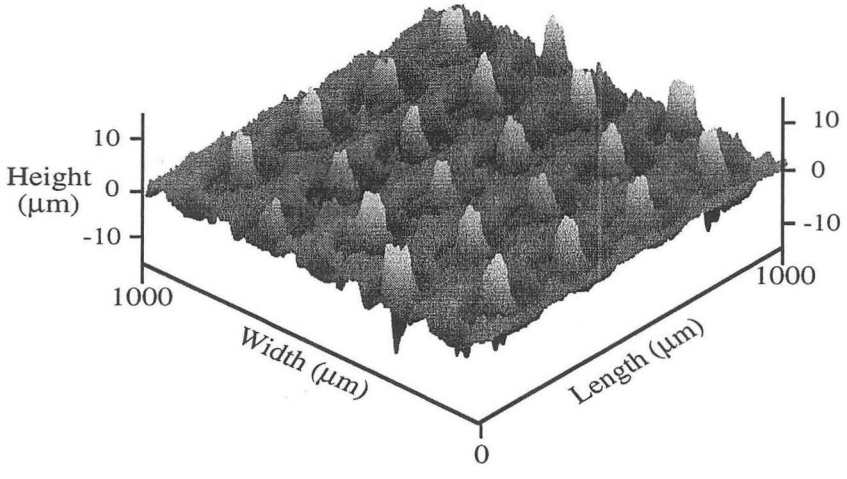

b)

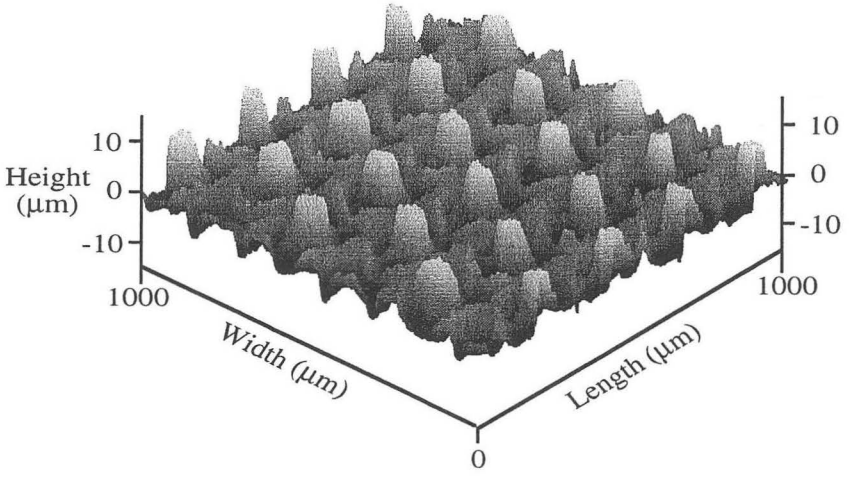

c)

Figure 33 Three dimensional plots of profilometry data for a nominally identical a) 2008 and b) 6111 pattern, showing the greater uplift in the 6111 pattern from smearing during rolling as well as c) from roll wear.

In addition to smearing of the pattern, the integrity of the discrete patterns also affected the forming friction. Loss of pattern integrity, i.e., degradation of the ring outline and formation of irregularities within the rings such as pits, relates to the wear of the roll used to imprint the patterns. The greater uplift for these patterns from roll wear is shown above in Figure 33. The contribution of these degraded patterns toward increasing forming friction is illustrated below in Figure 34. Side A of the AA6111 sheets was imprinted with a worn roll while Side B was imprinted with a newer roll, where the patterns were nominally identical to those on roll A before the wear resulting from the rolling process itself.

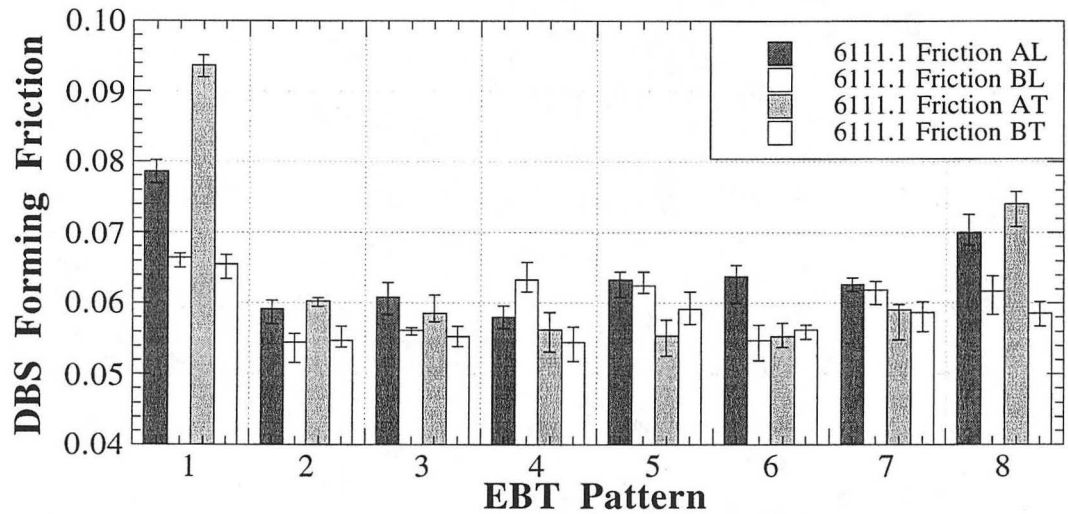

Figure 34 Column plot illustrating greater forming friction in the single-sided DBS test from pattern degradation resulting from greater roll wear. Side A represents worn roll, side B represents newer, less worn, roll; test scatter is shown by error bars.

3.5 Post-DBS Test Surface Appearance

3.5.1 Overall Tested Surface Appearance

Overall the FFT power spectra for tested EBT surfaces supported optical observations as to the reduction of or almost total destruction of the various patterns. Polynomially leveling the tested specimen data transverse to the test direction did not change the power spectra when compared to only polynomially leveling in the test direction, indicating little or no curving across the width of the test specimen. The power spectra for patterns that were not completely destroyed by testing showed some pattern elongation in the test direction as well as the degree of surface roughening (Figure 35). Pattern elongation is visible in Figure 35 by the shifting of the power spectra peaks to a slightly longer wavelength. Roughening of the tested surface is visible from the greater wavelength contributions shown compared to the untested surface contributions. While

all patterns were affected by surface roughening, the larger ring-sized patterns retained much of their lubricant carrying capacity, albeit following the topography of the roughened surface (Figure 36). All small ring-sized patterns were completely dominated by surface roughening, as was one large pattern; the critical pattern depth below which this destruction took place was approximately 2 μm (78 μin). The largest pattern ring depth tested here averaged 6 μm (235 μin).

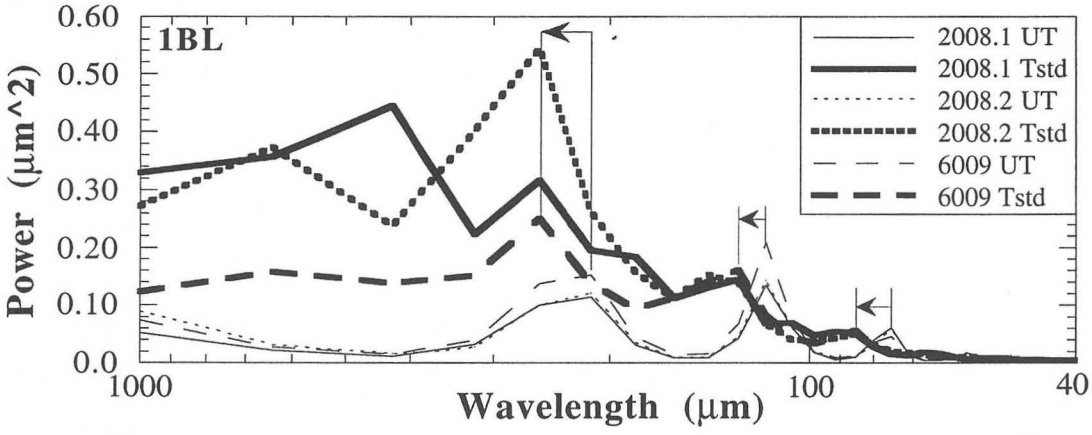

Figure 35 Tested versus untested 1BL surfaces for AA2008 and AA6009 showing pattern lengthening from stretching during testing, greater initial contribution from the untested AA6009 pattern from greater smearing during rolling, and greater tested roughnesses from AA2008.

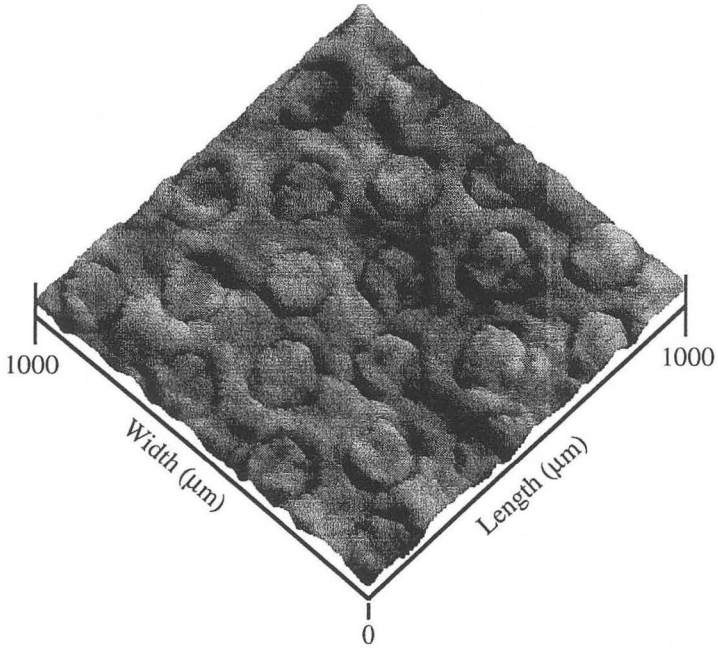

Figure 36 Three dimensional plot of tested surface showing the EBT imprinted pattern following the roughened surface topography.

3.5.2 Influence of Alloy on Tested Surface Appearance

For nominally the same surface patterns, AA2008 showed consistently greater roughening than AA6009 and AA6111 after testing, while AA6111 roughening was approximately the same as AA6009. In addition, 2008-T sheet specimens displayed significantly greater post-test roughening than the 2008-L specimens, and thus also the 6009 and 6111 specimens in both the -L and -T directions. This greater roughening, displayed in both Figure 35 and Figure 37, was consistent across all patterns tested, and appeared to correlate with increasing grain thickness rather than grain size in the rolling plane. This supports a prior author's contention that grain thickness is the most important parameter in determining post-test surface roughening.[R12] The 6111 pattern shown in Figure 37 illustrates the greater untested pattern wavelength contributions from pattern smearing. This smearing effect resulted in greater starting roughnesses for almost all 6111 patterns compared to the 2008 and the 6009 patterns. For the largest 6111 patterns, which include the one shown below, the tested surface actually contained lower wavelength contributions than the untested surface. This resulted from the discrete peaks, shown in Figure 33, deforming and smashing down during testing.

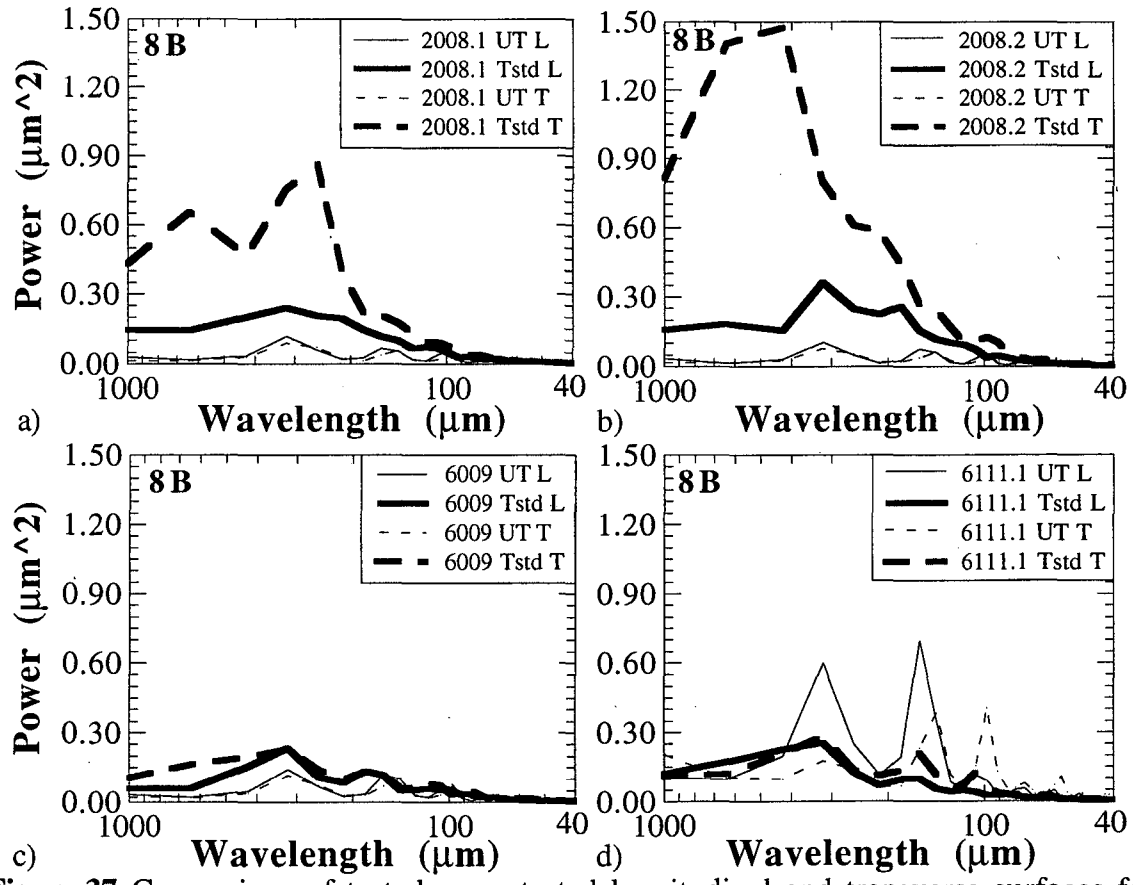

Figure 37 Comparison of tested vs. untested longitudinal and transverse surfaces for a) AA2008.1, b) AA2008.2, c) AA6009, and d) AA6111, showing greater roughening for AA2008-T and greater initial pattern contribution for AA6111.

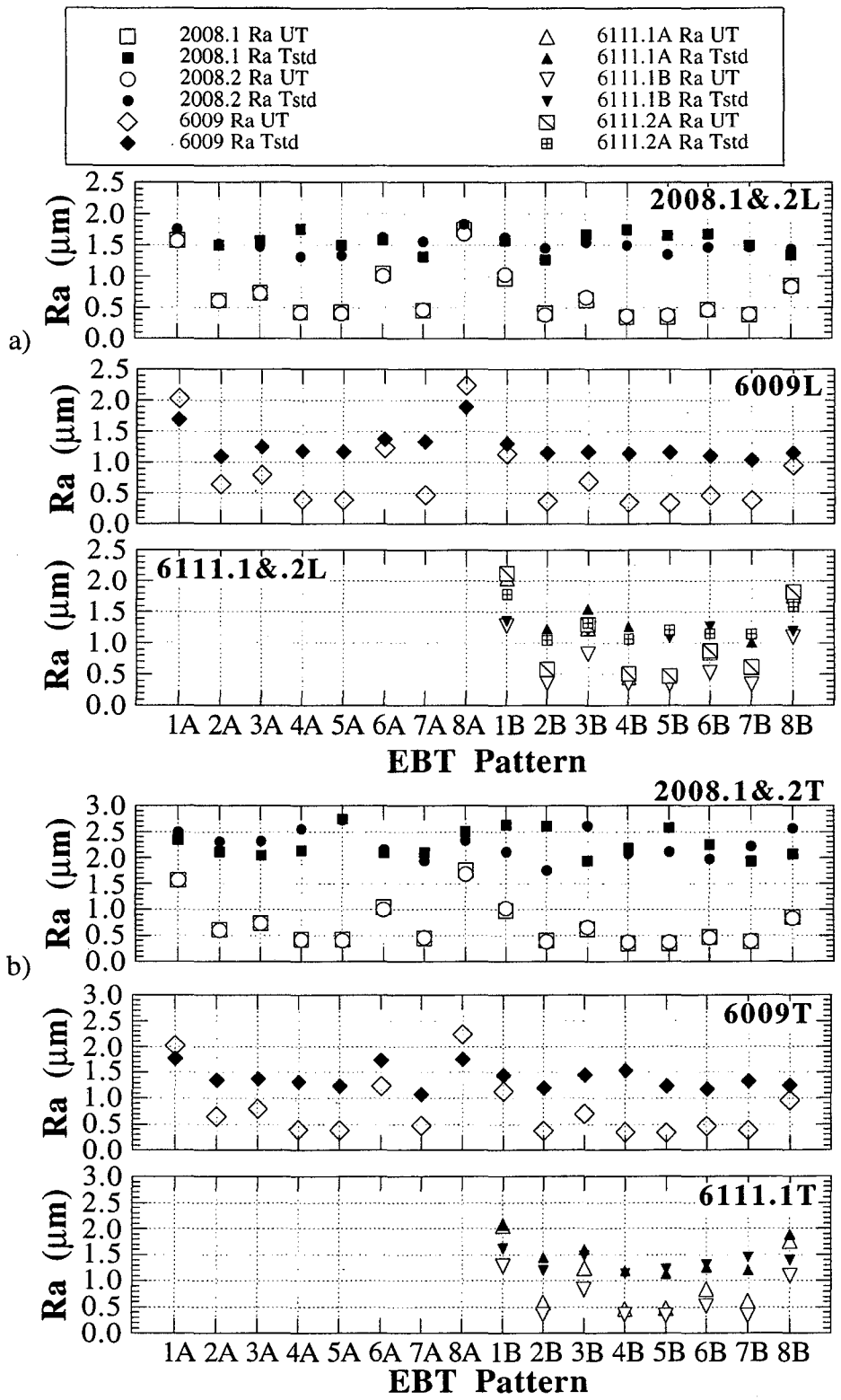

Figure 38 Three dimensional roughness averages (3D R_a) for untested versus tested a) longitudinal specimens and b) transverse specimens showing surface homogenization and greater post-test roughness of the 2008 sheets.

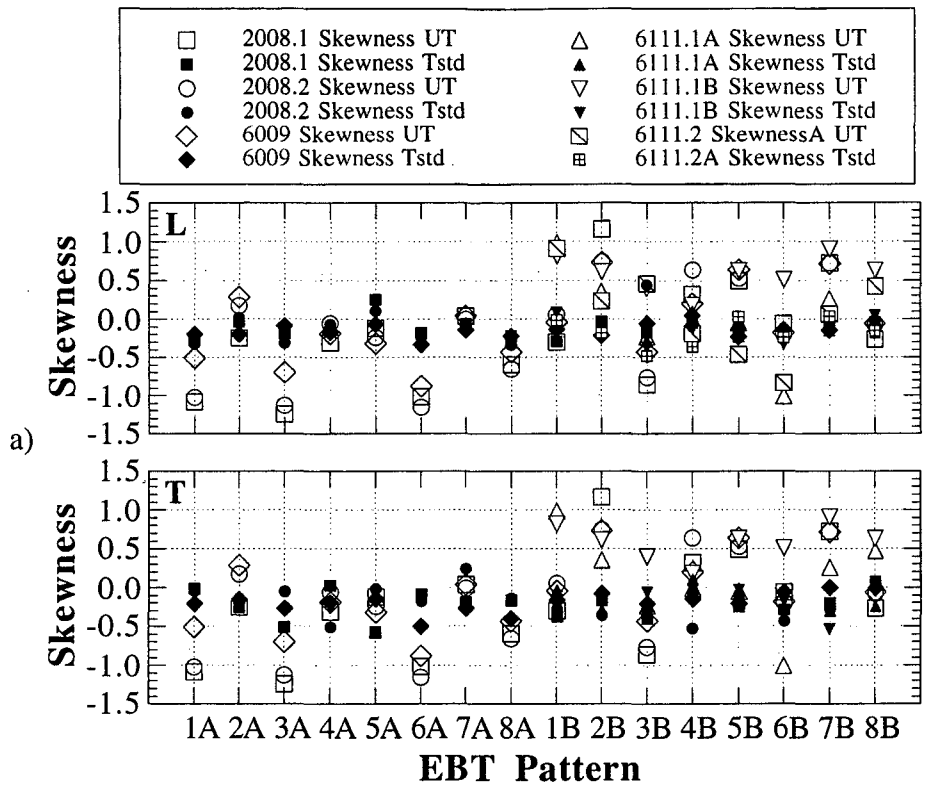

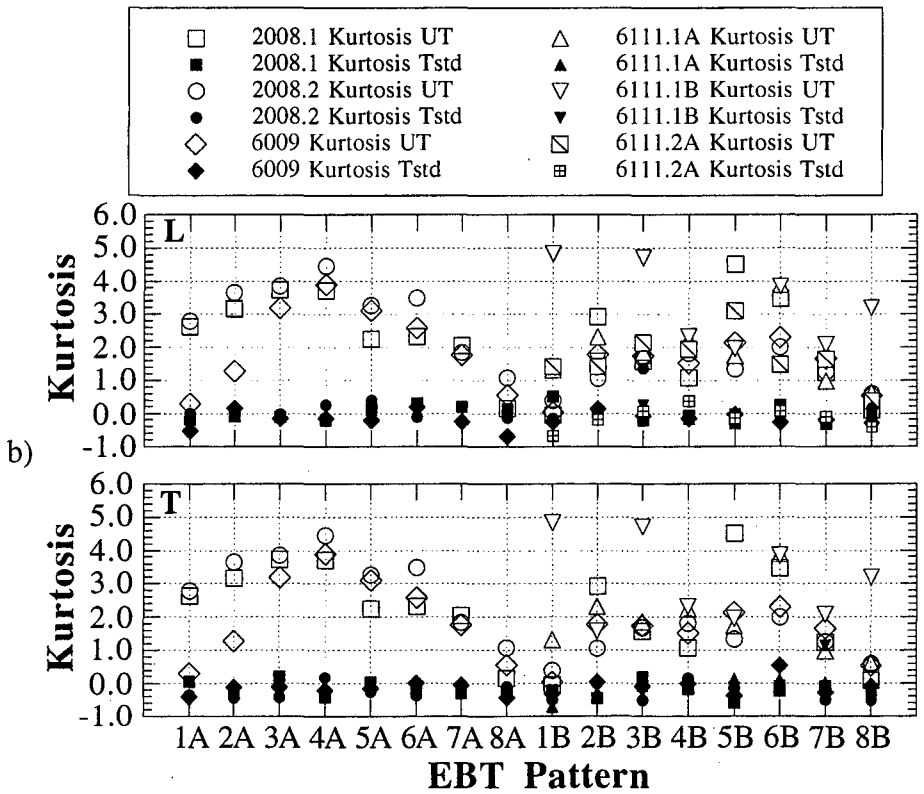

Figure 39 a) 3D Skewness and b) 3D Kurtosis for untested versus tested longitudinal specimens and tested transverse specimens showing homogenization of the different surfaces.

The homogenization of all tested patterns, regardless of starting size, depth, and distribution is illustrated in Figures 38 and 39. The R_a roughness calculation displayed in Figure 38 reveals that the differences between the untested patterns lessen dramatically for the tested specimens because of surface roughening from individual grains and groups of grains rotating to accommodate strain in the specimen. The R_a plots for the different alloys also show the greater tested roughness of the 2008-T specimens. The skewness and the kurtosis of the tested surfaces show the same homogenization effect (Figure 39).

3.5.3 Influence of Single-Sided vs. Double-Sided Test on Tested Surface Appearance

For MF surfaces the degree of roughening on the tested surface facing the fixed male bead was the same whether the test was performed using the fixed bead setup or the mixed bead setup (Figure 40). This indicates that there should be no practical difference in the resulting post-test surface appearance between single sided and double sided tests.

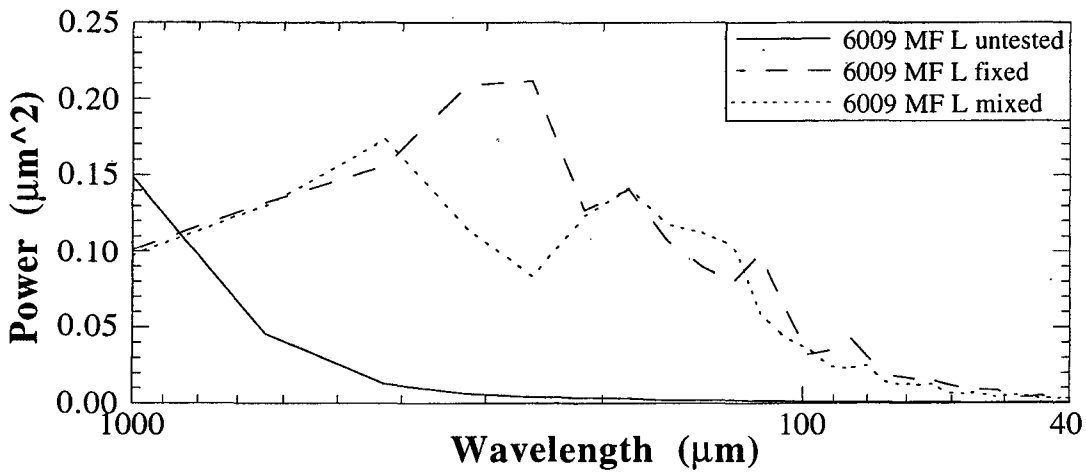

Figure 40 Plot of wavelength change for fixed and mixed MF sheet tests showing same degree of roughening.

3.5.4 Change in Lubricant Carrying Capacity After Testing

The measured lubricant carrying capacity results for each pattern both before and after testing, where the tested surface volumes include surface roughening effects, are compared in Figure 41. For both tested directions of the 2008 EBT sheets, the starting surface volume had virtually no effect on the ending volume, indicating that the ending volume was overwhelmingly dependent on the large amount of surface roughening. For both the 6009 and 6111 EBT sheets, however, there was a slight dependence on the initial volume, indicating that the roughening did not completely remove the possibility of post-DBS pattern effectiveness for these alloys.

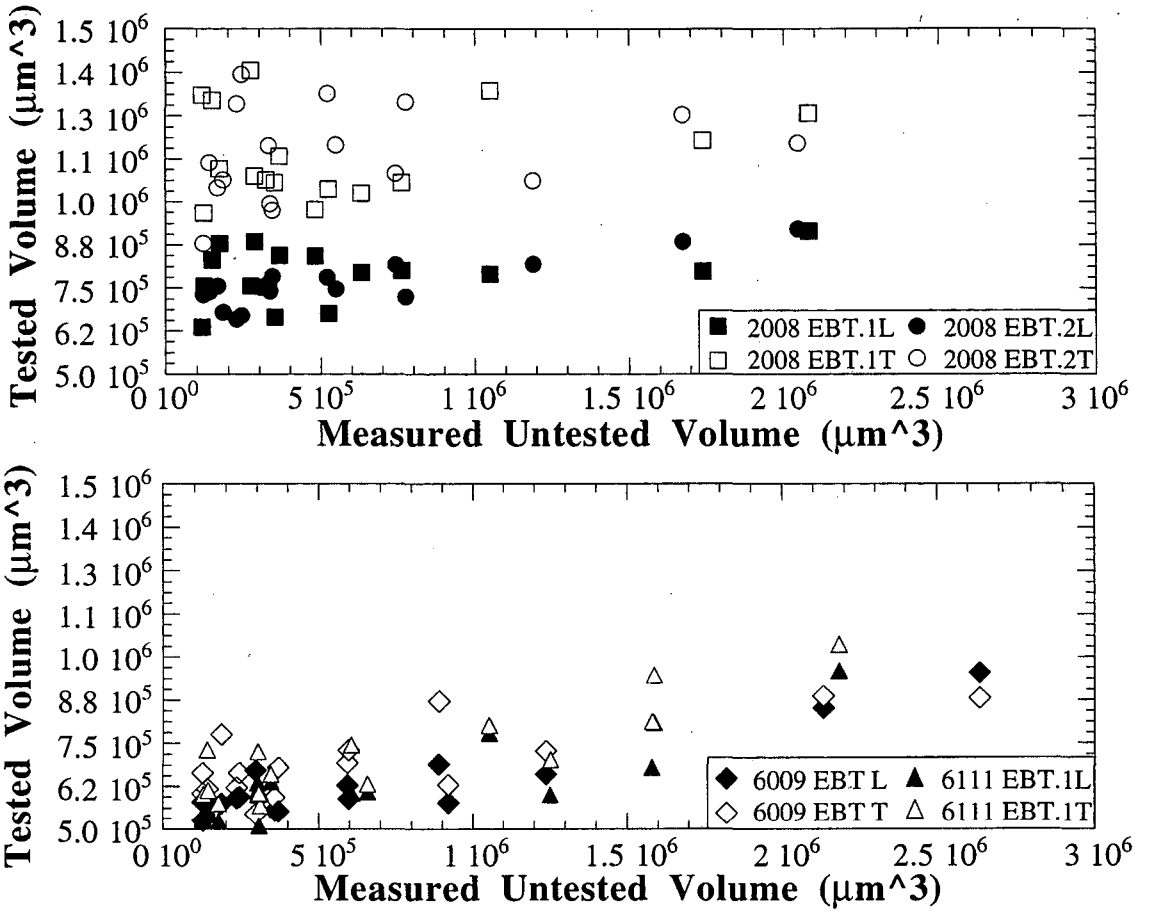

Figure 41 Plot of tested versus untested pattern lubricant carrying capacity, where the tested volume includes surface roughening effects.

The height histogram of the large ring patterned tested surfaces did not show the bimodal distribution characteristic of the untested surfaces (Figure 11), where one spike represented the unpatterned MF surface height and the other spike represented the ring depth. Instead, the histogram of the tested surfaces (Figure 42) showed a spread of heights distributed around a central point, as with the histogram of the untested small ring patterned surfaces, but with much wider peaks.

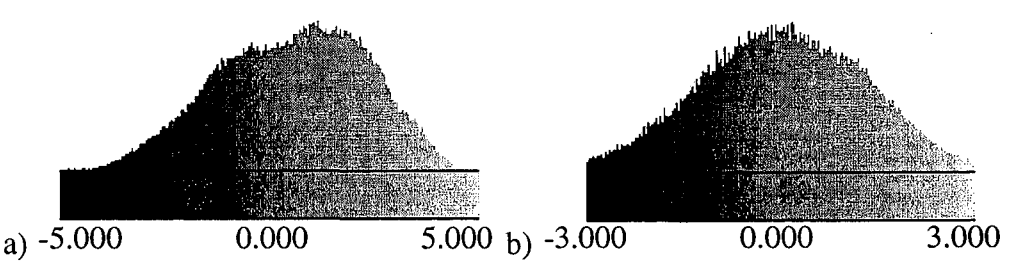

Figure 42 Height histogram of tested surfaces, a) large and b) small rings, with the tested surfaces for the deeper patterns showing a loss of the distinctive representation of the discrete pattern.

As with the height histograms, the bearing area curves of the tested surfaces also indicate a removal of the isolated lubricant pocket effectiveness (Figure 43). Instead of the distinctive knee in the untested pattern representation, the tested bearing area curve shows a smoother distribution. It is striking to note that the initial pattern did not greatly affect the tested bearing area. Figure 43 shows the similar final tested appearance for initially different patterns. The surface height change shown in these plots arises from a combination of the sheet surface being flattened from sliding over the test beads and from the surface roughening during testing. The tested bearing area curves for the MF and the EDT patterns are similar to the tested EBT patterns shown below.

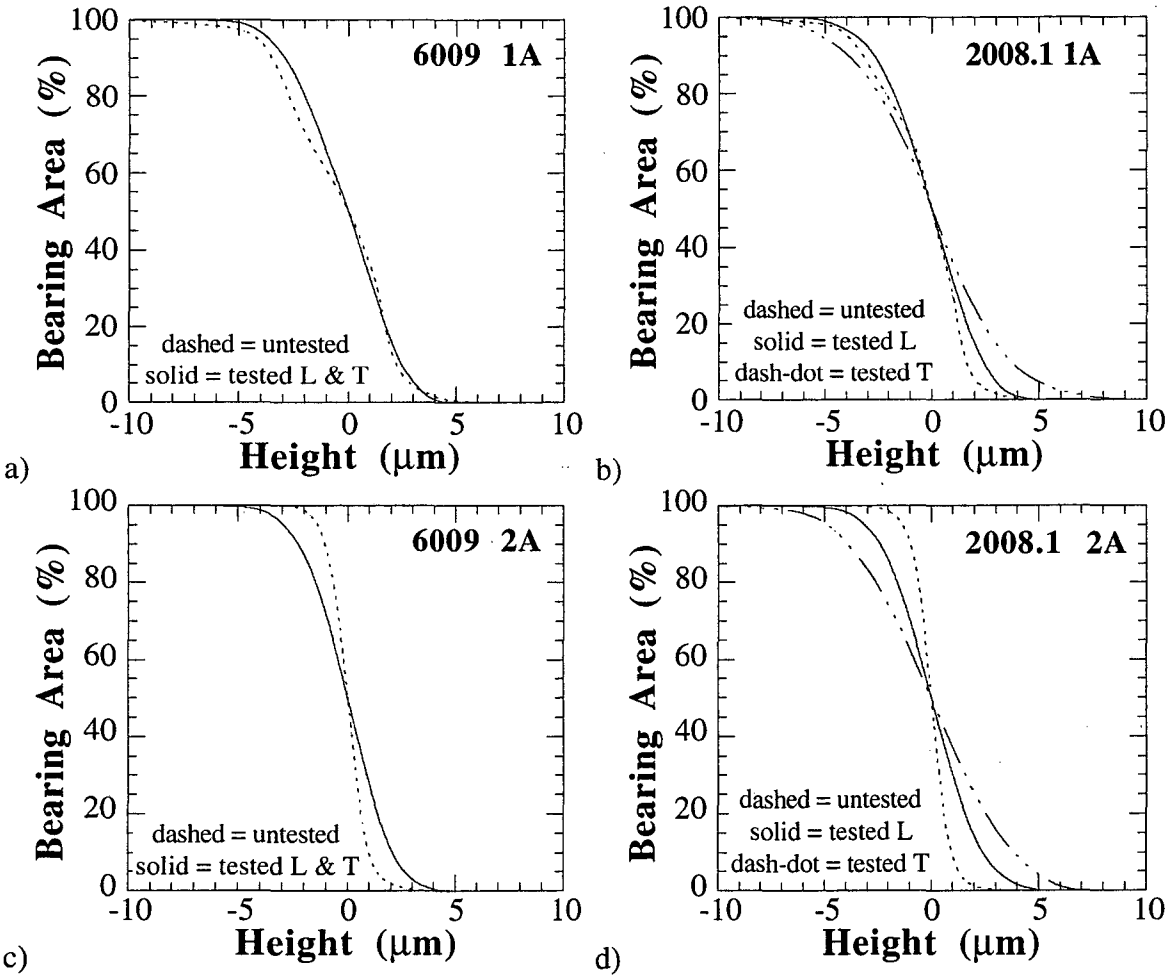

Figure 43 Bearing area curves for tested a) 6009 EBT 1A, b) 2008.1 EBT 1A, c) 6009 EBT 2A, and d) 2008.1 EBT 2A patterns. a) and b) show a removal of the lubricant pocket effectiveness (no more knee) for the deeper patterns, while all plots and show a change in the overall height for the tested surfaces.

4. DISCUSSION

The results given above are combined and discussed as three main points. These include validity of the results from the fabricated test machine, material properties and effects, and pattern effects. Material and pattern effects are combined in a fourth section to develop a constitutive equation for use in predicting the forming friction of EBT patterned surfaces.

4.1 Validation of DBS Test Results

As with any fabricated machine, validity of the test results from the DBS tester was of some concern, and so measures were taken to explore both the machine and the specimen parameters. Seven main areas of investigation took place to ensure confidence in the test data. First, die deflection was measured to ensure that the test strip was not being pinched during drawing. Second, two different setups were tested on the fabricated machine and the results compared to ensure consistent performance from the machine. Third, testing was performed on another DBS machine to check if results were similar. Fourth, bluing tests were performed to measure the actual contact angle of the sheet with the test beads. This was done to check the simple assumption of halving the geometric angle of contact for single-sided tests (Section 1.8, Eqn. 2) as well as to check for skipping of the test specimen over the male fixed bead. Fifth, the two specimen widths described above were tested both single-sided and double-sided on both machines, also to check the geometric contact angle assumption and to check any other synergistic effects. Sixth, two different specimen widths were tested both locally and on the Denver machine to ensure confidence in the results from using 25.4 mm (1.00 in) wide specimens versus 50.8 mm (2.00 in) wide specimens. Last, estimated error calculations were performed to check if specimen scatter was greater than what was reasonably expected.

4.1.1 Machine Validity

Validity of the DBS test machine was confirmed by four main results. These included die deflection, consistency within the fabricated machine's test setups, consistency between the fabricated machine and another DBS test machine, and comparison of estimated error to actual test scatter for the test setups.

Movement of the dies during testing was of concern, because there was the possibility of pinching the test strip with the consequence of falsely high forming friction values.[D1] The die deflection tests, performed to ensure maximum possible die deflection, showed that die movement was minimal and that the test strip was not being pinched during testing.

The second step confirming the validity of the fabricated machine was the repeatably linear relationship between the gauge setup tests and the load cell setup tests

(Figure 21). This relationship shows that the behavior for the machine remained the same between the two setups, with only the numerical value of the forming friction changing slightly. This robust behavior lends confidence to both the trends recorded by the machine and to the numerical values calculated from the test results.

Perhaps the most important confirmation of the results from the fabricated machine was the comparison testing performed on another DBS machine at the University of Colorado, Denver. The linearly consistent difference between the DBS forming friction values for the two machines (Figure 22) indicates that they are not identical, but repeatably similar enough for their differences to be corrected. The relationship also indicates that the fabricated machine is similar enough to the Denver machine to be considered a candidate for the round robin testing the NADDRG performs to standardize results between different DBS machines.

The final confidence in the output of the test setups came from calculating the estimated error for those setups. The fact that the error calculations and the test scatters were within one percent of each other indicates that both the fabricated machine and the Denver machine were performing within reasonable expectations. These calculations also indicate that the desires of some to reduce the test scatter of a given material and pattern to less than 1%, both within and between machines, are unrealistic, unless the machine error can be reduced substantially through machine redesign and by using load cells of even greater accuracy.

4.1.2 Specimen Validity

Confidence in the forming friction values obtained from the different specimens and test configurations used came from three main areas of investigation. These included measurement of the actual contact angle between the test specimen and the fixed beads, comparing single- and double-sided tests, and comparing test results for two different specimen widths.

Contact angle measurements obtained from bluing tests gave two main results. First, they showed that the specimen thicknesses tested here did not skip when travelling over the test beads. This was important, as other research indicated some material thicknesses may do so, influencing the final output of the tests. [D2] Second, the measurements showed that the specimen contact with the male bead is greater than the summed female bead contact and that the sum of these contact angles did not equal the assumed contact angle used in the forming friction equation (Eqn. 1). The slight difference from the assumed angle is a possible source of error between different machines, as contact angles may vary based on manufacturing differences. For single-sided specimens the implication is that the forming friction values would be slightly

higher than for double-sided test results, as the single-sided test contact angle is actually greater than half the double-sided test contact angle (see Section 1.8). Since the measurement of the contact angle varied slightly within the bluing tests performed, better confirmation of single- and double-sided test differences was needed. This was obtained by performing mixed and fixed bead tests both locally and at Denver.

Figure 24 shows that both the Denver results and the local results show a repeatably linear increase in the DBS-μ value of approximately 7% for single sided tests over double sided tests, agreeing with the bluing test results. Because of this difference, if it is necessary to compare single-sided and double-sided test results, double- and single-sided calibration tests should be run using material similar to that which will be tested but with the same nominal pattern on both sides. These tests should give a plot similar to Figure 24, where the effect of contact angle differences can be quantified and corrected for. The slight difference between the single-sided versus double-sided slope for the two machines in Figure 24 likely arises from the differences in design and manufacture of the two machines resulting in slightly different die deflections during testing and therefore different contact angles.

The last constraint on specimen configuration was imposed by the patterning layout of the EBT sheets (Figure 8). In order to obtain enough specimens per pattern, 25.4 mm (1.00 in) wide specimens were used rather than the more commonly used 50.8 mm (2.00 in) wide specimens. To confirm the use of this narrower specimen, both single-sided and double-sided tests were performed both locally and on the Denver machine using the two specimen widths. Despite their manufacturing differences, both machines display a one-to-one linear relationship between the two specimen widths tested. This relationship, shown in Figure 25, confirms the acceptability of using 25.4 mm (1.00 in) wide specimens versus 50.8 mm (2.00 in) wide specimens for the sheet thicknesses tested here and agrees with the same conclusion reached by Schey for 0.82 mm (0.032 in) thick electrogalvanized steel specimens.[D3]

4.2 Material Effects

The effect of the material properties of these alloys fall into three main areas of interest. First, the composition and processing of the alloys affect their tensile and frictionless forming properties. Second, these tensile and frictionless forming properties indicate an influence on the forming properties with friction. Third, processing apparently affected the post-test surface roughening of the sheets.

4.2.1 Effects of Composition and Processing on Mechanical Properties

Even though the alloys were split ingot cast, leading to the expectation that neither composition (Table 5) nor fabricating practice should affect the formability, the final

processing of MF, EDT, and EBT pattern rolling did appear to affect the mechanical strengths and elongations of AA2008. While these tensile differences were small, they are significant based on the frictionless forming properties of the alloys. The roller bead pulling forces shown in Figure 14 display the same effect as the tensile properties, but to a greater degree. That is, the directional differences both within and between the alloys is significantly repeatable, suggesting that the DBS drawing loads may display a directional dependence on mechanical strength. For the frictionless drawing forces it is possible that the greater differences arise from the cyclic nature of the deformation involved in the DBS test versus the unidirectional deformation of the uniaxial tensile test.

Two possibilities for these differences exist, keeping in mind that the fabricating process was supposed to be identical. First, it may be that residual strain from the discrete impressions, combined with some possible variation in various reductions during rolling to identical final thicknesses, resulted in these differences. It was assumed that polishing of the specimen faces removed all residual deformation from the pattern, which may not actually be the case. One way to check if the surface impressions are responsible would be to perform microhardness tests across the width of mounted, polished cross-sections of MF, EDT and various EBT patterns. Another way to check different pattern influence for the 2008 and 6009 alloys would be to tensile test both unpolished and polished specimens from each pattern, as was done in the longitudinal direction for AA6111 EBT1.

A second cause of the tensile and frictionless drawing force differences may be that the processing was not identical. It is possible that different processing resulted in different dominant textures in the two AA2008 EBT sheets. While the exact texture of the alloys tested here is unknown, support for texture being the likely cause of the directional formability differences for the 2008 alloy sheets was found in the literature. Zonker, et al., found the predominant textures of AA2008 sheet, processed around the same time as the material tested here, are cube and Goss.[D4,D5] They found anisotropy during forming of a 2008 alloy containing both textures (cube and Goss both with intensities of 11) and found an increase in the isotropic formability of a 2008 alloy processed to have a cube texture (cube intensity 10, Goss intensity 1). This result demonstrated the greater anisotropic effect of the Goss texture compared to the cube texture. In addition to this, Zonker has observed the same effect on pulling forces displayed in Figure 14 for the alloys tested here.[D5] He performed texture measurements on his material and ascertained that the greater Goss texture was the cause of the forming anisotropy for AA2008. He also found indications that closer pulling load values

between the longitudinal and transverse directions for aluminum alloys indicated a greater percentage of the more isotropic cube texture.

Interestingly, both AA6111 and AA6009 are also known to contain a mixture of cube and Goss textures, yet these alloy sheets did not show the anisotropic forming behavior in the roller bead tests that the 2008 alloy sheets did.[D4,D5] For AA6111 the intensities of cube (4) and Goss (5) cited by Zonker, et al., however, indicate a lower anisotropic texture effect in this alloy, and the AA6009 intensities of cube (8) and Goss (4) indicate a greater effect from the more isotropic cube texture. Story, et al., also indicate both the lesser degree of anisotropy in AA6111-T4 and the virtual lack of anisotropy in AA6009-T4 versus AA2008-T4 with their data on planar anisotropy gathered from tensile tests where they measured the plastic strain ratio, and state that planar anisotropy's effect on formability is an issue.[D6] As discussed earlier, planar anisotropy is an issue because the directional properties of an alloy affect its directional formability. The desired properties of a forming alloy are for it to have the same properties in all directions, preventing worry about preferential deformation and tearing in a particular sheet direction, and resulting in a more robust manufacturing condition. It is recommended, therefore, that sheet be processed to have properties that are as non-directional as possible to optimize formability.

4.2.2 Effect of Mechanical Strength on Forming Friction

The influence of mechanical strength on forming friction for nominally identical patterns between different alloy sheets is illustrated in Figure 28; this effect occurred in both the longitudinal and the transverse directions for all patterns tested. The increase of forming friction with mechanical strength indicates that the desired aluminum alloy should be formed at the lowest strength possible, then strengthened after forming. This is currently a common practice in the automotive industry because of the greater elongation possible with the -T4, or naturally aged, condition; the material is then strengthened by precipitate growth during the paint bake cycle.

A possible mechanism as to why the forming friction scaled monotonically with mechanical strength is that the mechanical strength of these alloys influenced the micro-PHD effectiveness of the imprinted patterns. The total spread of friction values for the EBT 6009 patterns was 40% in the L direction and 22% in the T direction, compared to EBT 2008.2 patterns which showed a 24% spread in the L direction and a 12% spread in the T direction. The greater strength of the 2008 alloys may have reduced the pliability of the discrete patterns in forming a micro-PHD seal against the drawbeads during testing. This is supported by Schey's citation of Kato, et al., that for a sheet with a

deterministic topography a critical pressure must be reached before the micro-PHD mechanism is activated, and this pressure is higher for harder sheet.[D7,D8]

4.2.3 Effect of Alloy Properties on Post-Test Surface Roughening

In addition to frictionless forming properties, alloy processing apparently affected the surface roughening of the tested sheets. Surface roughening is of concern both during the forming process and in the finished sheet surface appearance. During the forming process, if the surface parameters change from those expected, prediction of formability will be made that much more difficult. An additional concern for a formed sheet is that greater surface roughening may result in an unacceptable painted surface appearance, leading to part rejection.

4.2.3 #1 Surface Roughening

In the alloys tested here, a greater degree of surface roughening was observed for all 2008 patterned sheets over the 6009 and 6111 sheets. When compared to the smaller grain size of the 6009 alloy sheets of the same thickness, this result is consistent with both Andersson and Balbach, who observed greater roughening for larger grained materials.[D9,D10] Interestingly the 6111 and 6009 alloy specimens roughened approximately the same amount for the similar patterns despite their three fold difference in the rolling plane grain size. Their grain thicknesses, however, were similar, lending support to the proposal by Jain, et al., that grain thickness is the most important grain size parameter when considering surface roughening resulting from an applied stress.[D11] The basis for this proposal arises from consideration of the out-of-plane rotation of individual grains and groups of grains of similar texture. The thicker the grain, the more it may stick out when rotating to accommodate strain in the material.

The different roughening observed within an alloy type, with the EBT 2008.2 specimens exhibiting greater post-test roughening than the EBT 2008.1 specimens, may arise from the thicker grains in the higher roughness sheets, as well as it may result from the texture effect discussed above. Support for the latter contention comes from the roller bead pulling loads indicating a greater amount of anisotropic texture in the EBT 2008.2 sheets than in the EBT 2008.1 sheets (Figure 14). This texture effect has been observed elsewhere, with the roughening of the surface in a particular direction being labeled "ridging."[D12]

The roughening of all specimens tested here almost completely destroyed discrete surface patterns that were at or below 2 μm (79 μin) in depth. If discrete patterns are completely destroyed travelling through the drawbead portion of the press, the lubricant carrying properties of the post-drawbead deformed surface will vary greatly compared to non-drawbead deformed areas. As the isolated pits generate micro-PHD lubrication

which reduces forming friction, loss of these discrete pits will have a detrimental effect on the sheet forming friction. The difference between hydrostatic lubrication and its loss was dramatically demonstrated by Lin and Wang.[D13] They performed deep drawing on an aluminum sheet using a punch, where part of the flange section of the punch was patterned with lubricant carrying pits. During the part of the forming process where hydrostatic lubrication took place, resulting from the pit presence, the forming friction dropped. When the process lost the hydrostatic capability and shifted to boundary lubrication, the forming friction increased.

4.2.3 #2 Formability and Paintability Implications

Surface roughening during forming alters the surface characteristics of the sheet, and consequently alters the formability of the sheet. While the DBS test has been linked to the overall formability performance of patterns and lubricants, the roughening observed here leads to the expectation that the material that travels through the drawbead will have dramatically different forming properties from patterned areas that have not undergone the cyclic deformation. It is also possible that this same caution applies to material drawn over the die edge, where roughening has been observed on the free surface.[D10] If the majority of deformation to form a part takes place on material that has not undergone drawbead or other free-surface bending deformation, however, the deterministic EBT surface should maintain its desired micro-PHD capabilities. For non-bending deformation, asperity deformation takes place with the discrete cavities acting as pressurized reservoirs of lubricant that feeds out to the rest of the sheet as the asperities flatten and the volume of held lubricant decreases with decreasing cavity depth.[D10]

Increased roughening of post-DBS tested surfaces varied in wavelength from 150 to 650 μm (0.006 in to 0.026 in). The spread in the additional wavelengths indicates that single grains as well as groups of grains are rotating during the forming to accommodate internal strain in the specimens. The limit of approximately 500 μm (0.020 in) for a paintable surface indicates that, while most of the surface roughness may be painted over without a problem, the longer wavelength contributions will show through to the finished surface. For both optimum formability and optimum paintability, therefore, the recommendation at this point is to keep the roughening to a minimum by keeping the grain size both in the rolling plane and through the thickness as small as possible.

4.2.3 #3 Mill Finish Pattern Roughening

While roughening is an undesired effect for the EBT patterns tested here, it can be said that it may actually be beneficial for the formability of the highly directional MF pattern. Saha and Wilson observed an improvement in the forming friction of mill finish AA1100-H14 sheet tested in the longitudinal direction resulting from the roughening

during the test reducing the contact between the sheet surface with the toolpiece.[D14] This indicates that, for formability purposes, roughening of the mill finish patterned sheet may actually be a desired occurrence. For paintability purposes, however, the same cautions apply as for EBT patterned sheets.

The degree of roughening for the mill finish patterns tested here was directionally the same whether the test was double-sided or single-sided, as is illustrated in Figure 40 for the longitudinal direction of AA6009. This indicates that the roughening seen here for the EDT and the EBT patterns for the single-sided test would also be similar for the double-sided test. This arises from the fact that the sheet surface facing the male fixed bead undergoes the same bending and sliding processes during both single- and double-sided testing.

4.3 Pattern Effects

The patterns imprinted on the alloys tested here clearly affect the forming friction properties of these alloys. The effect of sheet reduction and roll wear on pattern smearing and on forming friction is discussed, and the effects of the different patterns are compared. Pattern comparisons are grouped as MF versus EDT, MF versus all EBT, and EBT versus different EBT.

4.3.1 Effect of Sheet Reduction and Roll Wear

The pattern elongation differences between the AA2008/AA6009 patterns and the AA6111 patterns shown in Figures 15 through 17 likely correspond to the amount of sheet reduction, for it has been demonstrated that pattern smearing increases with an increase in final sheet thickness reduction.[D15] For reductions over 9%, pattern transfer to the sheet was unacceptable because the amount of smearing completely destroyed the desired pattern. This smearing of the pattern from the final reduction of the aluminum sheet has essentially the same effect on the pattern as slipping during rolling. The degree of pattern elongation obviously influenced surface volume lubricant carrying capacity (Figure 20), as well as changed the surface from what was desired, i.e., the mirror image of the roll surface. Figure 44 illustrates how a smeared imprinted surface could result from the ideal roll surface slipping during the rolling process. It is important to note that too great of a smearing effect can destroy the whole idea behind the surface patterning in the first place, i.e., imprinting discrete surface microcavities to maintain micro-PHD lubricant pockets during forming in order to reduce friction.

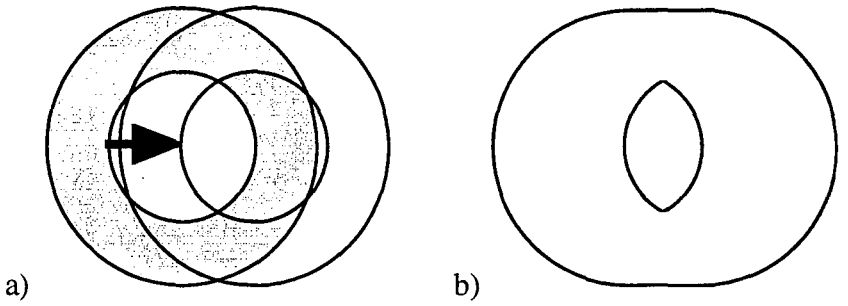

Figure 44 Schematic of a) how an ideal pattern on a roll smears on the sheet surface during rolling, b) resulting in an elongated pattern appearance.

While thickness differences and large pattern differences between the AA6111 sheets and the other alloy sheets make direct comparison of forming friction results difficult, it can be noted that the correlation of decreasing longitudinal forming friction with increasing pattern volume for the 2008 and 6009 alloy sheets did not hold for the 6111 alloy sheets for two reasons. First, as indicated above, smearing of the surface pattern during final sheet rolling reduction can wipe out the desired isolation of the imprints. This destruction was the case with the AA6111 sheet surfaces, where smearing was such that some of the surface patterns overlapped in the rolling direction of the sheet. Second, not only did the pattern overlap result in semi-continuous valleys along the rolling direction of the sheet, the smearing displaced material upward above the main sheet surface. The smearing resulted in a greater measured lubricant carrying capacity, but that larger lubricant carrying capacity also represented a greater amount of material that had been forced upward during rolling, above the sheet surface. This uplift created a series of discrete contact points that prevented the sheet from reaping the benefits of the micro-PHD capability of the discrete microcavities. Instead, the sheet rode on these contact points during the test, with higher forming friction resulting from a larger contact area which arose from a greater amount of uplift in the larger patterns (Figure 33).

In addition to smearing, roll wear may affect the forming friction by changing the size and shape of the desired microcavities, as is evidenced in Figures 17 and 33. Previous research has shown that wear of EDT rolls affects the resulting sheet surface output by shifting wavelength contributions in the power spectra toward longer wavelengths.[D16] Research here demonstrates that roll wear is also of concern for EBT surfaces, perhaps more so because of the desired perfection and discreteness of the microcavities in the final surface.

4.3.2 Mill Finish and Electro-Discharge Texture Patterns

All mill finish and EDT patterned material behaved as expected, based both on the surface topography and on other data available in the literature.[D8,D17,D18] The surface

topography of the mill finish pattern is highly directional, and indicates quite clearly the lubricant retention capability, or lack of it, in the different sheet directions. The topography of the EDT patterns are much more non-directional, indicating a similar lubricant retention effect in all directions of forming. Insufficient EDT pattern variety was available to conclude absolutely that wavelengths under 500 μm (0.020 in) affect the forming friction more than wavelengths over 500 μm (0.020 in), but based on the reasoning behind that finding there is no reason to suspect that it is not also the case for aluminum alloys.

4.3.3 Electron Beam Texture Patterns

Figure 26 illustrates the fact that all the discrete patterns tested here show a vast improvement in equalizing the longitudinal and transverse forming friction properties over the highly directional mill finish surface. Story and Englemann, who tested double-sided DBS specimens of AA6009 with eight patterns matching on both sides, also found this improvement.[D17] Differences between those results and load cell single sided test results are illustrated in Figure 45. The differences in friction values for the two test sets, which would be even greater if the single sided test results were reduced by 7%, partly arise from the differences in manufacturing between the two test machines, similar to the differences between the forming friction results obtained from the Denver machine and the fabricated machine. Some of the differences may also arise from the double sided specimens having effectively different patterns on the two sheet sides from roll wear, as with the 6111 sheets tested here. This would change the overall test value from a single sided test, as the second pattern may act either beneficially or detrimentally on the first pattern's effects.

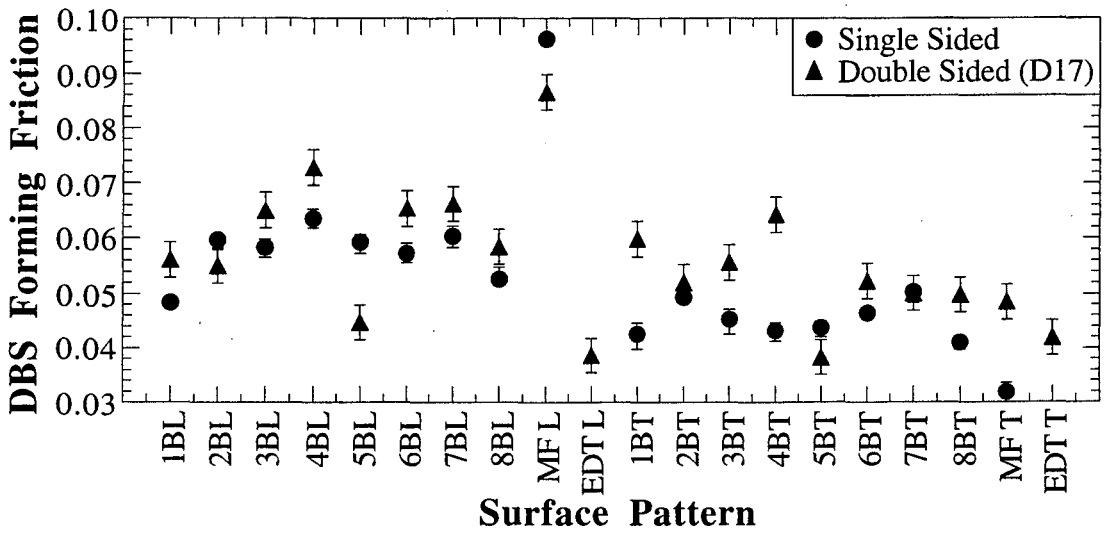

Figure 45 Comparison of load cell mixed bead test data to fixed bead test data for similar surfaces tested elsewhere (D17).

4.3.4 Lubricant Carrying Capacity

The ideal volumes calculated from the roll surface information did not correlate as well as the measured sheet pattern volumes with longitudinal forming friction of the sheets because transfer of the ideal roll pattern to the sheet surface was degraded both by smearing and by roll wear. The scatter in the dependence of forming friction on both pattern volume and pattern area most likely arose from the method that was chosen to calculate these parameters. Despite the scatter, the best way to determine the lubricant carrying capacity of a sheet is from the actual sheet surface rather than from information about the roll surface. If pattern transfer effects are well understood, however, a general idea of material behavior with a particular pattern volume may be obtained from ideal pattern information corrected for these effects.

The fact that the forming friction for all alloys tested in the transverse direction was essentially independent of both pattern volume and area arises from the residual MF pattern on the alloys. This indicates that the discrete patterns work extremely well in the longitudinal MF direction, where no other surface feature is available to hold the lubricant in place, but are less important when other surface patterns beneficially influence the surface's lubricant carrying capacity and micro-PHD capability.

4.4 Constitutive Equation Relating Forming Friction to Sheet Parameters

In order to develop a constitutive equation relating DBS forming friction to sheet parameters, those parameter must first be defined. Based on the results discussed above, two independent variables come to light. These variables are pattern lubricant carrying capacity (Figures 29 and 31) and material strength (Figures 14 and 28). The general form of a constitutive equation based on these two variables would be

$$\mu = \mu_0 + a*L + b*\sigma \qquad \text{Eqn. 7}$$

where μ_0 is a constant, a represents the dependence of forming friction on pattern lubricant carrying capacity, L is the lubricant carrying capacity, either volume or area, b represents the dependence of forming friction on material strength and σ is the material strength, either flow stress or bending deformation. The constants are the slopes obtained from plotting forming friction versus the active parameter in two dimensions, where both the dependencies noted above are directionally linear for the range of values tested here. It should be noted that, based on the differences discovered between the fabricated DBS machine and the University of Colorado, Denver DBS machine, as well as the differences between double sided testing and single sided testing, the absolute value of these dependencies will vary slightly from test setup to test setup, as will the value of μ_0. The

dependencies should, however, remain directionally the same, with forming friction dropping with increasing pattern volume and rising with increasing material strength.

The dependence of forming friction on pattern lubricant capacity for ideal calculations and measured calculations were found to be directly linear over the entire range for volume and area, respectively. As the ultimate tensile strength obtained from a uniaxial tensile test has been used in previously derived equations representing forming processes as a direct substitution for the material's flow stress, it was chosen over bending deformation as the material strength parameter for these equations.

Using the above form of the equation for the ideal surface volume calculated from the roll surface patterning information, and assuming the same smearing as seen here with the 6009 and 2008 alloy sheets, the equation becomes

$$\mu_L^i = \mu_{L_0}^i + c * V_i + b * \sigma_{UTS} \qquad \text{Eqn. 8}$$

where c is the two dimensional linear dependence of forming friction on ideal pattern volume, V_{ideal} is the ideal volume calculated from information about the roll surface pattern, b is the two dimensional linear dependence of forming friction on tensile strength, and σ_{UTS} is the tensile strength measured from a uniaxial tensile test. For measured surface area, the equation would be

$$\mu_L^m = \mu_{L_0}^m + a * A_m + b * \sigma_{UTS} \qquad \text{Eqn. 9}$$

where a is the two dimensional linear dependence of forming friction on measured pattern area, A_m is the surface volume measured directly from the sheet surface pattern, b is the same as for the ideal calculation, and σ_{UTS} is the tensile strength.

As the transverse friction properties were both lubricant carrying capacity independent, the forming friction may be represented by the equation

$$\mu_T = \mu_{T_0} + b * \sigma_{UTS} \qquad \text{Eqn. 11}$$

For all three of the above equations, a least squares fit in three dimensions was used with the two dimensional curve fits to give

$$\mu_L^i = -0.216 - 1.25\text{x}10^{-8} * V_i + 1.01\text{x}10^{-3} * \sigma_{UTS} \qquad \text{Eqn. 12}$$

$$\mu_L^m = -0.203 - 3.21\text{x}10^{-8} * A_m + 1.01\text{x}10^{-3} * \sigma_{UTS} \qquad \text{Eqn. 13}$$

$$\mu_T = -0.351 + 1.50\text{x}10^{-3} * \sigma_{UTS} \qquad \text{Eqn. 14}$$

where the friction value scatter for all equations is approximately ±0.005. The large μ_0 for all equations results from forcing the curve fit to the two dimensional parameters and from the assumptions of linearity through the origin for the three dimensional fit of the parameters.

Further investigation using materials with greater strength differences and greater volume differences should be performed to investigate the robustness of this equation, as there is no guarantee that the linearity observed for the present results will remain for a larger range of volumes or material strengths. For example, it is very likely that there exists an upper volume or area limit beyond which the forming friction will be represented by the shear strength of the lubricant itself. Similarly for material strengths, a lower limit of forming friction will be obtained below which a reduction in material strength will not result in a reduction in forming friction.

5. SUMMARY

A draw bead simulator was designed and fabricated to determine the dependence of forming friction on discrete surface patterning. The test results from this machine were validated using comparison tests both within two different test setups and between the fabricated machine and a machine at the University of Colorado, Denver. Automotive aluminum alloys with mill finish, electro-discharge texture and electron beam texture patterning were tested. Analysis of the surfaces indicated that Fourier transformation was useful for the more random surfaces, such as EDT and post-test roughening.

All of the EDT and EBT patterns decreased the difference between longitudinal and transverse forming friction values compared to the anisotropic MF pattern, which should translate into better bi-directional forming properties for these patterns. The forming friction of EBT patterned specimens in the rolling direction of the sheet displayed an inversely linear dependence on both pattern volume and area, and a monotonic dependence on material strength. These properties were combined into a constitutive equation for use in predicting the forming friction of other patterns that may be used on these alloys and for use in future EBT pattern design. Transverse forming friction properties for the EBT patterns appeared to be overwhelmed by the residual mill finish pattern, indicating that discrete patterns are most useful when no other beneficial patterning already exists.

Post-DBS test roughening of all patterns appeared to scale with grain thickness, with thicker grains causing greater roughening and resulting in discrete EBT patterning less than 2 μm (79 μin) in depth being completely destroyed. Anisotropic roller bead behavior and greater roughening for the 2008 sheets, known as "ridging," were attributed to texture effects.

6. CONCLUSIONS

The desire to increase the use of sheet Al alloys in automobiles necessitates investigating these alloys to improve the understanding of their part formability. This understanding encompasses the behavior of the entire sheet, from the effect of processing on mechanical properties to the effect of surface patterning on lubricant retention. The most striking result of the work performed here, that discrete pattern area linearly affects sheet forming friction, can be used as a guide for future EBT pattern design.

6.1 Patterning

As both EDT and EBT patterning equalized the bi-directional forming properties evident with the mill finish patterning, both are recommended over the anisotropic MF pattern. For EBT patterning, as post-test roughening obliterates patterns under 2 μm (79 μin), a pattern depth greater than 2 μm should be used. In addition, as this work showed that greater pattern areas lead to lower forming friction, a greater pattern area rather than a lesser pattern area should be maintained in order to maximize the micro-plastohydrodynamic effects of the discrete cavities. In order to maintain paintability, however, pattern dimensions should remain below 500 μm. For both EDT and EBT patterning, roll wear should be carefully monitored during the patterning roll in order to prevent a detrimental influence on the pattern transferred to the sheet.

6.2 Material

Since forming friction scaled with material strength, the formability of a material should be maximized by keeping the -T4 strengths as low as possible. Another way to maximize bi-directional formability is to keep the texture of a material as isotropic as possible. Keeping the texture isotropic should also reduce the amount of anisotropic deformation induced surface roughening, or "ridging," which could detrimentally affect both the subsequent formability and paintability. Keeping a material's grain thickness as small as possible should also reduce roughening from grain rotation by reducing the amount of material that may stick out of the sheet surface.

7. FUTURE WORK RECOMMENDATIONS

It is essential that future work continues to investigate the different parameters that affect sheet formability. These include surface patterning and material parameters as well as understanding the various influences within the chosen forming simulation test. Based on the work performed here, some specific recommendations are made for future investigation.

7.1 Patterning

In order to find if there is an upper limit to the forming friction dependence on EBT pattern area, imprint a sheet with greater pattern areas than those used here. The knowledge from these experiments will help determine if the linear relationship found here remains linear over a wider array of pattern areas, and will assist in determining if there is an upper limit to the beneficial micro-plastohydrodynamic effect provided by the discrete cavities.

7.2 Material

Tests on EBT patterned material should be performed using materials with a wider range of mechanical strengths than those tested here in order to determine more clearly the influence of mechanical strength on DBS forming friction. This information would be valuable in furthering the understanding of formable materials and may influence material choice for parts in the future.

7.3 DBS Test

To further explore the difference between male and female bead contact influence on the output of the DBS test, perform DBS tests using the same side of specimens cut from a single sheet with a single-sided test setup first using a fixed male bead then using a fixed female bead set. To expand understanding of the synergistic reactions of sheets with mismatched patterns on the two sides, test as above then test using fixed beads to explore the combined effects of the two sheet sides. This information is important in manufacturability of a sheet, as the patterning on both sheet sides does not always match to the degree desired.

8. REFERENCES

I1. P.J. Alvarado, *Steel vs. Plastics: The Competition for Light-Vehicle Fuel Tanks*, JOM, 48 (7), (1996) pp. 22-25

I2. J.R. Fekete, *Overview of Sheet Metals for Stamping*, SAE Paper No. 970715 SAE Trans.: J. Mater. and Manuf., 106 (5), (1997) pp. 125-137

I3. J.M. Story, G.W. Jarvis, H.R. Zonker, S.J. Murtha, *Issues and Trends in Automotive Aluminum Sheet Forming*, Sheet Metal and Stamping Symposium, International Congress and Exposition, Detroit, MI, SAE Paper No. 930277 in SP-944 (1993) pp. 1-25

I4. Aluminum: Properties and Physical Metallurgy, ed. J.E. Hatch, American Society for Metals, Metals Park, OH (1984)

I5. Personal communication with Harry Zonker, Alcoa, January 1998

I6. H.D. Nine, *Drawbead Forces in Sheet Metal Forming*, in Mechanics of Sheet Metal Forming, eds. D.P. Kaistinen and N.-M. Wang, Plenum Press (1978) pp. 179-211

I7. W.R.D. Wilson, *Friction and Lubrication in Sheet Metal Forming*, in Mechanics of Sheet Metal Forming, eds. D.P. Kaistinen and N.-M. Wang, Plenum Press (1978) pp. 157-177

I8. J. Schey, *Friction in Working 5052 Aluminum Alloy Sheet*, in Light Metals Processing and Applications, C. Bickert et al, eds., TMS of CIM, Montreal (1993) pp. 571-580

I9. R. Balbach, *Optimierung der Oberflächenmikrogeometrie von Aluminiumfeinblech für das Karosserieziehen (Optimization of the Surface Microgeometry of Aluminum Sheet for Autobody Drawing)*, Ph.D. Thesis, University of Stuttgart (1993)

I10. J.A. Schey, Tribology in Metalworking: Friction, Lubrication and Wear, American Society for Metals, Metals Park, OH (1983)

I11. J.A. Schey, *Friction in Sheet Metalworking*, SAE Paper No. 970712, SAE Trans.: J. Mater. and Manuf., 106 (5), (1997) pp. 113-124

I12 M.K. Smith and J.A. Dunn, *Lubricant Considerations for Automotive Sheet*, Lubrication Engineering, (Dec 1988) pp. 914-918

I13. S. Ashley, *Building an Aluminum Car*, Mechanical Engineering, (May 1994) pp. 65-68

I14. H. Hayashi and T. Nakagawa, *Recent Trends in Sheet Metal and Their Formability in Manufacturing Automotive Panels*, J. Mater. Proc. Tech., 46, (1994) pp. 455-487

I15. H.N. Han and J.P. Clark, *Lifetime Costing of the Body-in-White: Steel vs. Aluminum*, JOM, (May 1995) pp. 22-28

I16. K.R. Brown, M.S. Venie, and R.A. Woods, *The Increasing Use of Aluminum in Automotive Applications*, JOM, (July 1995) pp. 20-23

I17. K. Siegert, M. Ziegler, and S. Wagner, *Closed Loop Control of the Friction Force. Deep Drawing Process*, J. Mater. Process. Technol., 71, (1997) pp. 126-133

I18. J. Story, *An Investigation of Galling in the Formation of Aluminum Sheet*, Ph.D. Thesis, Michigan Technological University (1979)

I19. J.M. Story and K.J. Weinmann, *The Effects of Surface Topography and Surface Chemistry on Metal Buildup on the Tools During the Forming of Aluminum Sheet*, 8th Mfg. Engin. Trans. Proc. (1980) pp. 245-251

I20. R.A. Overfelt, J.J. Wert, and W.H. Hunt, Jr., *The Influence of Thermal Oxide Characteristics on the Frictional Behavior of Aluminum Auto Body Sheet Alloys*, Trans. ASME, 24 (2), (1981) pp. 175-185

I21. L.B. Sargent, Jr., *The Influence of Aluminum Oxides on the Transfer of Some Aluminum Alloys to Steel in Sliding Contact*, Lubrication Engineering, 38 (10), (1982) pp. 615-621

I22. P.C. Nautiyal and J. Schey, *Transfer of Aluminum to Steel in Sliding Contact: Effects of Lubricant*, Trans. ASME, 112 (4), (1990) pp. 282-287

I23. H. Ike, *Properties of Metal Sheets with 3-D Designed Surface Microgeometry Prepared by Special Rolls*, J. Mater. Process. Technol., 60, (1996) pp. 363-368

I24. R. Müller, *Evaluation of the Properties of Sheet with Lasertex Surface Texture*, Proc. 15th IDDRG, Dearborn, MI (1988) pp. 99-107

I25. G. Monfort, J. Defourny and A. Bragard, *Progress in the Roughness Texture of the Cold Rolled Steel Sheets Relating to Deep Drawing and Forming*, Proc. 15th IDDRG, Dearborn, MI (1988) pp. 91-98

I26. M. Imanaka, T. Fujiwara, T. Furubayashi, T. Obara, K. Tunoyama and K. Furukawa, *Development of High Image Clarity Steel Sheet by the Application of Laser Texturing*, Proc. 15th IDDRG, Dearborn, MI (1988) pp. 109-116

I27. V. Cascioli, A. Segala and P. Antoniucci, *Influence of Surface Morphology on the Appearance of Cold Rolled Steel Sheet After Painting*, Proc. 15th IDDRG, Dearborn, MI (1988) pp. 117-124

I28. P. Skarpelos and J.W. Morris, Jr., *The Effect of Surface Morphology on Formability of Electrogalvanized Sheet Steel*, Wear, 212 (2), (1997) pp. 165-172

I29. B. Andersson, *The Influence of Surface Topography on the Forming Performance of Aluminum*, Proc. 13th IDDRG, Melbourne, Australia (1984) pp. 467-475

I30. M. Jain, D.J. Lloyd and S.R. Macewen, *Hardening Laws, Surface Roughness and Biaxial Tensile Limit Strains of Sheet Aluminum Alloys*, Int. J. Mech. Sci., 38 (2), (1996) pp. 219-232

I31. E. Saur and P. Millet, *Preparation of Work Rolls and Manufacturing of Textured Aluminum Sheets*, METEC Congress 94, Dusseldorf, Germany (1994) pp. 477-479

I32. D. DeSoete, *Roll Texturing Techniques and their Implementation at Sidmar*, Seminar on the Influence of Surface Roughness in the Application of Sheet Steel, 22-23 October 1992, Zelzate, Belgium

I33. O. Pawelski, W. Rasp, W. Zwick, H.-J. Nettelbeck, K. Steinhoff, *The Influence of Different Work-Roll Texturing Systems on the Development of Surface Structure in the Temper Rolling Process of Steel Sheet Used in the Automotive Industry*, J. Mater. Process. Technol., 45, (1994) pp. 215-222

I34. K. Steinhoff, R. Bünten, W. Rasp, R. Kopp, O. Pawelski, *Development of a Model for the Simulation of the Transfer of Surface Structure in the Temper-Rolling Process*, Steel Research, 66 (12), (1995) pp. 520-525

I35. R. Bünten, K. Steinhoff, W. Rasp, R. Kopp, O. Pawelski, *Development of a FEM-Model for the Simulation of the Transfer of Surface Structure in Cold-Rolling Processes*, J. Mater. Process. Technol., 60 (1996) pp. 369-376

I36. J. Simao, D.K. Aspinwall, M.L.H. Wise, M.F. El-Menshawy, *Mill Roll Texturing Using EDT*, J. Mater. Process. Technol., 45, (1994) pp. 207-214

I37. J.A. McGeough and H. Rasmussen, *A Theoretical Model of Electrodischarge Texturing*, J. Mater. Process. Technol., 68, (1997) pp. 172-178

I38. P.A. Kramer and P. Skarpelos, Unpublished Research, (1995)

I39. J.A. Schey, *A Critical Review of the Applicability of Tribotesters to Sheet Metalworking*, SAE Paper No. 970714, SAE Trans.: J. Mater. and Manuf., 106 (5), (1997) pp. 113-124

I40. S. Shaffer, *Micromechanisms of Friction in Electrogalvanized Sheet Steel with Emphasis on the Role of Texture*, Ph.D. Thesis, U.C. Berkeley (1990)

I41. N-M. Wang, *A Mathematical Model of Drawbead Forces in Sheet Metal Forming*, J. Appl. Metalworking, 2 (3), (1982) pp. 193-199

I42. H.D. Nine, *The Applicability of Coulomb's Friction Law to Drawbeads in Sheet Metal Forming*, J. Appl. Metalworking, (1982) pp. 200-210

I43. B.S. Levy, *Development of a Predictive Model for Drawbead Restraining Force Utilizing the Work of Nine and Wang*, J. Appl. Metalworking, 3 (1), (1983) pp. 38-44, Letter to Editor pp. 45

I44. J.M Yellup, *Modelling of Sheet Metal Flow Through a Drawbead*, Proc. 13th IDDRG, Melbourne, Australia (1984) pp. 166-177

I45. J.M Yellup and M.J. Painter, *The Prediction of Stripe Shape and Restraining Force for Shallow Drawbead Systems*, J. Appl. Metalworking, 4 (1), (1985) pp. 30-38

I46. T.B. Stoughton, *Model of Drawbead Forces in Sheet Metal Forming*, Proc. 15th IDDRG, Dearborn, MI (1988) pp. 205-215

I47. L.R. Sanchez and K.J Weinmann, *A General Computer Model for Plane Strain Sheet Flow and its Application to Flow Between Circular Drawbeads*, Proc. 15th IDDRG, Dearborn, MI (1988) pp. 217-226

I48. J. Cao and M.C. Boyce, *Drawbead Penetration as a Control Element of Material Flow*, Proc. Sheet Metal Stamping Symposium, International Congress and Exposition, Detroit, MI, SP-944 (1993) pp. 145-153

I49. S.S. Tufecki, C.-T. Wang, G.L. Kinzel and T. Altan, *Estimation and Control of Drawbead Forces in Sheet Metal Forming*, SAE Paper No. 940941, J. Materials and Manufacturing, 103 (5), (1994) pp. 738-747

I50. L.R. Sanchez and K.J. Weinmann, *An Analytical and Experimental Study of the Flow of Sheet Metal Between Circular Drawbeads*, Trans. ASME, J. Eng. Ind., 118 (1), (1996) pp. 45-54

I51. P. Chabrand, F. Dubois and J.C. Gelin, *Modelling Drawbeads in Sheet Metal Forming*, Int. J. Mech. Sci., 38 (1), (1996) pp. 59-77

I52. G. Dalton and J. Schey, *Effects of Bead Surface Preparation on Friction in the Draw Bead Test*, Proc. Autobody Stamping Technology Progress Conference, SAE Paper No. 910511 (1991) pp. 29-39

I53. G. Dalton and J. Schey, *Effect of Bead Finish Orientation on Friction and Galling in the Drawbead Test*, SAE Paper No.920632, in Autobody Stamping Applications and Analysis, SP-897 (1992) pp. 123-133

I54. M.Y. Demery, *Drawbeads in Sheet Metal Forming*, J. Materials Engineering and Performance, 2 (6), (1993) pp. 863-866

I55. J. Schey and M. Smith, *Report of NADDRG Friction Committee on Reproducibility of Friction Tests Within and Between Laboratories,* Proc. Sheet Metal Stamping Symposium, International Congress and Exposition, Detroit, MI, SAE Paper No. 930811 in SP-944 (1993) pp. 261-267

I56. J. Schey, *Geometric Factors Affecting Results from the Drawbead Simulation (DBS) Test,* Lubrication Engineering, 50 (3), (1994) pp. 255-260

I57. J. Schey, *Causes of Random Variations of Friction in Sheet Metalworking*, Lubrication Engineering, 50 (10), (1994) pp. 821-829

I58. J. Schey, *Speed Effects in Drawbead Simulation*, J. Mater. Process. Technol., 57 (1-2), (1996) pp. 146-154

I59. I9, I11, I18, I19, I23-I25, I28, I29, I40, I52, I53

I60. M. Sulonen, P. Eskola, J. Kumpulainen, A. Ranta-Eskola, *A Reliable Method for Measuring the Friction Coefficient in Sheet Metal Forming,* IDDRG Working Group Meetings, Paper WG III/4, Tokyo, Japan (1981)

I61. E. Schedin, K. Fredriksson, C. Gustafsson, *Characterization of Friction Properties During Sheet Forming,* Proc. 15th IDDRG, Dearborn, MI (1988) pp. 55-61

I62. W.C. Emmens, *The Influence of Surface Roughness on Friction*, Proc. 15th IDDRG, Dearborn, MI (1988) pp. 63-70

I63. R. Zheng, D. Overby, *Strip Friction Experimental Study on Galvanized Steel Sheet,* Proc. 15th IDDRG, Dearborn, MI (1988) pp. 85-90

I64. H.D. Nine, *Friction Measurement for Forming of Zinc-Based Coated Sheet Steel*, Zn-Based Steel Coating Systems, eds. G. Krauss and D.K. Matlock, TMS (1990) pp. 233-242

I65. S.J. Shaffer, W.E. Nojima, P.N. Skarpelos, J.W. Morris, Jr., *Research on the Metallurgical Determinants of Formability in Electrogalvanized Sheet*, Zn-Based Steel Coating Systems, eds. G. Krauss and D.K. Matlock, TMS (1990) pp. 251-261

I66. T.A. Hylton, G.J. Wenzloff, C.J. VanTyne, D.K. Matlock, *The Importance of Microstructure, Surface Roughness, and Properties on the Frictional Behavior of EG Sheet Steels,* Proc. Galvatech '92, Amsterdam, The Netherlands, ed. Centre de Recherches Metallurgiques, Verlag Staleisen, Dusseldorf, Germany (1992) pp. 166-170

I67. T.A. Hylton, C. J. VanTyne, D.K. Matlock, *Frictional Behavior of EG Sheet Steels*, Proc. Sheet Metal and Stamping Symposium, International Congress and Exposition, Detroit, MI, SAE Paper No. 930809 in SP-944 (1993) pp. 241-253

I68. P. Skarpelos, *The Effect of Surface Morphology on the Friction of Electrogalvanized Sheet Steel in Forming Processes*, MS Thesis, U.C. Berkeley (1993)

I69. J.M. Story and D.M. Engelmann, *Surface Topography Effects on Friction in the Forming of Aluminum Sheet*, in Recent Developments in Sheet Metal Forming Technology, Proc. 18th IDDRG, Lisbon (1994) pp. 165-176

I70. J.P. Haruff, T.A. Hylton, C.J. VanTyne, D.K. Matlock, *Frictional Response of EG Sheet Steels,* Phys. Met. ZA-C. Steel, ed. A.R. Marder, TMS (1993) pp. 295-307

I71. T.A. Hylton, *Frictional Behavior of Electrogalvanized Sheet Steels*, Ph.D. Thesis, Colorado School of Mines (1994)

I72. E. Saur, *The Manufacture of Coated Aluminum Sheets*, Recent Developments in Sheet Forming, Proc. Metal Working Symposium, Stuttgart (1992) pp. 285-305

I73. S. Wagner, *Determination of the Friction Coefficients for the Drawing of Aluminum Sheets*, Proc. Metal Working Symposium, Stuttgart (1992) pp. ??-??

I74. Aluminium Materials Technology for Automobile Construction, ed. R. Woodward, Mechanical Engineering Publications Ltd., London (1993)

I75. I3

I76. I9,I16

E1. Constructed by Roger Emigh (1986)

E2. Donated by Jim Story at Alcoa

E3. Analyses performed at Anamet Laboratories, Inc., Hayward, CA

E4. Profiling performed on a UBM Microfocus laser profilometer at Ford Scientific Research Labs, Dearborn, MI, courtesy of Larry Reatherford and Robert McCune, 3-9 February 1997; Data translation performed using Windows 95 version of UBM program, provided courtesy of Peter Joshua, UBM, Santa Clara, CA

E5. Alcoa Confidential Information

E6. Marks Mechanical Engineering Handbook, 8th Edition (1978) pp. 2-12 - 2-15

E7. J. Schey, *Causes of Random Variations of Friction in Sheet Metalworking*, Lubrication Engineering, 50 (10), (1994) pp. 821-829

E8. Donated by Mike Reynolds at Parker Amchem

E9. J.M. Story and D.M. Engelmann, *Surface Topography Effects on Friction in the Forming of Aluminum Sheet*, in Recent Developments in Sheet Metal Forming Technology, Proc. 18th IDDRG, Lisbon (1994) pp. 165-176

E10. G. Dalton and J. Schey, *Effects of Bead Surface Preparation on Friction in the Draw Bead Test*, Proc. Autobody Stamping Technology Progress Conference, SAE Paper No. 910511 (1991) pp. 29-39

E11. Personal communication with John Schey, March 1996, and Rafael Sanchez, June 1996

E12. Courtesy of Rafael Sanchez and Dave Robertson, University of Colorado, Denver

R1. Aluminum Alloy 6111 Patent No.4,614,552, Issued Sep. 30, 1986

R2. C. Barrett and T.B. Massalski, Structure of Metals: Crystallographic Methods, Principles, and Data, 3rd ed., Pergamon Press, Oxford, England (1980) pp. 499-504

R3. Aluminum: Properties and Physical Metallurgy, ed. J.E. Hatch, American Society for Metals, Metals Park, OH (1984)

R4. J. Schey, *Causes of Random Variations of Friction in Sheet Metalworking*, Lubrication Engineering, 50 (10), (1994) pp. 821-829

R5. J.M Yellup, *Modelling of Sheet Metal Flow Through a Drawbead*, Proc. 13th IDDRG, Melbourne, Australia (1984) pp. 166-177

R6. R. Balbach, *Optimierung der Oberflächenmikrogeometrie von Aluminiumfeinblech für das Karosserieziehen (Optimization of the Surface Microgeometry of Aluminum Sheet for Autobody Drawing)*, Ph.D. Thesis, University of Stuttgart (1993)

R7. J. Schey, *Friction in Working 5052 Aluminum Alloy Sheet*, in Light Metals Processing and Applications, C. Bickert et al, eds., TMS of CIM, Montreal (1993) pp. 571-580

R8. J.M. Story and D.M. Engelmann, *Surface Topography Effects on Friction in the Forming of Aluminum Sheet*, in Recent Developments in Sheet Metal Forming Technology, Proc. 18th IDDRG, Lisbon (1994) pp. 165-176

R9. P. Skarpelos and J.W. Morris, Jr., *The Effect of Surface Morphology on Formability of Electrogalvanized Sheet Steel*, Wear, 212 (2), (1997) pp. 165-172

R10. T.A. Hylton, *Frictional Behavior of Electrogalvanized Sheet Steels*, Ph.D. Thesis, Colorado School of Mines (1994)

R11. F.P. Bowden and D. Tabor, The Friction and Lubrication of Solids, Oxford, Clarendon Press (1950)

R12. M. Jain, D.J. Lloyd and S.R. Macewen, *Hardening Laws, Surface Roughness and Biaxial Tensile Limit Strains of Sheet Aluminum Alloys*, Int. J. Mech. Sci., 38 (2), (1996) pp. 219-232

D1. J. Schey, *Geometric Factors Affecting Results from the Drawbead Simulation (DBS) Test*, Lubrication Engineering, 50 (3), (1994) pp. 255-260

D2. S. Shaffer, *Micromechanisms of Friction in Electrogalvanized Sheet Steel with Emphasis on the Role of Texture*, Ph.D. Thesis, U.C. Berkeley (1990)

D3. J. Schey, *Causes of Random Variations of Friction in Sheet Metalworking*, Lubrication Engineering, 50 (10), (1994) pp. 821-829

D4. H.R. Zonker, J.C. Brem, and J.L. Morson, *Verification of Crystallographic Texture Based FLD Predictions for Aluminum Sheet*, 1995 SAE draft

D5. Personal communication with Harry Zonker, Alcoa, January 1998

D6. J.M. Story, G.W. Jarvis, H.R. Zonker, S.J. Murtha, *Issues and Trends in Automotive Aluminum Sheet Forming*, Sheet Metal and Stamping Symposium (SP-944), International Congress and Exposition, Detroit, MI, SAE Paper No. 930277 (1993) pp. 1-25

D7. J.A. Schey, *Friction in Sheet Metalworking*, SAE Paper No. 970712, SAE Trans.: J. Mater. and Manuf., 106 (5), (1997) pp. 113-124

D8. T. Kato, E. Iizuka, T. Hira, O. Furukimi, T. Obara, *Effects of Strength and Surface Roughness of Steel Sheets on Frictional Behaviour During Sheet Forming*, Proc. IDDRG 1996, pp. 497-504

D9. B. Andersson, *The Influence of Surface Topography on the Forming Performance of Aluminum*, Proc. 13th IDDRG, Melbourne, Australia (1984) pp. 467-475

D10. R. Balbach, *Optimierung der Oberflächenmikrogeometrie von Aluminiumfeinblech für das Karosserieziehen (Optimization of the Surface Microgeometry of Aluminum Sheet for Autobody Drawing)*, Ph.D. Thesis, University of Stuttgart (1993)

D11. M. Jain, D.J. Lloyd and S.R. Macewen, *Hardening Laws, Surface Roughness and Biaxial Tensile Limit Strains of Sheet Aluminum Alloys*, Int. J. Mech. Sci., 38 (2), (1996) pp. 219-232

D12. P.M.B Rodrigues and R. Akeret, *Surface Roughening and Strain Inhomogeneities in Aluminum Sheet Forming*, Proc. 12th IDDRG Congress, Margherita Ligure, Italy (1982) pp. 73-84

D13. J.F. Lin and L.Y. Wang, *Friction in Deep Drawing of Aluminum Sheet*, Wear, 156, (1992) pp. 189-199

D14. P.K Saha and W.R.D. Wilson, *Influence of Plastic Strain on Friction in Sheet Metal Forming*, Wear, 172, (1994) pp. 167-173

D15. E. Saur, *The Manufacture of Coated Aluminum Sheets*, Recent Developments in Sheet Forming, Proc. Metal Working Symposium, Stuttgart (1992) pp. 285-305

D16. P. Skarpelos and P. Kramer, unpublished research showing increase in longer wavelengths and loss of shorter wavelengths with increase in roll wear

D17. J.M. Story and D.M. Engelmann, *Surface Topography Effects on Friction in the Forming of Aluminum Sheet*, in Recent Developments in Sheet Metal Forming Technology, Proc. 18th IDDRG, Lisbon (1994) pp. 165-176

D18. J. Schey, *Friction in Working 5052 Aluminum Alloy Sheet*, in Light Metals Processing and Applications, C. Bickert et al, eds., TMS of CIM, Montreal (1993) pp. 571-580

A1. Constructed by Roger Emigh (1986)

A2. S. Shaffer, *Micromechanisms of Friction in Electrogalvanized Sheet Steel with Emphasis on the Role of Texture*, Ph.D. Thesis, U.C. Berkeley (1990)

A3. P. Skarpelos, *The Effect of Surface Morphology on the Friction of Electrogalvanized Sheet Steel in Forming Processes*, MS Thesis, U.C. Berkeley (1993)

A4. *Surface Texture (Surface Roughness, Waviness, and Lay)*, ANSI/ASME Standard B46.1-1985

Appendix A: Fabrication and Modification of a DBS Forming Friction Test Machine

A draw bead simulator was designed and constructed utilizing a tension/compression hydraulically driven load frame already in existence.[A1] Utilizing this digital testing machine (DTM) necessitated rotating the test setup from the vertical pull used on the majority of other DBS testers to horizontal. Figure 5 shows a photograph of the overall test setup, while Figure 6 shows a top view of the grips and pulling assembly and Figure 7 shows a rear view of the beads with a specimen inserted before the top bead is lowered into place. The beads consisted of 9.525 mm (0.375 in) diameter D2 tool steel rods hardened to HRC 62. The drawing force, provided by a Compumotor ZX635 brushless servomotor connected to an ActionJac screwdrive, was measured by an Interface 2000 lb load cell with 150% overload protection wired to a Daytronic Model 3000 Strain Gauge Conditioner in line with the specimen friction grips. The clamping force, provided by the DTM pull rod, was measured using four Transducer Techniques 500 lb button load cells with 150% overload protection, wired to two Honeywell Accudata 218 Bridge Amplifiers, directly under the top die. Tests were run and recorded using a Quick Basic program(Appendix B) on a Compaq 386/25 computer with a CyberResearch PCL818H A/D card. Specimen location and test velocity were recorded using a MagneTek linear motion transducer.

For purposes of matching testing performed previously by others within the author's research group at another location,[A2,A3] the decision was made to purchase the DBS tooling and tooling support assembly from the manufacturer of that equipment. All other fabrication was designed and performed on site. All items, including the purchased tooling, were designed to attach to a jig plate which then attached to the DTM. The only modification the design did not originally account for was a rotation of the screw, and therefore the grips and the test specimen, while pulling the test. An adapter with linear rotational bearings running on support rods attached to the side support plates around the pulling assembly (shown in Figure 6) was fabricated to stop this rotation; the adapter clamps around the screwdrive/load cell connector behind the drawing load cell, so any friction from the bearings is not recorded during the test.

A number of modifications were necessary before the acquired tooling worked satisfactorily. The load support plate inside the top shoe (Figure A1) which prevented forward movement of the die during testing severely galled against the inside of the front support plate of the box, necessitating significant grinding down of both plates over their contact area. The plate from the shoe was ground on a planar grinder while the inside of the box was ground by hand. This reduction resulted in a forward shift of the male insertion bead (toward the front of the box). A 0.127 mm (0.005 in) shim placed between

the top die and the shoe load support plate returned the male bead to center position at full insertion between the female die beads.

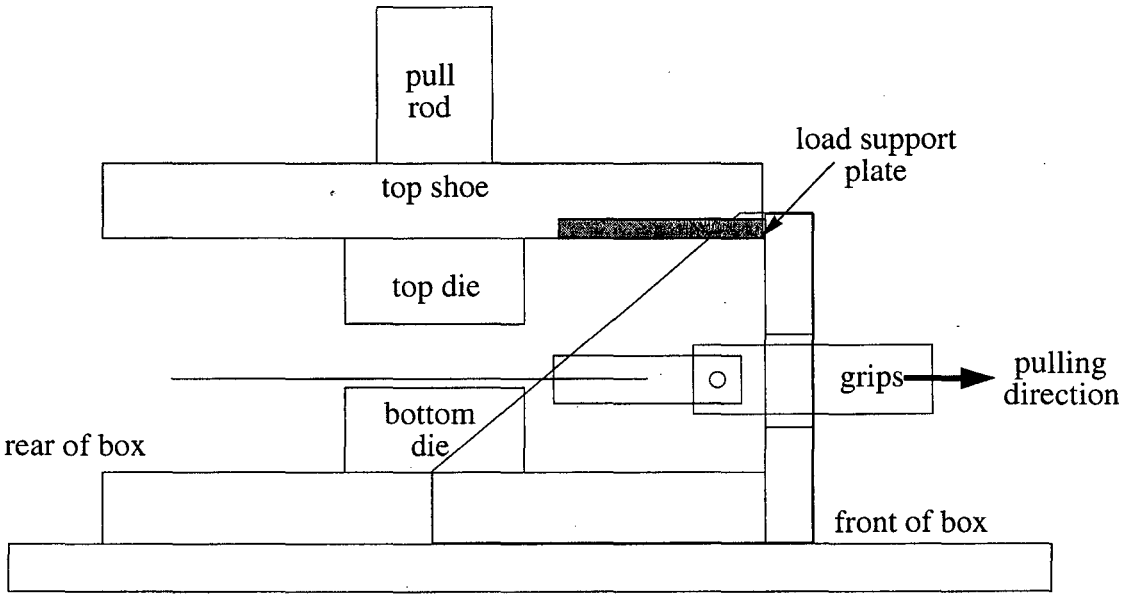

Figure A1 Side view schematic of DBS tooling box, indicating parts.

Friction between the load pins and the bronze bushings used to align the top shoe, and therefore the male die, negated the original idea of reading the clamping load with the column load cell in the existing load frame. Slight shifts in the valve pressure in the DTM resulted in a large shift in the load recorded at the DTM column load cell. Springs inserted over the load pins to compensate for the friction resulted in a compressive load on the column load cell, but the position controller in the load frame could not correct quickly enough to hold a steady position during testing. At the time, extra long roller bearings that could perform the task of the bushings were prohibitively expensive, in addition to the fact that the outer diameter of such bearings was greater than the amount of material that could be comfortably machined from the top shoe and still leave an acceptable amount of material around the bearing.

To minimize corrective machining of the purchased tooling, MicroMeasurements 120Ω strain gauges were cemented directly on the v-notched fixed bead support of the top die to form a Wheatstone bridge. Gauges were not installed on the male roller bead die because of insufficient output signal. Initial tests with the gauge setup were extremely sensitive to initial loading condition, i.e., whether the specimen was preloaded in tension or whether the die had been over-inserted during setup then raised back up so the specimen started the test "loose", and calibration data indicated that the gauges were too sensitive to the rate of die loading to reliably choose a calibration curve (Figure A2a). Gauges moved further down the support, away from the v-notch, were not as sensitive to

die load rate (Figure A2b) but were still sensitive to initial specimen load condition, and showed a significant clamping load increase during the tests.

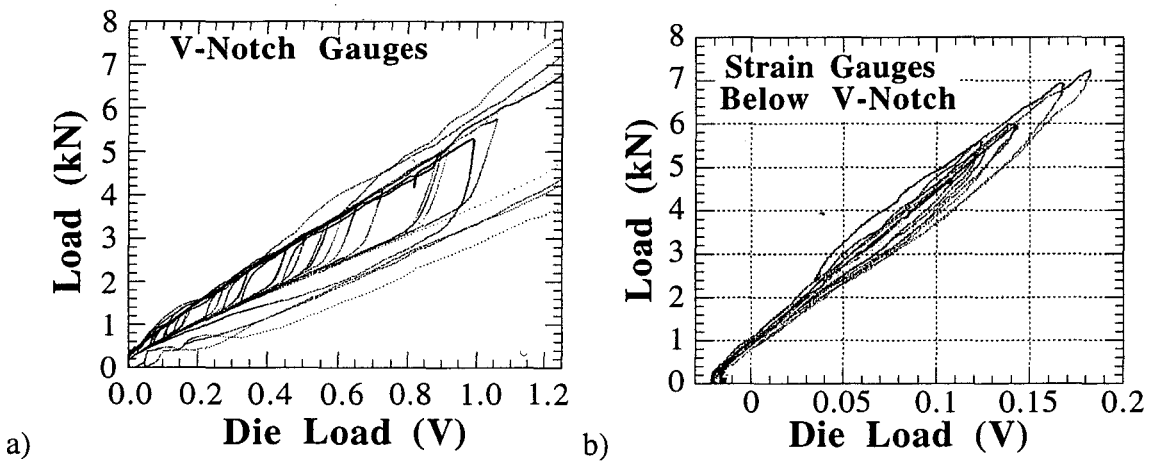

Figure A2 Calibration curves for strain gauges a) on V-notch and b) below V-notch.

Pinching of the strip between the top bead and the bottom exit bead during the test was not expected as the source of this load increase for two reasons. First, die deflections were measured prior to all tests using two inch wide, 0.82 mm (0.032 in) thick steel specimens in order to obtain maximum anticipated deflections. Deflection measurements showed both male and female bead deflection such that pinching of the test strip and corresponding influence of the test results should not occur. Second, there was no corresponding drawing load increase, to be expected if the effect was real. This left the gauges themselves, which were checked by separating out the output of the front and rear active gauges of the bridge. While the front gauge output showed an even load during the test, the rear gauge output showed an unevenly decreasing tensile load, which showed up as an increasing compressive load during the test. The decreasing load was attributed to the bead pulling forward at the test start and "relaxing" unevenly through the test duration. Using the front gauge only was not an option as its output was a combination of the clamping load and the pulling load from the test, the latter of which was presumed removed by the rear gauges of the bridge.

A variety of options using load cells were considered. The possibility of placing a load cell inside the fixed male die itself was negated when it was found that the slot depth within which the bead support piece fit was fully 1/4 less in depth than the blueprints indicated. Instead, the top shoe was disassembled and machined in order to insert four compressive button load cells not available at the time of the initial gauge installation. The load cells were wired into two bridge amplifiers, combining the output from the two front load cells into one amplifier and the output from the two rear load cells into the other. The machine was reassembled, realigned and recalibrated, with little evident

difference in the clamping load dependent on the direction of loading. Subsequent testing also showed no indication of the separate clamping load increase the strain gauge setup had shown.

In addition to the improvement in clamping load reliability, the load cells proved to be more robust with regard to initial test condition. Sample preloading for mixed bead tests increased the clamping load by a set 40 N (9 lb) for the 0.941 mm (0.036 in) specimens while roller bead tests were insensitive to all preloading conditions.

Appendix B: DBS Test QuickBasic Program

```
' ************** DBS Test Program  (DBSTEST.BAS) *****************
' *** Sub Routine Listing: ***
DECLARE SUB ad.card
DECLARE SUB bead.type
DECLARE SUB board.param
DECLARE SUB buffer.set
DECLARE SUB cable.pot
DECLARE SUB cable.buffer
DECLARE SUB card.call
DECLARE SUB conversion.channel
DECLARE SUB die.insert
DECLARE SUB dieinsert.boardparam
DECLARE SUB dieinsert.buffer
DECLARE SUB display.data
DECLARE SUB gain.array
DECLARE SUB gainarray.print
DECLARE SUB grpaxisb (xmin!, xmax!, ymin!, ymax!, wpage%, dpage%)
DECLARE SUB home.position
DECLARE SUB initial.buffer
DECLARE SUB initial.data
DECLARE SUB longgrip.setup
DECLARE SUB longgrip.test
DECLARE SUB motor.home
DECLARE SUB motor.off
DECLARE SUB save.question
DECLARE SUB set.time
DECLARE SUB setup.question
DECLARE SUB setup.test
DECLARE SUB shortgrip.setup
DECLARE SUB shortgrip.test
DECLARE SUB tension.buffer
DECLARE SUB tension.card
DECLARE SUB tension.specimen
DECLARE SUB test.boardparam
DECLARE SUB test.question
DECLARE SUB write.data
DECLARE SUB write.initialdata
DECLARE SUB write.dieinsertdata

'********** Declare Parameter Array for Board and Buffers *************
DIM param%(60)              ' If two boards installed, need to declare
DIM cbl%(50)            ' Cable Pot buffer  'the second parameter array
DIM die%(9800)              ' Die Insertion Data Buffer (1 min 10 sec)
DIM init%(350)              ' Zero Point Values Data Buffer
DIM pre%(700)               ' Pretension Data Buffer
DIM dat%(14007)             ' Test Data Buffer (5 sec max)
DIM ff%(7)                  ' Gain Array Table Buffer

KEY 1, "long" + CHR$(13):       ' to long grip test point on this key
KEY 5, "short" + CHR$(13):      ' go to short grip test start point on this
KEY 9, "home" + CHR$(13):       ' return to home position on this key

dbsload = 399.976: cblpos = 2.0572: cblvel = 565:
dtmload = -1001: dtmlvdt = .0222275: lvdt3 = .217822: lvdt30 = .0222275

1 CLS 0
GOSUB motor.off
PRINT "PCL818H Data Collection Program (DBSTEST)"
GOSUB test.question
GOSUB bead.type
INPUT "Enter File Name: ", file$    'File to save data from buffer
INPUT "Enter Die Offset (in lb): ", dieoffset
```

```
'INPUT "Enter DBS (draw) Load Cell Calibration Slope: ", dbsload
IF testtype = 1 THEN
   GOSUB cable.pot
   GOSUB setup.test
END IF
IF testtype = 2 THEN
   GOSUB setup.question
END IF
GOSUB initial.data
IF testtype = 1 THEN
   GOSUB die.insert
END IF
IF testtype = 2 THEN
   dievar = 2
END IF
GOSUB tension.specimen
GOSUB test.boardparam
GOSUB buffer.set
GOSUB set.time
GOSUB conversion.channel
GOSUB gain.array
GOSUB gainarray.print
CALL grpaxisb(xmin!, xmax!, ymin!, ymax!, wpage%, dpage%)
GOSUB card.call
GOSUB display.data
GOSUB save.question
LOCATE 41, 20: PRINT "                                        "
LOCATE 41, 20: INPUT "Perform another test (y or n)? ", moretst$
IF moretst$ = "y" THEN GOTO 1
IF moretst$ = CHR$(13) THEN GOTO 1
LOCATE 41, 20: PRINT "                                        "
LOCATE 41, 20: PRINT "Hit Enter to return to DOS."
DO
     LOOP UNTIL INKEY$ = CHR$(13)
100 CLS 0
END


' ***********************************************************************
' ************************ SUB ROUTINES ********************************
' ***********************************************************************
test.question:
' *************** Find out if Test is New or Continuation ***********
testtype = 0
3 INPUT "Is this a new (n) test or a continuing (c) test w/ bead in place? (n) ", new$
IF new$ = "" THEN testtype = 1
IF new$ = "n" OR new$ = "N" THEN testtype = 1
IF new$ = "c" OR new$ = "C" THEN testtype = 2
IF testtype = 0 THEN GOTO 3
RETURN

bead.type:
' ************** Check Bead Type and Specimen Width ***************
beadcheck = 0
4 INPUT "Fixed(f) or roller(r) bead test? (r) ", bead$
IF bead$ = "" THEN beadtyp = 2
IF bead$ = "f" OR bead$ = "F" THEN beadtyp = 1
IF bead$ = "r" OR bead$ = "R" THEN beadtyp = 2
IF bead$ = "" OR bead$ = "f" OR bead$ = "F" OR bead$ = "r" OR bead$ = "R" THEN
   beadcheck = 1
END IF
IF beadcheck <> 1 THEN GOTO 4
IF beadtyp = 1 THEN        'AND widthtyp = 1 THEN
     dieloadf = 150
```

```
      dieloadr = 150
      dieloadsum = 150
END IF
IF beadtyp = 2 THEN
      dieloadf = 150
      dieloadr = 150
      dieloadsum = 150
END IF
RETURN

cable.pot:
' ************ Check That Starting at Home Position *****************
10 GOSUB board.param
GOSUB cable.buffer
GOSUB gain.array
GOSUB ad.card
I = 1: cblvolt = 0: cable = 0: sum = 0: num = 0:
FOR I = 1 TO 49
   num = (cbl%(I) * 20! / 4096! + (-10!))
   sum = sum + num
NEXT I
cblvolt = sum / 49
LOCATE 7: PRINT cblvolt
IF cblvolt > 7.618 THEN
   LOCATE 8: PRINT "The pull rod is not out far enough!"
   cable = 1
END IF
IF cblvolt < 7.613 THEN
   LOCATE 8: PRINT "The pull rod is out too far!"
   cable = 1
END IF
IF cable = 1 THEN
   LOCATE 9: PRINT "Hit Enter to move the pull rod to home position."
   DO
      LOOP UNTIL INKEY$ = CHR$(13)
   GOSUB home.position
END IF
RETURN

home.position:
' ******************* Move Pull Rod to Home Position ******************
GOSUB board.param
GOSUB cable.buffer
GOSUB gain.array
GOSUB ad.card
LOCATE 8: PRINT "                                        "
I = 1: cblvolt = 0: cable = 0: sum = 0: num = 0:
FOR I = 1 TO 49
   num = (cbl%(I) * 20! / 4096! + (-10!))
   sum = sum + num
NEXT I
cblvolt = sum / 49
LOCATE 7: PRINT cblvolt
IF cblvolt < 7.613 OR cblvolt > 7.618 THEN
   OPEN "com1:9600,n,8,1,rs,cs,ds,cd" FOR RANDOM AS #2
   PRINT #2, "on"
   PRINT #2, "mc"
   LOCATE 9: PRINT "Proceeding to home position.                    "
   PRINT #2, "1sld3"
END IF
LOCATE 8: PRINT "                                        "
I = 1: cblvolt = 0: cable = 0: sum = 0: num = 0:
FOR I = 1 TO 49
   num = (cbl%(I) * 20! / 4096! + (-10!))
```

```
   sum = sum + num
NEXT I
cblvolt = sum / 49
LOCATE 7: PRINT cblvolt
IF cblvolt < 7.5 THEN
  PRINT #2, "h+"
  PRINT #2, "a50 ad50 v3 g"
 DO
  I = 1: sum = 0: num = 0: cblvolt = 0: home = 0
  GOSUB ad.card
  FOR I = 1 TO 49
     num = (cbl%(I) * 20! / 4096! + (-10!))
     sum = sum + num
  NEXT I
  cblvolt = sum / 49
  LOCATE 7: PRINT cblvolt
 LOOP UNTIL cblvolt < 7.613 AND cblvolt > 7.5
 PRINT #2, "s"
END IF
IF cblvolt < 7.613 AND cblvolt > 7.5 THEN
  PRINT #2, "h+"
  PRINT #2, "a10 ad10 v.05 g"
END IF
IF cblvolt > 7.618 THEN
  PRINT #2, "h-"
  PRINT #2, "a10 ad10 v.05 g"
END IF
DO
  I = 1: sum = 0: num = 0: cblvolt = 0: home = 0
  GOSUB ad.card
  FOR I = 1 TO 49
     num = (cbl%(I) * 20! / 4096! + (-10!))
     sum = sum + num
  NEXT I
  cblvolt = sum / 49
  LOCATE 7: PRINT cblvolt
LOOP UNTIL cblvolt < 7.618 AND cblvolt > 7.613
PRINT #2, "s"
PRINT #2, "z"
LOCATE 9: PRINT "Hit Enter when ready to continue."
DO
     LOOP UNTIL INKEY$ = CHR$(13)
PRINT #2, "off"
CLOSE #2
RETURN 10

setup.test:
' ************** Setup Test After Specimen In Grips *****************
KEY(1) ON: KEY(5) ON:
ON KEY(1) GOSUB longgrip.setup
ON KEY(5) GOSUB shortgrip.setup
longgrip = 0: shortgrip = 0
LOCATE 7: PRINT "                                    "
LOCATE 8: PRINT "To setup a long grip test hit F1."
LOCATE 9: PRINT "To setup a short grip test hit F5."
DO
     LOOP UNTIL INKEY$ = "short" OR INKEY$ = "long"
20 KEY(1) OFF: KEY(5) OFF:
RETURN

shortgrip.setup:
'************ Short Grip Test Start Position *************
OPEN "com1:9600,n,8,1,rs,cs,ds,cd" FOR RANDOM AS #2
PRINT #2, "on"
```

```
PRINT #2, "a10 ad10 v1 d-111000 g"
LOCATE 8: PRINT "Proceeding to short grip test start point."
LOCATE 9: PRINT "Hit Enter when ready to continue.          "
DO
     LOOP UNTIL INKEY$ = CHR$(13)
PRINT #2, "off"
CLOSE #2
shortgrip = 1
LOCATE 8: PRINT "                                    "
LOCATE 9: PRINT "                                    "
RETURN 20

longgrip.setup:
'************ Long Grip Test Start Position ***************
OPEN "com1:9600,n,8,1,rs,cs,ds,cd" FOR RANDOM AS #2
PRINT #2, "on"
PRINT #2, "a10 ad10 v1 d-163500 g"
LOCATE 8: PRINT "Proceeding to long grip test start point."
LOCATE 9: PRINT "Hit Enter when ready to continue.          "
DO
     LOOP UNTIL INKEY$ = CHR$(13)
PRINT #2, "off"
CLOSE #2
longgrip = 1
LOCATE 8: PRINT "                                    "
LOCATE 9: PRINT "                                    "
RETURN 20

setup.question:
' ************* Continuing Test Short or Long Grips? ****************
longgrip = 0: shortgrip = 0
6 INPUT "Continuing test using long (l) or short (s) grips? ", grip$
IF grip$ = "l" OR grip$ = "L" THEN longgrip = 1
IF grip$ = "s" OR grip$ = "S" THEN shortgrip = 1
IF longgrip = 0 AND shortgrip = 0 THEN GOTO 6
RETURN

initial.data:
' ********* Collect Initial (Zero Point) Data Points ******************
LOCATE 9: PRINT "                                                    "
LOCATE 10: PRINT "                                                    "
LOCATE 11: PRINT "                                                    "
LOCATE 12: PRINT "                                                    "
LOCATE 13: PRINT "                                                    "
LOCATE 14: PRINT "                                                    "
LOCATE 15: PRINT "                                                    "
IF testtype = 2 THEN
   LOCATE 9: PRINT "Raise bead so no load is on it, put LVDT to 3, then after"
   LOCATE 10: PRINT "initial values are read re-insert bead with LVDT at 30."
   PRINT "Hit Enter when Ready to Read Initial Values     "
   DO
      LOOP UNTIL INKEY$ = CHR$(13)
   LOCATE 11: PRINT "Reading Initial Values                    "
END IF
IF testtype = 1 THEN
 LOCATE 9: PRINT "Reading Initial Values"
END IF
  inivar = 1: initcheck = 1: arraytype = 1
GOSUB board.param
GOSUB initial.buffer
GOSUB gain.array
GOSUB ad.card
IF testtype = 2 THEN
  LOCATE 9: PRINT "                                                    "
```

```
  LOCATE 10: PRINT "                                                    "
  LOCATE 11: PRINT "                                                    "
  LOCATE 12: PRINT "                                                    "
END IF
LOCATE 10: PRINT "Hit Enter to Continue"
DO
     LOOP UNTIL INKEY$ = CHR$(13)
LOCATE 9: PRINT "                                        "
LOCATE 10: PRINT "                                        "
LOCATE 11: PRINT "                                        "
RETURN

die.insert:
' ***************** Collect Data During Die Insertion ******************
diecheck = 0
25 LOCATE 9: INPUT "Collect Die Insertion Data? (y or n) (n) ", insert$
IF insert$ = "y" OR insert$ = "Y" THEN
   dievar = 1
   diecheck = 1
   LOCATE 9: PRINT "                                        "
   LOCATE 9: INPUT "Die Insertion Data File Name: ", dieinsert$
   PRINT "Lower on LVDT3 to roughly 400mils, Hit Enter to Start Data Collection."
   PRINT "Resume Lowering Top Die:"
   PRINT "Fixed:  LVDT3 to between -   & -   mils, then LVDT30 to -  .  mils."
   PRINT "Mixed:  LVDT3 to between -20 & -35 mils, then LVDT30 to -2.7 mils."
   PRINT "Roller: LVDT3 to between -40 & -55 mils, then LVDT30 to -23.7 mils."
   PRINT "   "
   PRINT "**THE DTM HEAD HAS A TENDENCY TO DROP QUICKLY WHEN PUMP IS
OFF!!!!**"
   DO
        LOOP UNTIL INKEY$ = CHR$(13)
   PRINT "Reading Values"
   GOSUB dieinsert.boardparam
   GOSUB dieinsert.buffer
   GOSUB gain.array
   GOSUB ad.card
END IF
IF insert$ = "" OR insert$ = "n" OR insert$ = "N" THEN
   dievar = 2
   diecheck = 1
   PRINT "Lower bead to test position (listed here)."
   PRINT "Fixed:  LVDT3 to between -   & -   mils, then LVDT30 to -  .  mils."
   PRINT "Mixed:  LVDT3 to between -20 & -35 mils, then LVDT30 to -2.7 mils."
   PRINT "Roller: LVDT3 to between -40 & -55 mils, then LVDT30 to -23.7 mils."
   PRINT "   "
   PRINT "**THE DTM HEAD HAS A TENDENCY TO DROP QUICKLY WHEN PUMP IS
OFF!!!!**"
   PRINT "Hit Enter When Bead is in Test Position"
   DO
     LOOP UNTIL INKEY$ = CHR$(13)
END IF
IF diecheck <> 1 THEN GOTO 25
LOCATE 10: PRINT "                                                    "
LOCATE 11: PRINT "                                                    "
LOCATE 12: PRINT "                                                    "
LOCATE 13: PRINT "                                                    "
LOCATE 14: PRINT "                                                    "
LOCATE 15: PRINT "                                                    "
LOCATE 16: PRINT "                                                    "
LOCATE 17: PRINT "                                                    "
RETURN

tension.specimen:
' ****** Pull Specimen Back Screw Drive Turn Fraction to Pre-Tension ******
```

```
precheck = 0
30 LOCATE 10: PRINT "                                        "
LOCATE 11: PRINT "                                        "
LOCATE 10: INPUT "Pretension specimen? (y or n): (n) ", preques$
OPEN "com1:9600,n,8,1,rs,cs,ds,cd" FOR RANDOM AS #2
PRINT #2, "on"
CLOSE #2
IF preques$ = "y" OR preques$ = "Y" THEN
   precheck = 1
   arraytype = 2
   LOCATE 10: PRINT "Hit Enter to Pre-tension Specimen                    "
   DO
       LOOP UNTIL INKEY$ = CHR$(13)
   OPEN "com1:9600,n,8,1,rs,cs,ds,cd" FOR RANDOM AS #2
   LOCATE 10: PRINT "Pre-tensioning Specimen                    "
   GOSUB dieinsert.boardparam
   GOSUB tension.buffer
   GOSUB gain.array
   GOSUB tension.card
   LOCATE 10: PRINT "Hit Enter to Continue                    "
   DO
       LOOP UNTIL INKEY$ = CHR$(13)
   CLOSE #2
END IF
IF preques$ = "" OR preques$ = "n" OR preques$ = "N" THEN
   precheck = 1
END IF
IF precheck <> 1 THEN GOTO 30
RETURN

' ********************************************************
' ************* Board Parameter Subroutines ***************
' ********************************************************
board.param:
' ******************* Board and Data Rate Parameters *********************
param%(0) = 0            ' Board number
param%(1) = &H300            ' Base I/O address
param%(4) = 2            ' IRQ level : IRQ2
param%(5) = 50            ' Pacer rate = 1M / (50 * 100) = 200 Hz
param%(6) = 100            ' param(5)=C1, param(6)=C2
param%(7) = 0            ' Trigger mode, 0 : pacer trigger
param%(8) = 0            ' Non-cyclic
RETURN

dieinsert.boardparam:
' ***** Board and Data Rate Params for Die Insertion/Pretensioning *****
param%(0) = 0            ' Board number
param%(1) = &H300            ' Base I/O address
param%(4) = 2            ' IRQ level : IRQ2
param%(5) = 250            ' Pacer rate = 1M / (250 * 200) = 20 Hz
param%(6) = 200            ' param(5)=C1, param(6)=C2
param%(7) = 0            ' Trigger mode, 0 : pacer trigger
param%(8) = 0            ' Non-cyclic
RETURN

test.boardparam:
' ******************* Board and Data Rate Parameters *********************
param%(0) = 0            ' Board number
param%(1) = &H300            ' Base I/O address
param%(4) = 2            ' IRQ level : IRQ2
param%(5) = 50            ' Pacer rate = 1M / (50 * 50) = 400 Hz
param%(6) = 50            ' param(5)=C1, param(6)=C2
param%(7) = 0            ' Trigger mode, 0 : pacer trigger
param%(8) = 0            ' Non-cyclic
```

```
RETURN

buffer.set:
' ******************** Set Buffer Addresses*******************
param%(10) = VARPTR(dat%(0))  ' Offset of A/D data buffer A
param%(11) = VARSEG(dat%(0))  ' Segment of A/D data buffer A
param%(12) = 0              ' Data buffer B address, if not used,
param%(13) = 0              ' must set to 0.
RETURN

cable.buffer:
' **************** Set Buffers for Cable Pot Check ***************
param%(10) = VARPTR(cbl%(0))        ' Offset of A/D data buffer A
param%(11) = VARSEG(cbl%(0))        ' Segment of A/D data buffer A
param%(12) = 0                  ' Data buffer B address, if not used,
param%(13) = 0                  ' must set to 0.
param%(14) = .25 * 1 * 200          ' A/D conversion number
param%(15) = 1                  ' A/D conversion start channel
param%(16) = 1                  ' A/D conversion stop channel
RETURN

dieinsert.buffer:
' *************** Buffer for Die Insertion Data **************
param%(10) = VARPTR(die%(0))        ' Offset of A/D data buffer A
param%(11) = VARSEG(die%(0))        ' Segment of A/D data buffer A
param%(12) = 0                  ' Data buffer B address, if not used,
param%(13) = 0                  ' must set to 0.
param%(14) = 70 * 7 * 20            ' A/D conversion number  (1 min)
param%(15) = 0                  ' A/D conversion start channel
param%(16) = 6                  ' A/D conversion stop channel
RETURN

initial.buffer:
'****************** Buffer for Zero Point Values *********************
param%(10) = VARPTR(init%(0))       ' Offset of A/D data buffer A
param%(11) = VARSEG(init%(0))       ' Segment of A/D data buffer A
param%(12) = 0                  ' Data buffer B address, if not used,
param%(13) = 0                  ' must set to 0.
param%(14) = .25 * 7 * 200          ' A/D conversion number (1/4 sec)
param%(15) = 0                  ' A/D conversion start channel
param%(16) = 6                  ' A/D conversion stop channel
RETURN

tension.buffer:
' ***************** Buffer for Pretensioning Data *********************
param%(10) = VARPTR(pre%(0))        ' Offset of A/D data buffer A
param%(11) = VARSEG(pre%(0))        ' Segment of A/D data buffer A
param%(12) = 0                  ' Data buffer B address, if not used,
param%(13) = 0                  ' must set to 0.
param%(14) = 5 * 7 * 20             ' A/D conversion number (5 sec)
param%(15) = 0                  ' A/D conversion start channel
param%(16) = 6                  ' A/D conversion stop channel
RETURN

set.time:
'************************** Set Test Time **************************
'***************** Determine the Number of Data Points *****************
'************* Input Voltage Input Parameters *************
INPUT "Length of test (5 sec maximum): ", time
35 IF time * 7 * 400 > 14000 THEN
  INPUT "Too many data points.  Reenter time: ", time
  GOTO 35
END IF
IF time < 0 OR time = 0 THEN
```

```
  INPUT "Please enter a time greater than zero: ", time
  GOTO 35
END IF
INPUT "Minimum input voltage to display (Negative # or Zero): ", ymin!
INPUT "Maximum input voltage to display (Positive # or Zero): ", ymax!
PRINT "The voltage range to display is from "; ymin!; "to"; ymax!; "V."
xmin! = 0: xmax! = time
wpage% = 0: dpage% = 0
RETURN

conversion.channel:
' ****************** Sets Number of Data Points ******************
' ********************** Sets Channels to Scan ********************
param%(14) = time * 7 * 400 + 7  ' A/D conversion number
param%(15) = 0                   ' A/D conversion start channel
param%(16) = 6                   ' A/D conversion stop channel
RETURN

gain.array:
' ************************** Define Gain Table **************************
ff%(0) = 0                 'channel 0 (DBS Load Cell)  0 = +/-5V
ff%(1) = 8                 'channel 1 (Cable Pot Position)  8 = +/-10V
ff%(2) = 8                 'channel 2 (Cable Pot Velocity)
ff%(3) = 1                 'channel 3 (DTM Load Cell)  1 = +/-2.5V
ff%(4) = 8                 'channel 4 (DTM LVDT)
ff%(5) = 8                 'channel 5 (Front Die Load Cells)
ff%(6) = 8                 'channel 6 (Rear Die Load Cells)
ff%(7) = 0                 'channel 7 (Die Calibration Load Cell)
param%(17) = &HFF                  ' tells to look for gain table
param%(18) = VARPTR(ff%(0))        ' offset address
param%(19) = VARSEG(ff%(0))        ' segment address
RETURN

gainarray.print:
'*************** Print Gain Array ************************
PRINT "The current gain table is: "
PRINT "Channel      Gain Code  (0=+/-5V; 1=+/-2.5V; 8=+/-10V)"
FOR I = param%(15) TO param%(16)
     PRINT I; CHR$(9); CHR$(9); ff%(I)
NEXT I
INPUT "Hit Enter to continue. ", continue$
RETURN

ad.card:
' ******************** A/D Card Call ************************
FUN% = 3                        ' hardware initialization
CALL PCL818H(FUN%, SEG param%(0))
IF param%(45) <> 0 THEN PRINT "Driver Initialization Failed!": STOP
FUN% = 100                      ' A/D initialization
CALL PCL818H(FUN%, SEG param%(0))
IF param%(45) <> 0 THEN PRINT "A/D Initialization Failed!": STOP
FUN% = 105                      ' pacer trigger A/D conversion with
CALL PCL818H(FUN%, SEG param%(0))       ' interrupt data transfer
IF param%(45) <> 0 THEN PRINT "A/D Interrupt Data Transfer Failed!": STOP
40 FUN% = 106                   ' check interrupt status
CALL PCL818H(FUN%, SEG param%(0))
CHK% = (param%(46) AND 1)
IF CHK% <> 0 THEN GOTO 40               ' 0 : Not active, 1 : Active
RETURN

tension.card:
' ************* A/D Card Call for Pretensioning Specimen **************
FUN% = 3                  ' hardware initialization
CALL PCL818H(FUN%, SEG param%(0))
```

```
IF param%(45) <> 0 THEN PRINT "Driver Initialization Failed!": STOP
FUN% = 100                ' A/D initialization
CALL PCL818H(FUN%, SEG param%(0))
IF param%(45) <> 0 THEN PRINT "A/D Initialization Failed!": STOP
IF longgrip = 1 THEN PRINT #2, "a5 ad2 v.5 d-161700 g"
IF shortgrip = 1 THEN PRINT #2, "a5 ad2 v.5 d-109200 g"
FUN% = 105                ' pacer trigger A/D conversion with
CALL PCL818H(FUN%, SEG param%(0))       ' interrupt data transfer
IF param%(45) <> 0 THEN PRINT "A/D Interrupt Data Transfer Failed!": STOP
45 FUN% = 106                ' check interrupt status
CALL PCL818H(FUN%, SEG param%(0))
CHK% = (param%(46) AND 1)
IF CHK% <> 0 THEN GOTO 45     ' 0 : Not active, 1 : Active
RETURN

card.call:
' ********************** A/D Card Function Calls **********************
FUN% = 3                  ' hardware initialization
CALL PCL818H(FUN%, SEG param%(0))
IF param%(45) <> 0 THEN PRINT "Driver Initialization Failed!": STOP
FUN% = 100                ' A/D initialization
CALL PCL818H(FUN%, SEG param%(0))
IF param%(45) <> 0 THEN PRINT "A/D Initialization Failed!": STOP
IF longgrip = 1 THEN GOSUB longgrip.test
IF shortgrip = 1 THEN GOSUB shortgrip.test
50  FUN% = 105                ' pacer trigger A/D conversion with
CALL PCL818H(FUN%, SEG param%(0))       ' interrupt data transfer
IF param%(45) <> 0 THEN PRINT "A/D Interrupt Data Transfer Failed!": STOP
55 FUN% = 106                ' check interrupt status
CALL PCL818H(FUN%, SEG param%(0))
CHK% = (param%(46) AND 1)
IF CHK% <> 0 THEN GOTO 55     ' 0 : Not active, 1 : Active
CLOSE #2
GOSUB motor.off
RETURN

longgrip.test:
'***************** 6 in Test Using Long Grips *****************
LOCATE 41, 10: PRINT "                                        "
rate = 200
accel = 100
vel$ = LTRIM$(STR$(rate / 10))
acc$ = LTRIM$(STR$(accel))
LOCATE 41, 20: PRINT "v"; vel$; ", a"; acc$; "  Hit Enter to start the test."
DO
     LOOP UNTIL INKEY$ = CHR$(13)
LOCATE 41, 20: PRINT "Running Test                                  "
OPEN "com1:9600,n,8,1,rs,cs,ds,cd" FOR RANDOM AS #2
PRINT #2, "a"; acc$; " ad300 v"; vel$; " d-55000 g"
RETURN 50

shortgrip.test:
'***************** 6 in Test Using Short Grips *********************
LOCATE 41, 10: PRINT "                                        "
rate = 200
accel = 100
vel$ = LTRIM$(STR$(rate / 10))
acc$ = LTRIM$(STR$(accel))
LOCATE 41, 20: PRINT "v"; vel$; ", a"; acc$; "  Hit Enter to start the test."
DO
     LOOP UNTIL INKEY$ = CHR$(13)
LOCATE 41, 20: PRINT "Running Test                                  "
OPEN "com1:9600,n,8,1,rs,cs,ds,cd" FOR RANDOM AS #2
PRINT #2, "a"; acc$; " ad300 v"; vel$; " d-3000 g"
```

```
RETURN 50

motor.off:
'************************* Turn Resolver Off ******************************
OPEN "com1:9600,n,8,1,rs,cs,ds,cd" FOR RANDOM AS #2
PRINT #2, "off"
CLOSE #2
RETURN

display.data:
' ****** Plots 40 points/channel/sec (for 400Hz collection/channel) ******
timeseg = 0
I = 0
60 IF timeseg <= time THEN
     IF I <= param%(14) - 6 THEN
        PSET (timeseg, dat%(I) * 10! / 4096! + (-5!)), 10
        j = I + 1: PSET (timeseg, dat%(j) * 20! / 4096! + (-10!)), 11
' (velocity)  k = I + 2: PSET (timeseg, dat%(k) * 20! / 4096! + (-10!)), 12
        l = I + 3: PSET (timeseg, (-1) * (dat%(l) * 5! / 4096! + (-2.5))), 13
' (lvdt)     m = I + 4: PSET (timeseg, dat%(m) * 20! / 4096! + (-10!)), 14
        n = I + 5: PSET (timeseg, (dat%(n) * 20! / 4096! + (-10!))), 15
        o = I + 6: PSET (timeseg, (dat%(o) * 20! / 4096! + (-10!))), 15
    timeseg = timeseg + .025
  I = I + 70
  GOTO 60
 END IF
END IF
RETURN

' ****************************************************************
' ********************** Save All Data *************************
' ****************************************************************
save.question:
' ************************** Ask to Save Data ***************************
GOSUB write.data
70 KEY(9) ON
ON KEY(9) GOSUB motor.home
LOCATE 41, 20: PRINT "To return to home position press F9.          "
DO
     LOOP UNTIL INKEY$ = "home"
75 KEY(9) OFF
RETURN

write.data:
'************************* Save Data to File ****************************
LOCATE 41, 20: PRINT "                                    "
LOCATE 41, 20: PRINT "Saving test data to "; file$; "."
OPEN file$ FOR OUTPUT AS #3
PRINT #3, "DBSTEST Program used on "; DATE$; "."
IF shortgrip = 1 THEN
PRINT #3, "Short Grip Test with V="; rate; "in/min and A="; accel; "in/min2"
END IF
IF longgrip = 1 THEN
PRINT #3, "Long Grip Test with V="; rate; "in/min and A="; accel; "in/min2"
END IF
PRINT #3, "dbsload ="; dbsload; "; cblpos ="; cblpos; "; cblvel ="; cblvel; ";"
PRINT #3, "dtmload = "; dtmload; "; lvdt3 ="; lvdt3; "; lvdt30 ="; lvdt30
PRINT #3, "Die Offset (subtracted from test data only) = "; dieoffset; " lb."
PRINT #3, "DBS Load (lb)"; CHR$(9); "Position (in)"; CHR$(9); "Velocity (V)";
PRINT #3, CHR$(9); "DTM Load (lb)"; CHR$(9); "DTM Pos'n (in)"; CHR$(9);
PRINT #3, "Die LoadF (lb)"; CHR$(9); "Die LoadR (lb)"; CHR$(9);
PRINT #3, "Die LdSum (lb)"; CHR$(13)
I = 7
80 PRINT #3, USING "#####.######"; dbsload * (dat%(I) * 10! / 4096! + (-5!));
```

```
  PRINT #3, CHR$(9);
  j = I + 1
  PRINT #3, USING "###.######"; cblpos * (dat%(j) * 20! / 4096! + (-10!));
  PRINT #3, CHR$(9);
  k = I + 2
  PRINT #3, USING "###.######"; cblvel * (dat%(k) * 20! / 4096! + (-10!));
  PRINT #3, CHR$(9);
  l = I + 3
  PRINT #3, USING "#####.#####"; dtmload * (dat%(l) * 5! / 4096! + (-2.5));
  PRINT #3, CHR$(9);
  m = I + 4
  PRINT #3, USING "###.######"; dtmlvdt * (dat%(m) * 20! / 4096! + (-10!));
  PRINT #3, CHR$(9);
  n = I + 5
  PRINT #3, USING "#####.#####"; -(dieoffset / 2) + (dieloadf * (dat%(n) * 20! / 4096! + (-10!)));
  PRINT #3, CHR$(9);
  o = I + 6
  PRINT #3, USING "#####.#####"; -(dieoffset / 2) + (dieloadr * (dat%(o) * 20! / 4096! + (-10!)));
  PRINT #3, CHR$(9);
  PRINT #3, USING "#####.#####"; -   dieoffset + ( dieloadsum * (( dat%(n) * 20! / 4096! + (-10!)) +
(dat%(o) * 20! / 4096! + (-10!))))
  I = I + 7
IF I <= param%(14) - 6 THEN GOTO 80
GOSUB write.initialdata
CLOSE #3
IF dievar = 1 THEN
   GOSUB write.dieinsertdata
END IF
RETURN 70

write.initialdata:
' ************ Data Collection Portion of Initial Data *******************
LOCATE 41, 20: PRINT "                                    "
LOCATE 41, 20: PRINT "Saving initial data to "; file$; "."
GOSUB initial.buffer
I = 7
PRINT #3, "0000.000000"; CHR$(9); "0000.000000"; CHR$(9); "0000.000000";
PRINT #3, CHR$(9); "0000.000000"; CHR$(9); "0000.000000"; CHR$(9);
PRINT #3, "0000.000000"; CHR$(9); "0000.000000"; CHR$(9); "0000.000000"
85  PRINT #3, USING "#####.#####"; dbsload * (init%(I) * 10! / 4096! + (-5!));
  PRINT #3, CHR$(9);
  j = I + 1
  PRINT #3, USING "###.######"; cblpos * (init%(j) * 20! / 4096! + (-10!));
  PRINT #3, CHR$(9);
  k = I + 2
  PRINT #3, USING "###.######"; cblvel * (init%(k) * 20! / 4096! + (-10!));
  PRINT #3, CHR$(9);
  l = I + 3
  PRINT #3, USING "#####.#####"; dtmload * (init%(l) * 5! / 4096! + (-2.5));
  PRINT #3, CHR$(9);
  m = I + 4
  PRINT #3, USING "###.######"; lvdt3 * (init%(m) * 20! / 4096! + (-10!));
  PRINT #3, CHR$(9);
  n = I + 5
  PRINT #3, USING "#####.#####"; dieloadf * (init%(n) * 20! / 4096! + (-10!));
  PRINT #3, CHR$(9);
  o = I + 6
  PRINT #3, USING "#####.#####"; dieloadr * (init%(o) * 20! / 4096! + (-10!));
  PRINT #3, CHR$(9);
  PRINT #3, USING "#####.#####";  dieloadsum * (( init%(n) * 20! / 4096! + (-10!)) + (   init%(o) * 20! /
4096! + (-10!)))
  I = I + 7
IF I <= param%(14) - 6 THEN GOTO 85
PRINT #3, "0000.000000"; CHR$(9); "0000.000000"; CHR$(9); "0000.000000";
```

```
PRINT #3, CHR$(9); "0000.000000"; CHR$(9); "0000.000000"; CHR$(9);
PRINT #3, "0000.000000"; CHR$(9); "0000.000000"; CHR$(9); "0000.000000"
IF dievar = 2 AND arraytype = 2 THEN
LOCATE 41, 20: PRINT "                                    "
LOCATE 41, 20: PRINT "Saving pretensioning data to "; file$; "."
   GOSUB tension.buffer
   I = 7
86  PRINT #3, USING "#####.######"; dbsload * (pre%(I) * 10! / 4096! + (-5!));
   PRINT #3, CHR$(9);
   j = I + 1
   PRINT #3, USING "###.#######"; cblpos * (pre%(j) * 20! / 4096! + (-10!));
   PRINT #3, CHR$(9);
   k = I + 2
   PRINT #3, USING "###.#######"; cblvel * (pre%(k) * 20! / 4096! + (-10!));
   PRINT #3, CHR$(9);
   l = I + 3
   PRINT #3, USING "#####.#####"; dtmload * (pre%(l) * 5! / 4096! + (-2.5));
   PRINT #3, CHR$(9);
   m = I + 4
   PRINT #3, USING "###.#######"; dtmlvdt * (pre%(m) * 20! / 4096! + (-10!));
   PRINT #3, CHR$(9);
   n = I + 5
   PRINT #3, USING "#####.#####"; dieloadf * (pre%(n) * 20! / 4096! + (-10!));
   PRINT #3, CHR$(9);
   o = I + 6
   PRINT #3, USING "#####.#####"; dieloadr * (pre%(o) * 20! / 4096! + (-10!));
   PRINT #3, CHR$(9);
   PRINT #3, USING "#####.#####";  dieloadsum * (( pre%(n) * 20! / 4096! + (-10!)) + (  pre%(o) * 20! /
4096! + (-10!)))
   I = I + 7
   IF I <= param%(14) - 6 THEN GOTO 86
END IF
CLOSE #3
RETURN

write.dieinsertdata:
' ************ Read Array Points Into Die Insertion Data File ************
LOCATE 41, 20: PRINT "                                    "
LOCATE 41, 20: PRINT "Saving insertion data to "; dieinsert$; "."
GOSUB dieinsert.buffer
OPEN dieinsert$ FOR OUTPUT AS #4
PRINT #4, "Die Insertion Values for "; file$; "."; CHR$(13)
PRINT #4, "DBS Load (lb)"; CHR$(9); "Position (in)"; CHR$(9); "Velocity (V)";
PRINT #4, CHR$(9); "DTM Load (lb)"; CHR$(9); "DTM Pos'n (in)"; CHR$(9);
PRINT #4, "Die LoadF (lb)"; CHR$(9); "Die LoadR (lb)"; CHR$(9); "Die LdSum (lb)"
I = 7
90 PRINT #4, USING "#####.#####"; dbsload * (die%(I) * 10! / 4096! + (-5!));
  PRINT #4, CHR$(9);
  j = I + 1
  PRINT #4, USING "###.#######"; cblpos * (die%(j) * 20! / 4096! + (-10!));
  PRINT #4, CHR$(9);
  k = I + 2
  PRINT #4, USING "###.#######"; cblvel * (die%(k) * 20! / 4096! + (-10!));
  PRINT #4, CHR$(9);
  l = I + 3
  PRINT #4, USING "#####.#####"; dtmload * (die%(l) * 5! / 4096! + (-2.5));
  PRINT #4, CHR$(9);
  m = I + 4
  lvdt = 1
  PRINT #4, USING "###.#######"; lvdt * (die%(m) * 20! / 4096! + (-10!));
  PRINT #4, CHR$(9);
  n = I + 5
  PRINT #4, USING "#####.#####"; dieloadf * (die%(n) * 20! / 4096! + (-10!));
  PRINT #4, CHR$(9);
```

```
  o = I + 6
  PRINT #4, USING "#####.#####"; dieloadr * (die%(n) * 20! / 4096! + (-10!));
  PRINT #4, CHR$(9);
  PRINT #4, USING "#####.#####";  dieloadsum * (( die%(n) * 20! / 4096! + (-10!)) + (   die%(n) * 20! /
4096! + (-10!)))
  I = I + 7
IF I <= param%(14) - 6 THEN GOTO 90
CLOSE #4
IF arraytype = 2 THEN
   GOSUB tension.buffer
   OPEN dieinsert$ FOR APPEND AS #4
   LOCATE 41, 20: PRINT "                                        "
   LOCATE 41, 20: PRINT "Saving tension data to "; dieinsert$; "."
   PRINT #4, "000.0000000"; CHR$(9); "000.0000000"; CHR$(9); "000.0000000";
   PRINT #4, CHR$(9); "000.0000000"; CHR$(9); "000.0000000"; CHR$(9);
   PRINT #4, "000.0000000"; CHR$(9); "000.0000000"; CHR$(9); "000.0000000"
   I = 7
91  PRINT #4, USING "#####.#####"; dbsload * (pre%(I) * 10! / 4096! + (-5!));
   PRINT #4, CHR$(9);
   j = I + 1
   PRINT #4, USING "###.#######"; cblpos * (pre%(j) * 20! / 4096! + (-10!));
   PRINT #4, CHR$(9);
   k = I + 2
   PRINT #4, USING "###.#######"; cblvel * (pre%(k) * 20! / 4096! + (-10!));
   PRINT #4, CHR$(9);
   l = I + 3
   PRINT #4, USING "#####.#####"; dtmload * (pre%(l) * 5! / 4096! + (-2.5));
   PRINT #4, CHR$(9);
   m = I + 4
   PRINT #4, USING "###.#######"; dtmlvdt * (pre%(m) * 20! / 4096! + (-10!));
   PRINT #4, CHR$(9);
   n = I + 5
   PRINT #4, USING "#####.#####"; dieloadf * (pre%(n) * 20! / 4096! + (-10!));
   PRINT #4, CHR$(9);
   o = I + 6
   PRINT #4, USING "#####.#####"; dieloadr * (pre%(o) * 20! / 4096! + (-10!));
   PRINT #4, CHR$(9);
   PRINT #4, USING "#####.#####";  dieloadsum * (( pre%(n) * 20! / 4096! + (-10!)) + (  pre%(o) * 20! /
4096! + (-10!)))
   I = I + 7
   IF I <= param%(14) - 6 THEN GOTO 91
   CLOSE #4
END IF
RETURN

motor.home:
' ***************** Return Motor to Starting Position ******************
OPEN "com1:9600,n,8,1,rs,cs,ds,cd" FOR RANDOM AS #2
PRINT #2, "on"
PRINT #2, "xr1"
PRINT #2, "a10 ad20 v.5 d-1000 g"
LOCATE 41, 20: PRINT "                                        "
LOCATE 41, 20: PRINT "Hit Enter when ready to continue."
DO
     LOOP UNTIL INKEY$ = CHR$(13)
PRINT #2, "off"
CLOSE #2
RETURN 75


SUB grpaxisb (xmin!, xmax!, ymin!, ymax!, wpage%, dpage%)
'plotting area setup routine
'need to input xmax!, xmin, ymin!, ymax!
'variables used -  xmin, xmax!, ymin!, ymax!, ytick, xtick, x1, x%, y1, y1
```

```
'INPUT xmax!, ymax!
'modified 2/3/95 to fit DBS test parameters
CLS 0
SCREEN 9, 0, wpage%, dpage%            '640x350 resolution requires EGA
WIDTH 80, 43                           'high resolution text
VIEW (56, 0)-(600, 300), 1, 11         'set physical viewport and box
WINDOW (xmin!, ymin!)-(xmax!, ymax!)   'window with logical max x, y.
LINE (xmin!, ymin!)-(xmax!, ymax!), , B  'draw axis
ytick = (ymax! - ymin!) / 100          'draw tick marks every 1/2 sec
x1 = (xmax! - xmin!) / (2 * xmax!)     'on x axis
FOR x% = 1 TO (xmax! * 2)
LINE (x1 * x% + xmin!, ymin!)-(x1 * x% + xmin!, ymin! + ytick)
NEXT x%
xtick = (xmax! - xmin) / 100           'ticks on y axis
y1 = (ymax! - ymin!) / 5
FOR y% = 1 TO 4
LINE (xmin, y1 * y% + ymin!)-(xmin + xtick, y1 * y% + ymin!)
NEXT y%
LOCATE 1, 1, 1
    PRINT USING "###.#"; ymax!
LOCATE 8, 1, 1                         'locate cursor  y axis labels
    PRINT USING "###.#"; ymax! - y1
LOCATE 16, 1, 1
    PRINT USING "###.#"; ymax! - y1 * 2
LOCATE 23, 1, 1
    PRINT USING "###.#"; ymax! - y1 * 3
LOCATE 31, 1, 1
    PRINT USING "###.#"; ymax! - y1 * 4
LOCATE 38, 1, 1
    PRINT USING "###.#"; ymin!
LOCATE 40, 4, 1                        'print x axis labels
    PRINT USING "###.#"; xmin
LOCATE 40, 18, 1
    PRINT USING "###.#"; xmax! / 5
LOCATE 40, 32, 1
    PRINT USING "###.#"; 2 * xmax! / 5
LOCATE 40, 45, 1
    PRINT USING "###.#"; 3 * xmax! / 5
LOCATE 40, 59, 1
    PRINT USING "###.#"; 4 * xmax! / 5
LOCATE 40, 73, 1
    PRINT USING "###.#"; xmax!
END SUB
```

Appendix C: Representative Micrographs of AA2008, AA6009, and AA6111

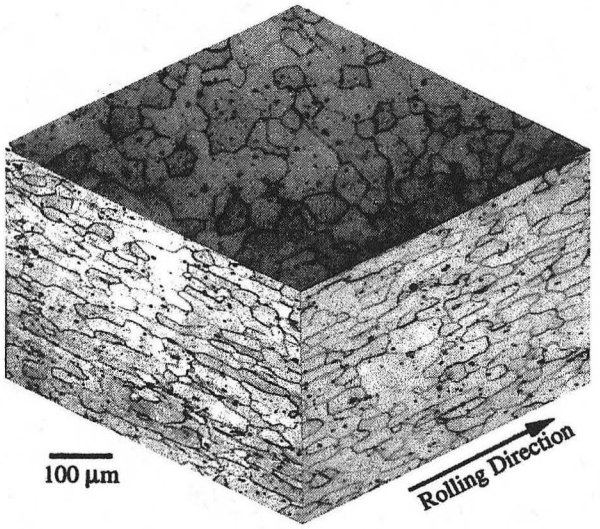

a)

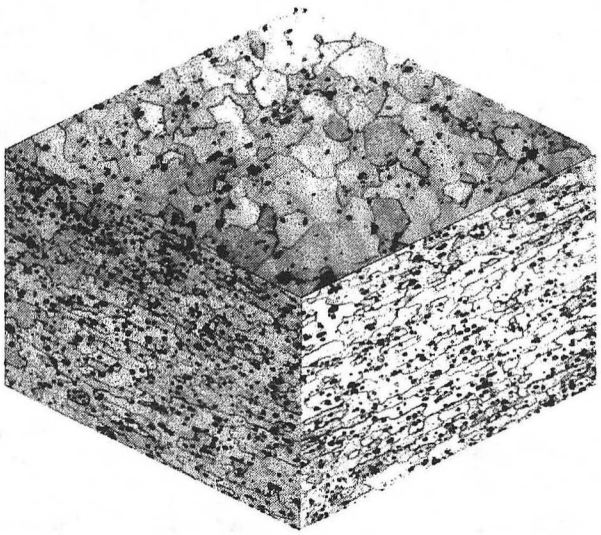

b)

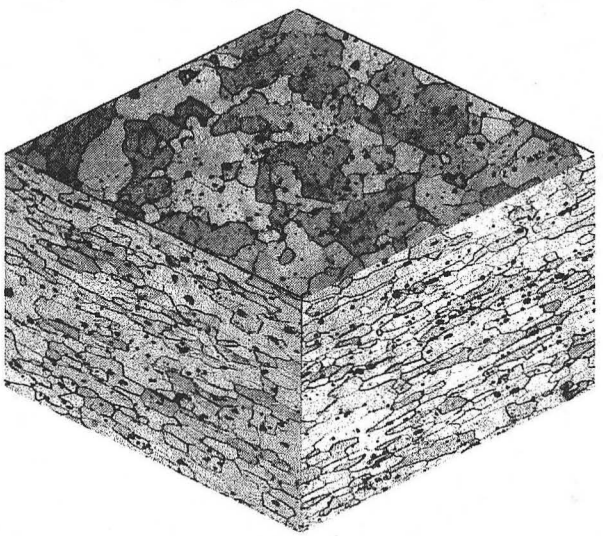

c)

Figure C1 Microstructures of a) 2008, b) 6009, and c) 6111 sheet alloys.

Appendix D: EBT Forming Friction Strain Gauge and Load Cell Results

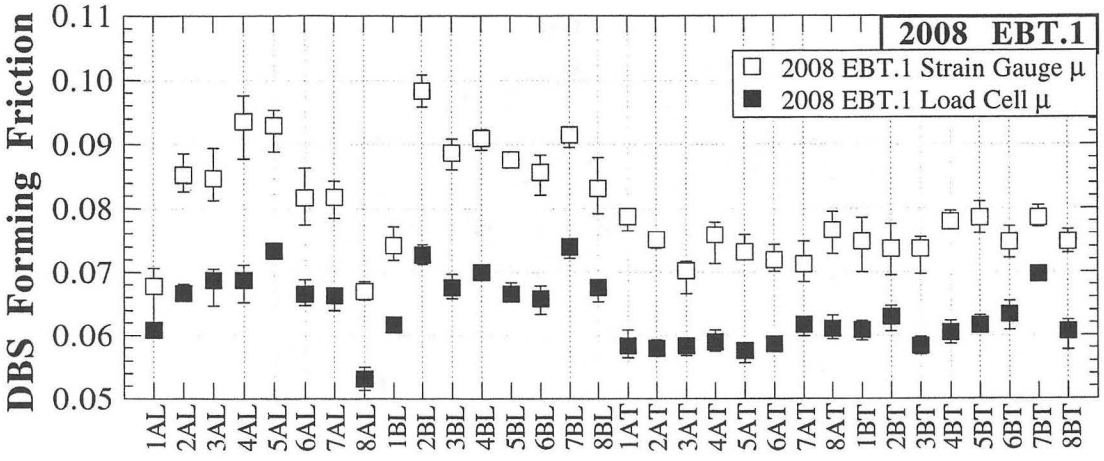

Figure D1 DBS-μ strain gauge and load cell setup results for 2008 EBT.1.

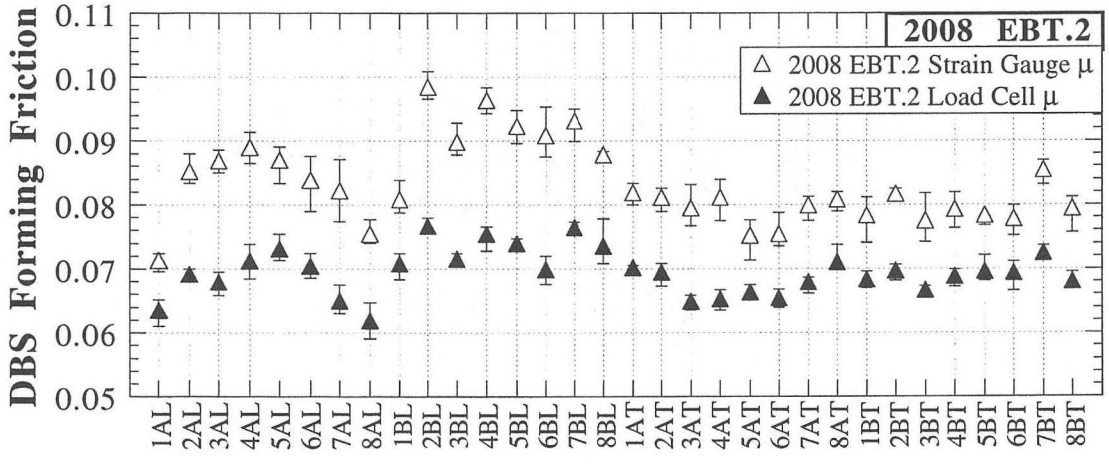

Figure D2 DBS-μ strain gauge and load cell setup results for 2008 EBT.2.

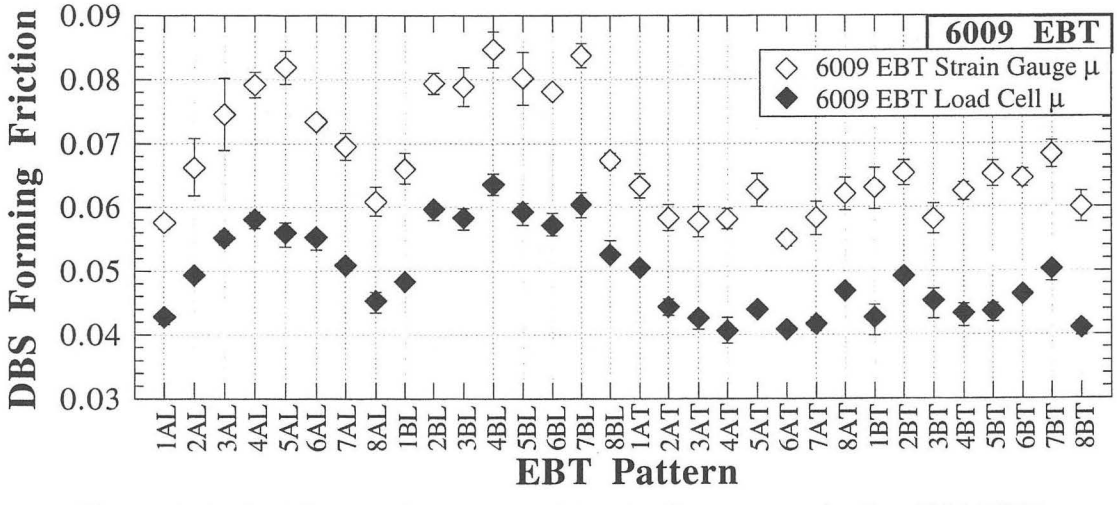

Figure D3 DBS-μ strain gauge and load cell setup results for 6009 EBT.

Appendix E:

DBS Load Cell Setup Forming Friction Data For All Patterns in Column Form

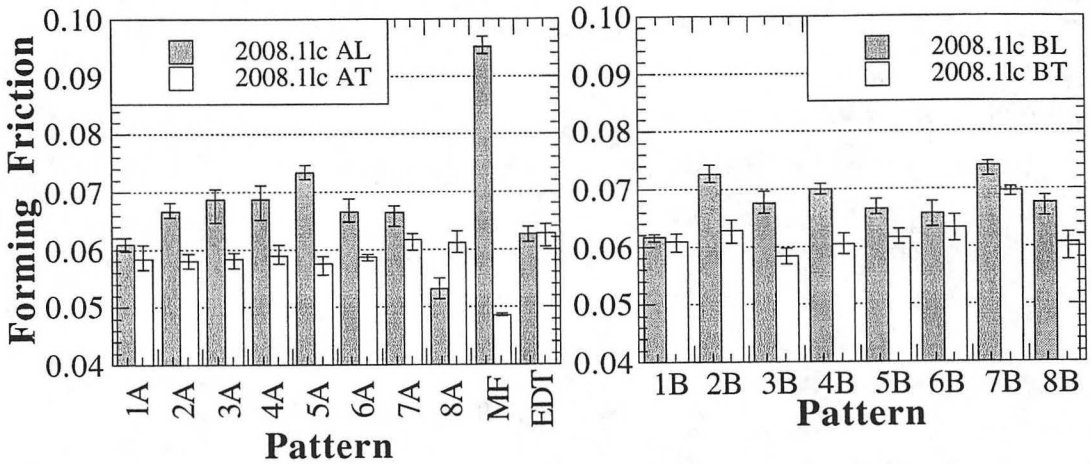

Figure E1 DBS-μ results for 2008 MF, 2008 EDT, and 2008.1 EBT sheets.

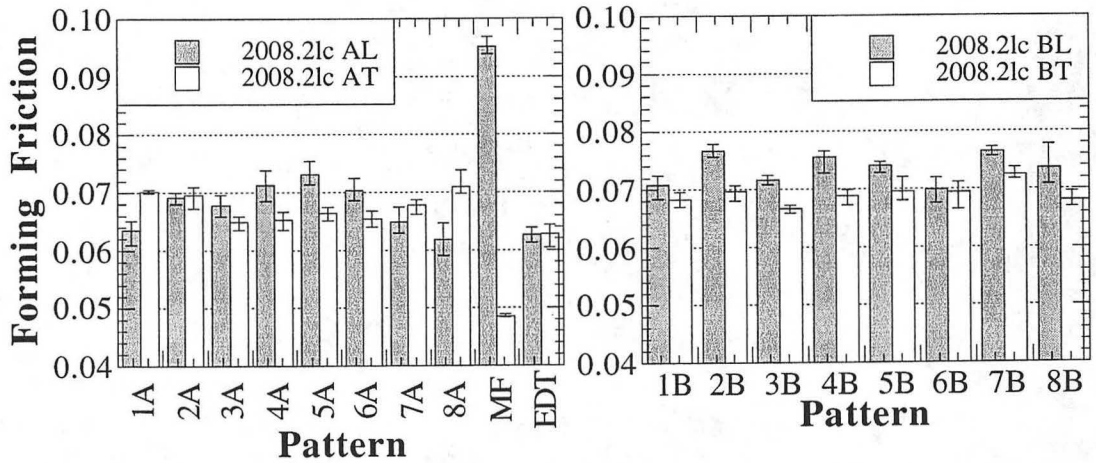

Figure E2 DBS-μ results for 2008 MF, 2008 EDT, and 2008.2 EBT sheets.

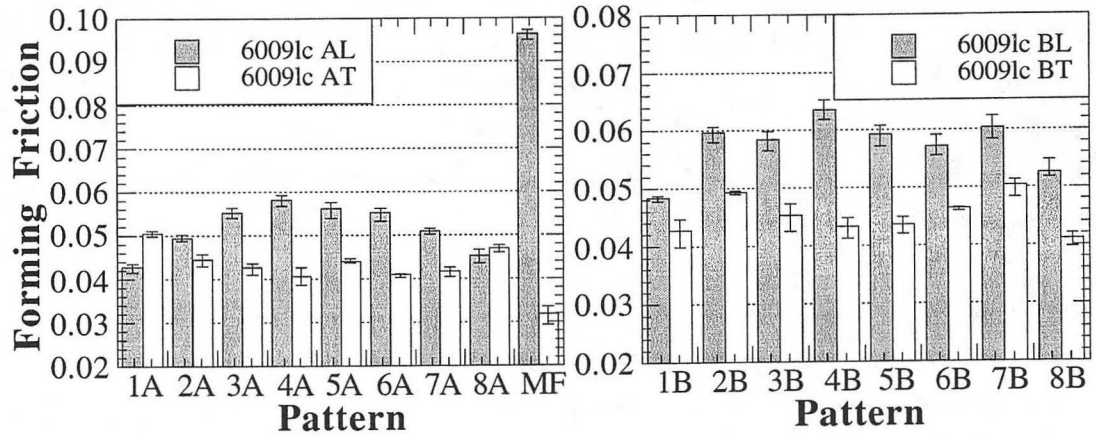

Figure E3 DBS-μ results for 6009 MF and 6009 EBT sheets.

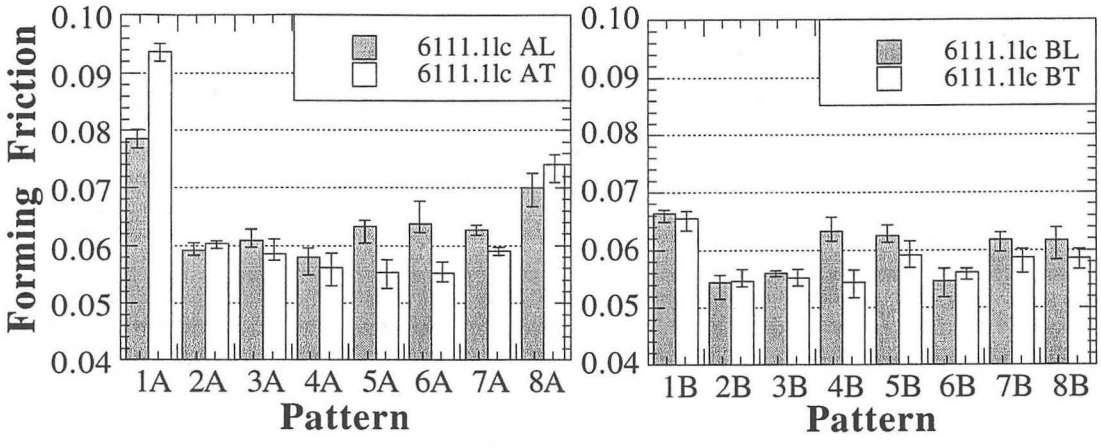

a)

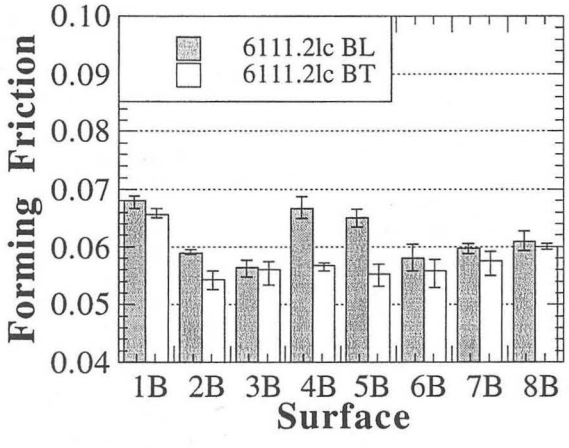

b)

Figure E4 DBS-μ results for a) 6111.1 EBT, and b) 6111.2 EBT sheets.

Appendix F: Calculation of Surface Parameters[A2]

Two Dimensional (2D) Surface Parameters:

Surface Parameter Name	Symbol	Equation
Roughness Average	R_a, AA, CLA	$R_a = \left(\frac{1}{L}\int_{x=0}^{x=L} \lvert y\rvert \, dx\right) = \frac{\sum_{i=1}^{N} \lvert y_i\rvert}{N}$
Root Mean Square Roughness	R_q	$R_q = \left(\frac{1}{L}\int_{x=0}^{x=L} y^2 \, dx\right) = \left(\frac{\sum_{i=1}^{N} \lvert y_i\rvert^2}{N}\right)^{\frac{1}{2}}$
Skewness	Skew	$\text{Skew} = \frac{1}{(R_q)^3}\frac{1}{N}\sum_{i=1}^{N} y_i^3$
Kurtosis	Kurt	$\text{Kurt} = \frac{1}{(R_q)^4}\frac{1}{N}\sum_{i=1}^{N} y_i^4$

L is the sampling length and y_i is the distance of point i from the center line along the sampling line of length N points.

Three Dimensional (3D) Surface Parameters:

Surface Parameter Name	Symbol	Equation
Roughness Average	R_a, AA, CLA	$R_a = \frac{\sum_{i=1}^{C}\sum_{j=1}^{R} \lvert y_{ij}\rvert}{R*C} = \frac{\sum_{i=1}^{N} \lvert y_i\rvert}{N}$
Root Mean Square Roughness	R_q	$R_q = \left(\frac{\sum_{i=1}^{C}\left(\sum_{j=1}^{R} \lvert y_{rc}\rvert^2\right)}{R*C}\right)^{\frac{1}{2}} = \left(\frac{\sum_{i=1}^{N} \lvert y_i\rvert^2}{N}\right)^{\frac{1}{2}}$
Skewness	Skew	$\text{Skew} = \frac{1}{(R_q)^3}\frac{1}{N}\sum_{i=1}^{N} y_i^3$
Kurtosis	Kurt	$\text{Kurt} = \frac{1}{(R_q)^4}\frac{1}{N}\sum_{i=1}^{N} y_i^4$

R and C are the number of rows and columns, respectively, of the 2D matrix, N is the total number of points, RxC, collected over the profiled area, and y_{rc} and y_i are the point distance from the average surface value calculated from all points in the profiled area.

ERNEST ORLANDO LAWRENCE BERKELEY NATIONAL LABORATORY
ONE CYCLOTRON ROAD | BERKELEY, CALIFORNIA 94720

Prepared for the U.S. Department of Energy under Contract No. DE-AC03-76SF00098